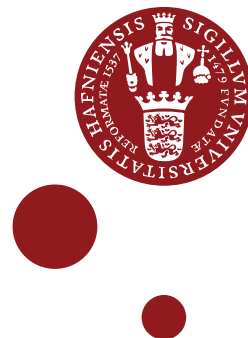


UNIVERSITY OF COPENHAGEN
FACULTY OF SCIENCE



MSc Climate Change thesis

Steffen Kristiansen, KU-ID: bnf783

Quantification of bipolar volcanic eruptions during the last glacial period (12-60 ka) based on Greenland and Antarctic ice cores

Supervisor: Anders Svensson

Submitted on: 28-Jun-20

Abstract

From historical records and measurements, it is evident that large volcanic eruptions can have an impact on the climate. Sulfate aerosols from an eruption can disperse in the atmosphere and with precipitation or dry fall-out over ice sheets, the sulfate can build up a record. Hence, sulfate concentration can be used to detect and quantify volcanic eruptions. First a thorough explanation on how volcanic aerosols are dispersed and how they impact climate will be introduced. Hereafter, several eruptions during the last glacial (12000 b2k – 60000 b2k) are identified. In order to validate the estimation of the sulfate levels and detection of eruptions, a replication of the methods used by Sigl *et al.* (2013) is presented and the methods are validated and applied on sulfate and sulfur data from three Greenland cores (GISP2, NEEM and NGRIP) and three Antarctic cores (EDC, EDML and WD). The detected eruptions and the sulfate depositions in kg/km^2 are synchronized with bipolar eruptions identified by Svensson *et al.* (2020). Further, a comparison in terms of the sulfate depositions and frequencies are compared with bipolar eruptions during the last 2500 years identified by Sigl *et al.* (2013, 2015). A comparison that reveals a glacial with a close to expected amount of eruptions, but with an elevated sulfate background level and eruptions with higher sulfate deposition. Together with eruptions with known latitudes, the sulfate depositions are further used in order to estimate latitudinal bands for the glacial bipolar eruptions showing an overweight of north hemispheric and tropical eruptions. Additionally, seven selected eruptions are investigated for possible climatic fingerprints using $\delta^{18}\text{O}$ records from both Greenland and Antarctica with two occurring just prior to cooling events.

Acknowledgements

Following the completion of this project, I have had the time to look back on the somewhat peculiar situation which largely has affected the process. About 1.5 month into the work, the corona virus caused as an almost complete lockdown which lasted through the remaining part of the project. Hence my apartment is where the vast majority of the work has been done.

Firstly, I want to draw my gratitude towards my supervisor Anders Svensson who has been a big support and a huge help in figuring out the necessary Matlab coding. I thank him for having an always-open door (before the lock-down) and adjusting his supervision to work under the special corona conditions with Zoom meetings and an endless amount of emails. Also, a huge thanks to PhD-student Jia-Mei Lin for her collaboration with Matlab coding and troubleshooting.

Secondly, I want to thank my partner for always being supportive and enduring being locked inside our apartment with me and my office mess. I reckon it has not been an easy task for either of us. Further, I also want to express my gratitude to my friends who, even though physical meetings have not been possible due to the virus, have always been there listening to my thoughts and encouraging me when needed.

Table of contents

1. Introduction.....	5
2. Background.....	6
2.1. Volcanism and the gaseous components	6
2.2. Geography and the effect on dispersion of gases	7
2.3. Effects on the radiation	8
2.3.1. How big quantities are needed?.....	10
2.4. Determining the size of an eruption.....	10
2.5. The climatic effects of eruptions	11
3. Ice cores.....	13
3.1. Ice cores in this project.....	14
3.1.1. Greenland ice cores	14
3.1.2. Antarctic ice cores	15
4. Methods	15
4.1. Reproduction of data from Sigl, M., et al., (2013).....	15
4.2. Modifications used on present data.....	17
5. Results	22
5.1. Bipolar eruptions	23
5.2. Sulfate concentration vs. latitude	25
6. Discussion	26
6.1. Data resolution and window width	26
6.2. Size of glacial eruptions compared to historical.....	28
6.2.1. Sulfate concentration during the glacial and last 2500 years	31
6.3. Latitudinal origin.....	33
6.4. The $\delta^{18}\text{O}$ -temperature relationship.....	36
6.5. Bipolar eruptions and climatic changes.....	36
6.5.1. The 29678 b2k eruption (Campi Flegrei)	37
6.5.2. The 41444 b2k eruption	38
6.5.3. The 45555 b2k eruption	39
6.5.4. The 52302 b2k eruption	40
6.5.5. The 55383 b2k eruption (NAAZ II)	40
6.5.6. Other eruptions of interest	41
Conclusion	45
7. Bibliography.....	47

Appendix A	51
A.1. Reproduction of Sigl et al., (2013), WAIS example	51
A.2. EDML script (high resolution).....	52
A.3. NEEM script (low resolution)	54
A.4. All bipolar events, Greenland.....	56
A.5. All bipolar events, Antarctica	59
A.6. SO ₄ dep. values, age, and reference for known and speculated origin of historical and glacial eruptions	62
A.7. Hemispheric and global averages of bipolar eruptions	63
A.8. Sulfate deposition difference between NH and SH.....	65
Appendix B.....	67
B.1. Scatter plots comparing Sigl et al. (2013) with replicated data	67
B.2. Sulfate records (12000-60000 b2k)	68

1. Introduction

The balance between incoming and outgoing energy in the Earth's climate system is our climate's primary controlling factor. Changes in the system, e.g. current human-induced increase of greenhouse gases alter the climate by increasing the global temperature. However, changes such as alterations in the albedo can too lead to climatic changes. Volcanic eruptions are an example of the latter (Cole-Dai, 2010). Through the Earth's history, volcanoes have played an important role in our planet's climate system. From Roman times, there are descriptions of the sun being moon-like for a year (Stothers, 1984) and in 1784, Benjamin Franklin noted a constant fog over Europe and great parts of North America that did not dissipate as normal fog would and concluded that the fog was not weather-induced. Additionally, he also noticed that the 1783 AD European summer and following winter were unusually cold and concluded that the cause of that must have been the 1783 AD to 1784 AD Laki eruption in Iceland (Franklin, 1784). Later, the 1815 AD Tambora eruption was followed by an exceptionally cold summer throughout the Northern Hemisphere with snow in June in parts of New England and crop failures and famine in Europe (Zielinski, 2002). Further studies on volcanoes have since verified that eruptions indeed can influence weather and climate, and the 1991 AD Pinatubo eruption hit the nail on the head by being the first eruption where it was possible to directly measure a global cooling effect (0.5°) (Robock, 2000; Holm, 2012).

This project investigates bipolar eruptions during the last glacial (12000-60000 b2k). First a thorough explanation on how volcanic aerosols are dispersed and how they impact climate will be introduced. In order to validate the estimation of the sulfate levels and detection of eruptions, a replication of the methods used by Sigl *et al.* (2013) is presented and the methods are validated and hereafter applied on sulfate and sulfur data from three Greenland cores (GISP2, NEEM and NGRIP) and three Antarctic cores (EDC, EDML and WD). The detected eruptions and the sulfate depositions in kg/km^2 are synchronized with bipolar eruptions identified by Svensson *et al.* (2020). Further, a comparison in terms of the sulfate depositions and frequencies is made with bipolar eruption during the last 2500 years identified by Sigl *et al.* (2013, 2015). Using the latitudinal origin of known eruptions during the last 2500 years and the glacial together with the difference in sulfate deposition between Greenland and Antarctica, bands of latitude are applied to the glacial bipolar eruptions with unknown origin. Lastly, using $\delta^{18}\text{O}$ records from Greenland and Antarctica, the climatic fingerprint of some of the largest detected glacial bipolar eruptions is investigated.

2. Background

Whether a volcanic eruption have an impact on the climate or not depends on a few factors: The nature and the total volume of the emitted products during the entire eruption and the explosivity. At least one to five megaton of sulfur gases need to be injected into the stratosphere in order to cause a global impact. If the two factors are fulfilled, the location of the eruption determines how widespread the impacts will be. Further, plinian eruption types which are most common in subduction zones, are the ones which are most likely to inject matter into the stratosphere due to their high explosivity (Zielinski, 2002).

2.1. Volcanism and the gaseous components

An erupting volcano injects vast amounts material into the atmosphere (Figure 1). One of the main products is the mineral matter, *tephra* (ash in Figure 1), which is ejected during the eruption's explosive phase. In big eruptions, vast amounts of tephra are produced, however, due to the size of the material, it only reaches the troposphere and thus stays in the atmosphere for a short period of time. Henceforth, while the local climatic effects due to blocking of the incoming sunlight might be significant for a short period, the global climatic impacts are very limited (Robock, 2000; Cole-Dai, 2010; Holm, 2012; Geology In, 2015). The composition of the emitted gases varies depending on the type of magma and is generally controlled by the equilibrium between a hydrous fluid at the top and the silicate melt in the magma chamber (Textor *et al.*, 2003). The components with the biggest climatic impact are the volcanic gases which are emitted both during the explosive and the quiescent phase with the most abundant types being sulfur (S), hydrogen chloride (HCl), hydrogen fluoride (HF), water (H₂O) and carbon dioxide (CO₂) (Table 1). The three latter gases are all important parts of the Earth's atmosphere, and while both H₂O and CO₂ are important greenhouse gases which are emitted in big quantities, the relative amount is small compared to the atmospheric content. Thus, their effect on the climate is neglectable.

Table 1: A general composition of the volcanic gases at the vent. (Textor *et al.*,2003)

Species	H ₂ O	CO ₂	SO ₂	H ₂ S	COS	CS ₂	HCl	HBr	HF
%/vol	50-90	1-40	1-25	1-10	10 ⁻⁴ - 10 ⁻²	10 ⁻⁴ -10 ⁻²	1-10	?	< 10 ⁻³
Tg/year	?	75	1.5- 50	1-2.8	0.006- 0.1	0.007- 0.096	0.4- 11	0.0078- 0.1	0.06-6

Instead, the most important climatic effect from explosive eruptions is mainly due to SO₂ and to a certain degree H₂S ejected into the stratosphere. Here, they react with OH and H₂O to form H₂SO₄, H₂S, however, for the most part oxidizes quickly and forms SO₂ which in the timespan of approx. a month forms H₂SO₄ (Eq. 1 – 3).



In the stratosphere, the reactions can take several weeks to months (Cole-Dai, 2010), and the aerosols that form here can, due to the dry and weather-less nature, stay aloft in the stratosphere for years. If produced in big enough quantities, they can impact the climate up to three to four years after the eruption. Aerosols formed in the troposphere will on the other hand be affected by the weather and will quickly be washed out by precipitation. The other acids such as HCl and HF are very soluble and do not stay in the atmosphere for a long time, due to many of them adsorbing on to the ash particles in the eruption column and thus, they will quickly fall to the ground (Robock, 2000; Zielinski, 2002).

2.2. Geography and the effect on dispersion of gases

Whether an eruption impacts the whole globe or just a part of it, highly depends on the geographical position of the eruption. Eruptions originating in the tropics, can due to the atmospheric circulation with a general airflow from the tropics to the poles, have a global impact, while eruptions taking place at higher latitudes mainly will only affect the hemisphere it is in. However, for an eruption to pass the tropopause, the eruption column in the equatorial zone will need to rise about 15 km while an eruption in the mid- to high latitudes only needs to reach about 10 km. The seasons play a rather big role in determining whether an eruption has an impact or not. While the location of the Intertropical Convergence Zone and the phase of the Quasi Biennial Oscillation play an important role, the seasons also affects the overall airflow and height of the tropopause. In the spring and

autumn, the equator to pole air exchange is greater, and thus, these times of the year, the volcanic aerosols will more easily spread out into each hemisphere. However, the dispersion into the two hemispheres is not uniform as shown by the three largest modern eruptions that affected the global climate (Agung, 1963, El Chichón, 1982, Pinatubo, 1991). Additionally, during winter, the tropopause moves downward and thus, an eruption taking place in the mid- to high latitudes during the winter months will only need to rise about 8 km to enter the stratosphere. Consequential, a smaller eruption can impact the climate if it is taking place outside the equatorial zone where it will primarily affect the hemisphere in which it occurs (Zielinski, 2002; Textor *et al.*, 2003).

At higher latitudes, after an equatorial eruption big enough to impact climate, the biggest cooling is experienced during the summer in the first and second year following the eruption. The cause of this is the quicker dispersion of aerosols from the tropics to the mid- to higher latitudes during spring. If the eruption is located within the mid- to high latitudes, the cooling effects from it would be felt immediately compared to an equatorial eruption. (Zielinski, 2002)

2.3. Effects on the radiation

The global sulfur emissions to the stratosphere from volcanoes is only about 14% of the total natural and anthropogenic contribution, however, their effect on changes in the radiation is much larger and thus, volcanic emissions has a bigger imprint relative to their size (Textor *et al.*, 2003).

The sulfate aerosols produced effectively both reflect and absorb the incoming solar light and cause a fog-like dimming of the sun as experienced (Franklin, 1784). The decrease in incoming solar light causes and overall cooling at the surface while the absorption triggers a stratospheric warming. The aerosols typically have an effective radius of 0.5 μm which is approx. the same size as radiation in the visible spectrum, however, the single scatter albedo is 1 and hence, they perfectly scatter solar radiation. The dominant radiative effect seen at the surface is reflection of the sunlight back to space (backscattering) which increases the Earth's albedo and cools the surface by decreasing the amount of sunlight reaching the surface. Counteracting this surface cooling is an enhanced downward diffuse radiation caused by forward scattering of the solar light. However, even though this effect opposes the backscattering effect, it does not complete equalize and thus, the surface will experience a net cooling. Conversely, at the top of the aerosol cloud in the stratosphere, the atmosphere sees an increase in temperature due to absorption of solar radiation in the near infrared spectrum (Figure 1) (Stothers, 1984; Robock, 2000; Zielinski, 2002) .

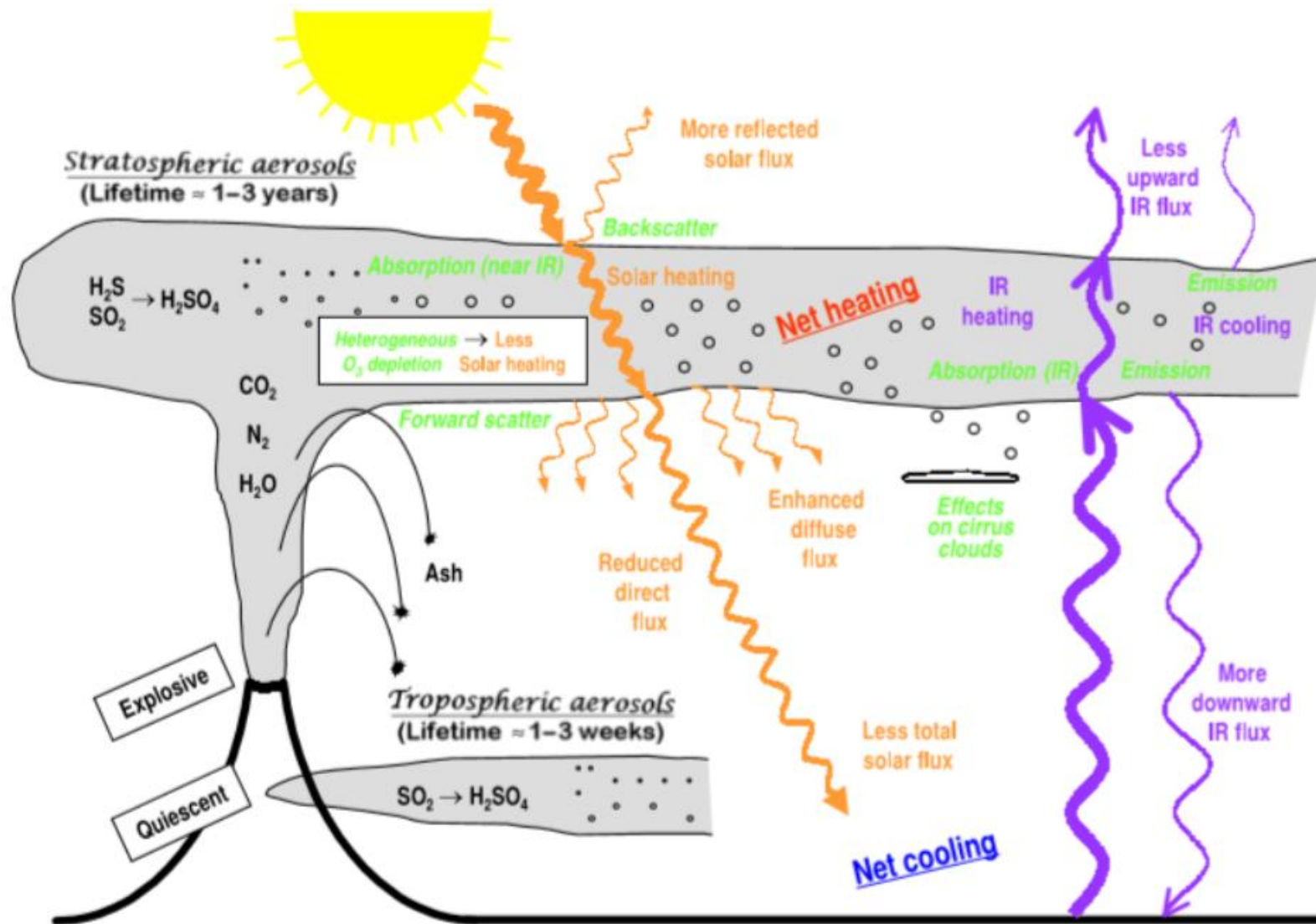


Figure 1: Overview of the volcanic inputs to the atmosphere and their effects. Particles emitted into the troposphere falls out quickly, while stratospheric injections will stay aloft for longer time. (Robock, 2000)

2.3.1. How big quantities are needed?

The total amount of sulfate aerosols produced after an eruption is important for whether the climate will be impacted or not. The question is *how much sulfur is needed?*

The optical depth (τ) determines how much light penetrates the atmosphere and hence it is the determining parameter on how much sulfur is needed in order to have an impact on the climate. An increasing optical depth value means that less solar radiation is reaching the Earth's surface.

Stothers (1996) investigated a series of volcanic eruptions and concluded that an optical depth of about 0.1 seems to have a cooling effect on the Earth's surface. The peak global aerosol loading of the stratosphere can be calculated using Eq. 4.

$$M_D = 1.5 \times 10^{14} \tau_D \text{ g} \quad 4$$

where M_D is total H_2SO_4 loading (Stothers, 1984). Hence, the H_2SO_4 mass needed in order to a cooling effect is

$$M_D = 1.5 \times 10^{14} \times 0.1 \text{ g} = 1.5 \times 10^{13} \text{ g}$$

which corresponds to approx. 10 megatons (Mt).

However, the mass of H_2SO_4 produced in the stratosphere is approx. double the mass of emitted SO_2 . On top of that, the mass of the total H_2SO_4 aerosol loading is 1.25 times the mass of the produced H_2SO_4 . Using a 75% H_2SO_4 and 25% H_2O aerosol ratio and a time series of volcanic SO_2 over 25 years, Zielinski (2002) calculated that an eruption needs to inject at least 1 to 5 Mt of SO_2 into the stratosphere in order for the eruption to be big enough to have a climatic effect.

2.4. Determining the size of an eruption

In order to estimate the size of an eruption, a classification is needed. Eruptions are typically indicated after a combination of how fine the ejected materials are and how far they are spread or on the base of the ejected material's volume or the height of the ejection column. The latter is referred to as the volcanic explosivity index (VEI) (Holm, 2012).

The VEI is a relative scale and is based on geological and historical sources of the ejected material and is very useful since it can both be used on present eruptions investigated by scientists and on eruptions that occurred several thousand years ago. The scale ranges from 0 to 8 with 0 being the smallest eruption and 8 the biggest. The amount of deposition increases with a factor ten for each step. For an eruption to possibly reach into the stratosphere, the VEI 3 is needed. For a VEI 4 or higher, the stratospheric injection is definite or significant (Table 2) (Newhall and Self, 1982). However, history shows that even though the VEI states that stratospheric injection is significant, it is not necessarily so. The AD 1980 Mt. St. Helens eruption was classified as a VEI 5, but the stratospheric impact was insignificant due to its low sulfur content (Zielinski, 2002)

Table 2: The VEI classification (Newhall and Self, 1982)

VEI	0	1	2	3	4	5	6	7	8
Description	Non-explosive	Small	Moderate	Mod-large	Large	Very large	Very large	Very large	Very large
Ejected vol. (m ³)	<10 ⁴	10 ⁴ -10 ⁶	10 ⁶ -10 ⁷	10 ⁷ -10 ⁸	10 ⁸ -10 ⁹	10 ⁹ -10 ¹⁰	10 ¹⁰ -10 ¹¹	10 ¹¹ -10 ¹²	>10 ¹²
Stratospheric injection	None	None	None	Possible	Definite	Significant	Significant	Significant	significant

2.5. The climatic effects of eruptions

When sulfuric acid is formed in the stratosphere, it initiates an immediate effect which will continue until it precipitates out of the atmosphere. Equatorial eruptions can affect the global climate while eruptions occurring in mid- to high latitudes will mainly impact the hemispheres, they occur in. Many models agree that tropical eruptions large enough to impact the climate cause a net surface cooling for 2 to 3 years (Zielinski, 2002), however, Sigl *et al.* (2015) found, using dendrochronology, that the temperature anomalies might span for a longer period of time than the models show. Even though a net cooling is observed, regional differences such as winter warming may also happen (Robock, 2000). This pattern was observed after the June AD 1991 Mt. Pinatubo eruption where satellite measurements revealed that in July, August, and September the same year, the Earth's albedo had increased. In August AD 1991, the aerosols had produced a forcing of -2.4 W/m², in August AD 1992 the forcing was -3 W/m² and in August AD 1993 it was approx. -1 W/m² which resulted in the largest tropospheric temperature anomaly of -0.5°C in AD 1992 (McCormick, Thomason and Trepte, 1995; Zielinski, 2002). However, the net cooling was not uniformly distributed, instead, an overall winter warming pattern was observed in the AD 1991-1992 winter; conversely an overall summer cooling was measured in the AD 1992 summer (Kirchner *et al.*,

1999). Further back in time, the AD 1815 Tambora caused “*the year without summer*” where the global temperature anomaly is estimated to have been between -0.4°C and -0.7°C (Cooper *et al.*, 2018).

The warming of the stratosphere caused by the aerosol cloud results in an enhanced temperature gradient between the tropics and the poles which is particularly strong during winter. A stronger gradient produces a stronger jet stream in the Northern Hemisphere (NH) which causes an egregious stationary wave pattern in the troposphere. The stronger NH jet stream correlates with an enhanced positive North Atlantic Oscillation (NAO) index which produces stronger westerlies and contrary the cooling effect causes a winter warming of Europe. Furthermore, the stronger jet stream also causes warm winter anomalies over Asia and North America; the Middle East adversely experiences cooling (Stenchikov *et al.*, 1998; Kirchner *et al.*, 1999; Robock, 2000). Robock and Mao (1992) examined the 12 largest eruptions from 1883-1992 and found that for tropical eruptions, the pattern is seen in the first winter following, for midlatitudes in the first or second and for high latitudes in the second winter.

The halogens, e.g. Cl, Br and F, depletes the stratospheric ozone. The ozone layer absorbs UV and thermal infrared radiation and depletion of the layer can thus result in further cooling of the surface acting like an amplifier of the cooling caused by the sulfate aerosols (Cadoux *et al.*, 2015; Baldini, Brown and Mawdsley, 2018).

On millennial timescales, very large hemispheric eruptions might, apart from cooling their own hemisphere, also warm the opposing due to temperature asymmetry between the two hemispheres. Baldini, Brown and McElwaine (2015) found that a large Southern Hemispheric (SH) eruption could trigger Dansgaard-Oeschger (DO) events and an Antarctic cooling by a northward shifting ITCZ which also displaces the Hadley cells to the north. A northward shifting Hadley cell circulation will force the NH polar front to higher latitudes causing an abrupt warming promoting collapse of the sea ice and retreat of continental ice sheets which are characteristic for DO events. A large NH eruption would conversely cool the NH relative to the SH, shift the ITCZ to the south and compressing the polar cell in the SH which shifts the SH polar front further south causing Antarctic warming.

3. Ice cores

As the sulfate aerosols reach the polar latitudes, they will eventually drop out of the stratosphere into the troposphere where they will be removed from the atmosphere by precipitation or by dry fall-out. If precipitated on a glacier, the snow and thus also the aerosols will accumulate. Due to the accumulating snow, old snow will metamorphose into firn which with further overlying accumulation will increase in density due to the pockets of air in between the crystals are reduced by mechanical packing and plastic deformation. At a density of approx. 0.83 kg m^{-3} , the air pockets are completely sealed off and exists as individual air bubbles which is when it is considered to be ice (Figure 2). The depth of which the firn is turned into ice varies considerably depending on the temperature and precipitation rate which also influence resolution.

High accumulation rates show great details within a short time scale and annual layers can be recognized; additionally, seasonal physical and chemical properties are distinguishable. On the other hand, ice sheets in areas with low accumulation rates show fewer details but span a longer

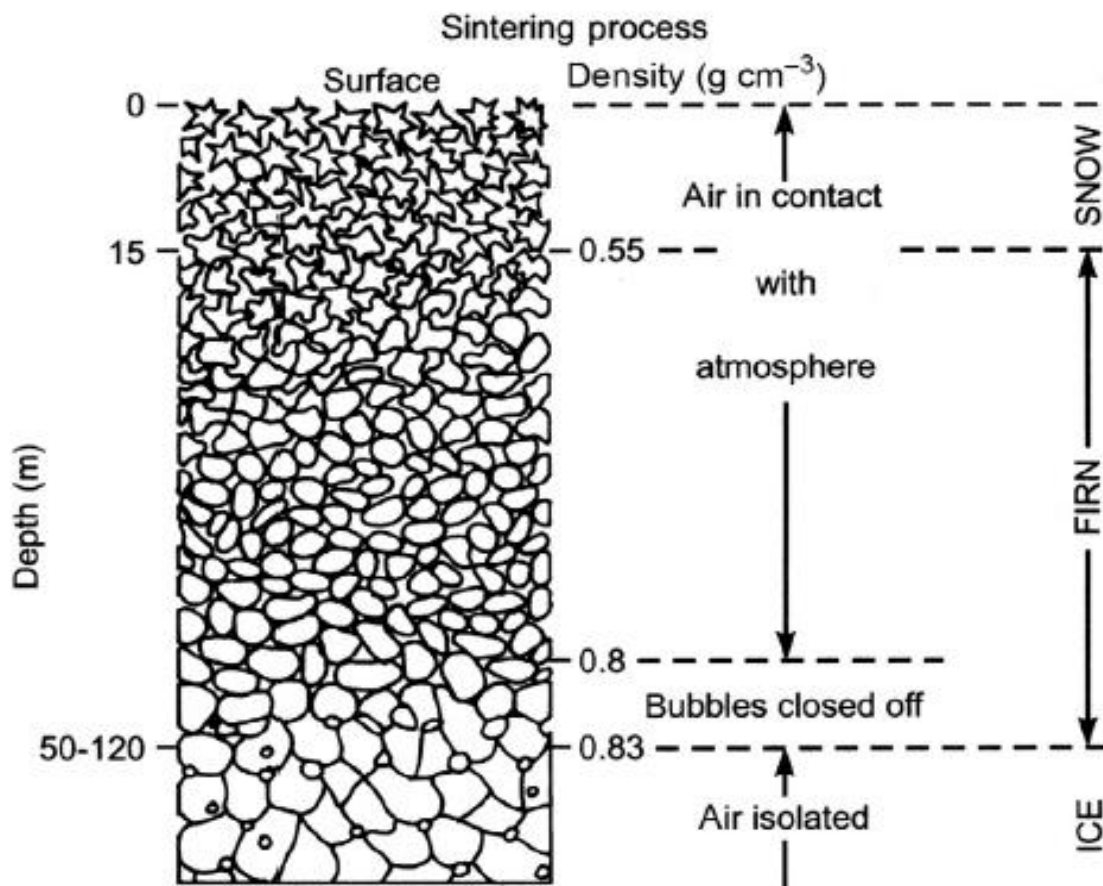


Figure 2: Illustration of how air is trapped due to compaction of snow to ice. The depth varies depending on the temperature and accumulation rate. (Bradley, 2015)

time scale. Overall, Antarctica falls under the latter with low accumulation rate and thus, ice-cores drilled there will generally show fewer details, while Greenland overall belongs to the former with higher accumulation. However, geographical variability also exists within Antarctica and Greenland with the maritime Antarctic and Southern Greenland experiencing higher accumulation rates than inland Antarctica and Northern Greenland.

Another property to consider is the thinning of the ice. As the glacier grows, its own weight deforms the ice. Due to ice flows, the deeper down in the ice, the more thinning of layers occur, and thus, the older the ice, the more layer thinning should be accounted for (Alley, 2000; Bradley, 2015).

3.1. Ice cores in this project

For this project, data from three Greenland and three Antarctic ice cores is analyzed.

3.1.1. Greenland ice cores

3.1.1.1. *GISP2 (Greenland Ice Sheet Project 2)*

The GISP2 ice core is a 3054.55-meter-long core located at $72^{\circ}6'N$ $38^{\circ}5'W$ close to Summit (Figure 3). Drilling began in 1988 and ended five years later July 1st, 1993 when the bottom of the ice was reached (The University of Maine, no date; Alley *et al.*, 1997).

3.1.1.2. *NEEM (North Greenland Eemian Ice Drilling)*

The NEEM ice core is a 2537.36-meter-long ice core located at $77^{\circ}45'N$ $51^{\circ}06'W$ (Figure 3). Drilling began in 2009 and one year later July 27th, 2010, when the bottom of the ice was reached (University of Copenhagen, no date b, no date a)

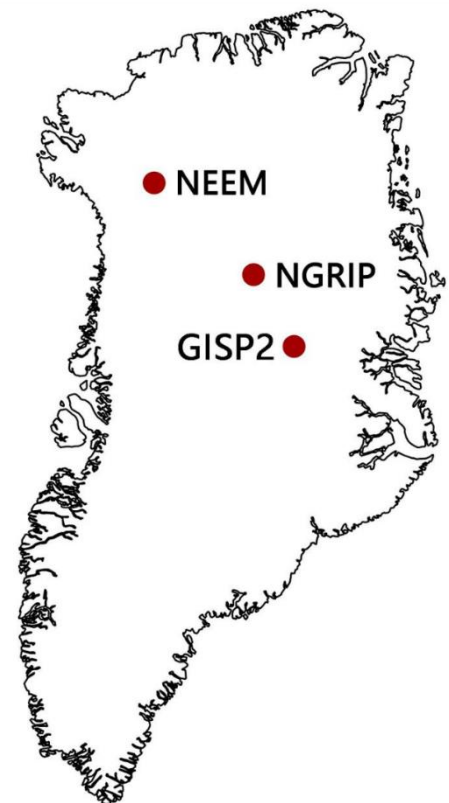


Figure 3: Location of the studied sites in Greenland

3.1.1.3. NGRIP (North Greenland Ice Core Project)

The NGRIP ice core is a 1755-meter-long ice core located at 75°1'N 42°3'W (Figure 3). Drilling began in 1996 and lasted until 2004 when the bottom of the ice was reached (University of Copenhagen, no date b; Svensson et al., 2005)

3.1.2. Antarctic ice cores

3.1.2.1. EDC (EPICA Dome C)

The EDC ice core project is located at 75°06'S 123°21'E which ended drilling on December 21st, 2004 at a depth of 3270.2 m (Figure 4)(European Science Foundation, no date).

3.1.2.2. EDML (EPICA Dronning Maud Land)

The EDML ice core project is located at 75°00'S 00°04'E which ended drilling on January 17th, 2006 at a depth of 2774.15 m (Figure 4) (European Science Foundation, no date)

3.1.2.3. WD (West Antarctic Ice Sheet Device)

The WD ice core project is located at 79°28'S 112°05'W. Drilling began in 2006 and ended in 2013 in a depth of 3405 m (Figure 4) (Fitzpatrick *et al.*, 2014)

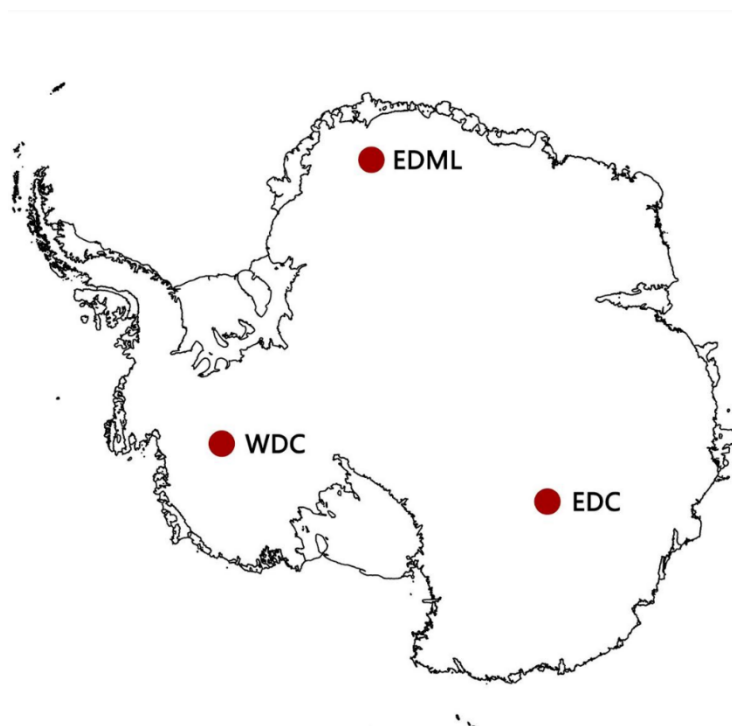


Figure 4: Location of the studied sites in Antarctica

4. Methods

4.1. Reproduction of data from Sigl, M., et al., (2013)

In order to validate the volcanic sulfate flux calculations on present data, data and methods from Sigl *et al.*, (2013) on the WAIS divide (WD) and NEEM ice cores was used. Furthermore, methods using Matlab to extract the volcanic eruption signals from the non-sea-salt sulfur (nssS) signal were replicated. The methods are as follows:

1. The nssS-signals are converted into an annually averaged time series.
2. To avoid not-a-number holes in the data, the nssS-signals are interpolated where holes in the dataset occur.

3. To estimate an average of the natural occurring background, a 31-year running median (RM) filter is applied (Eq. 5).

$$RM_i = \text{median}(x_i - n, \dots, x_i + n) \quad (5)$$

where x_i is the sulfate concentration at point i , and n is the width of the window. Since the median value is not affected by larger peaks, this is preferred rather than the mean value.

4. As a good measure of variability in the data in the presence of volcanic signals and long-term changes in the background signal, the median of absolute deviation (MAD) is applied. Matlab has an inbuilt median of absolute deviation function which has been used.

If the threshold value (y) in Eq. 6 is exceeded, peaks are detected

$$y = z \times MAD_i + RM_i \quad (6)$$

where z is factor that adjusts the threshold value. In this case, $z = 3$ is used.

5. To avoid that the volcanic signals having an influence on the RM and 3xMAD-filters, the signals exceeding the 3xMAD threshold are excluded applying a reduced running median (RRM) filter and hereafter, a 3xMAD filter (calculated in the same ways as Eq. 5 and 6 respectively) is applied using the RRM again assuming that the signals exceeding the threshold are volcanic.
6. Finally, the volcanic signals are integrated, and the start and end year of the eruption and the total sulfur which is converted into sulfate are listed. Sulfur weighs approx. 32 g mol^{-1} while sulfate approx. weighs 96 g mol^{-1} thus being a factor three more heavy. Conversion from sulfur to sulfate thus applies by multiplying with 3.

See Appendix A.1. for an example of the Matlab scrips.

A list of total sulfate deposition (kg/km^2) from volcanic eruptions is made for both the NEEM and WAIS ice cores and the results are compared to the results presented in the Sigl *et al.* (2013) paper. In order to check if the replication data agree with Sigl *et al.* (2013), the two data sets are plotted together in a scatter diagram with Sigl *et al.* (2013) data on the x-axis and the replicated data on the y-axis (Appendix B.1.), hence the more linearity the plot shows, the closer the data are together. Regression analysis on both NEEM and WAIS shows that the R^2 value is 0.9192 and 0.9264 respectively; the WAIS reproduction is thus slightly better than the NEEM. Since the same methods

have been applied, the R^2 -value idealistically should equal one. Though, the same methods have been used, slight deviations may occur. Sigl *et al.* (2013) uses a manual equation from Traufetter *et al.* (2004) to calculate the median of absolute deviation while the automatic MAD-function in Matlab has been applied during the replication. Hence, the result is influenced by this and might be an explanation of why the data does not agree completely. Also, Sigl *et al.* (2013) states that they “*applied a 31 year running median (RM) filter on the annually averaged nssS time series*”, but does not show how data has been annually averaged. Thus, different approaches in doing that could also contribute to the slight deviations.

Even though the replication does not agree 100%, the R^2 -values are both > 0.9 and the methods accepted, and the same approach will be used on the present data from the Greenland and Antarctic ice cores

4.2. Modifications used on present data

By default, the methods used in the replication of the (Sigl *et al.*, 2013) are applied on the data from the GISP2, NGRIP, NEEM, EDC, EDML and WD ice cores. However, due to differences in data, modifications have been necessary to apply to get the best fit.

The data resolution in the cores differs from core to core. The two Greenland cores, GISP2 and NEEM, are low-resolution while the remaining Greenland core, NGRIP, and the three Antarctic cores, EDML, EDC and WD have higher resolution. Tests have revealed that different running medians are needed on the different resolutions in order to get the best result. Different attempts have shown that the best running median (and reduced running median) fit best with a running median of 181 years on the GISP2 and NEEM cores, while 91 years have been used in the remaining cores (Figure 5, Figure 6) except NGRIP. To be able to detect DO-events, the window width is lowered to 51 years. Furthermore, the resolution in GISP2 and NEEM is too low to convert the sulfate signal into an annual averages times series. Instead, the raw, integrated sulfate signal is used in the data processing.

Data from the replication covers the last 2500 years on the WAIS divide core and the last 2000 years on the NEEM core where the climate has not experienced any big fluctuations, and thus the background signal is relatively steady. The present data the methods are applied on, spans approx. 50000 years (12000-60000 b2k) and the signals show that the background fluctuations are big in cold periods and small in warm periods. Hence, using a variable MAD instead of a set MAD allows

for more eruption detections in the warmer periods and thus smaller bipolar eruptions will also be detected in these periods. Conversely, a variable MAD also excludes big fluctuations in the cold periods, thus not detecting them as eruptions. A variable MAD is calculated using same window width as used calculating the RM/RRM

The raw data is in all cores but WD given in sulfate with WD given in sulfur. Thus, only WD needs to be adjusted to sulfate using the same approach as previously described.

Furthermore, Sigl *et al.* (2013) is only using data from the upper part of the ice cores, thus layer thinning is insignificant. Data presented here originates from the deeper parts of the core, and layer thinning needs to be accounted for (thinning correction references are found in Table 3).

Additionally, a water eq. depth correction needs to be applied too (Eq. 7)

$$y_i = \frac{SO4_{\text{uncorrected},i}}{z_i} \times w \quad (7)$$

where z_i is the thinning correction at point i , and w is the water eq. correction.

Example of Matlab scripts for high-resolution core (EDML) and a low-resolution core (NEEM) can be found in Appendix A.2. and Appendix A.3. respectively. The applied criteria and data references for the reproduction of Sigl *et al.* (2013) and the present data are found in Table 3

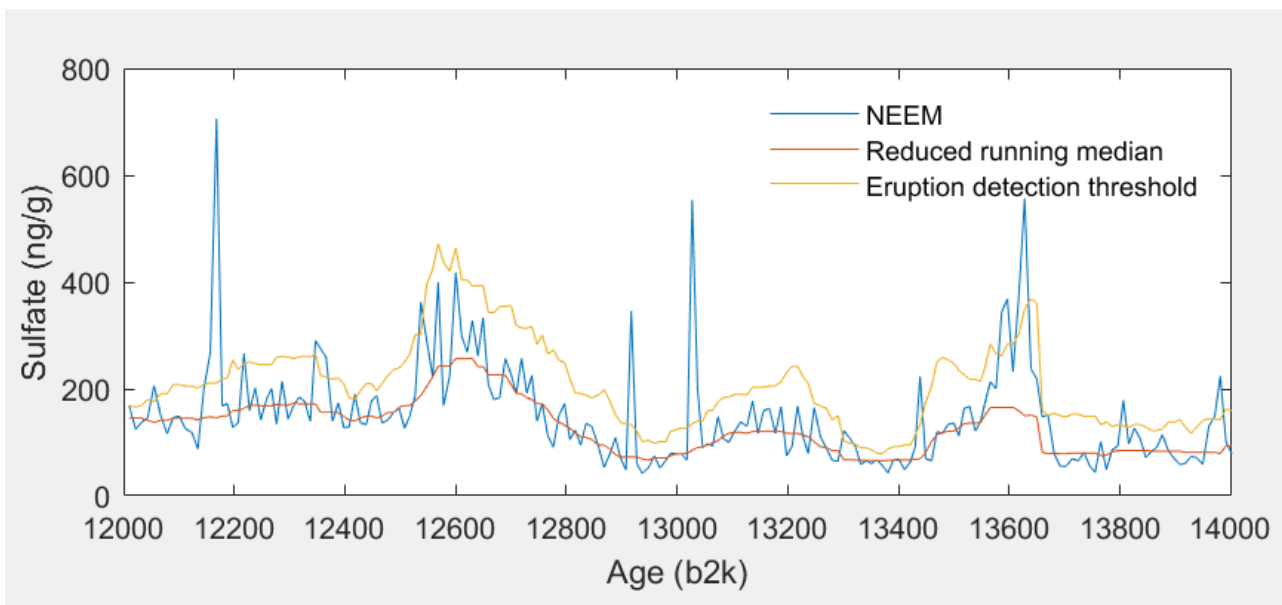


Figure 5: Sulfate record from the low-resolution NEEM ice core, Greenland, spanning 12000 b2k – 14000 b2k. The red line is the reduced running median while the yellow is the eruption detection threshold both with a window width of 181 years.

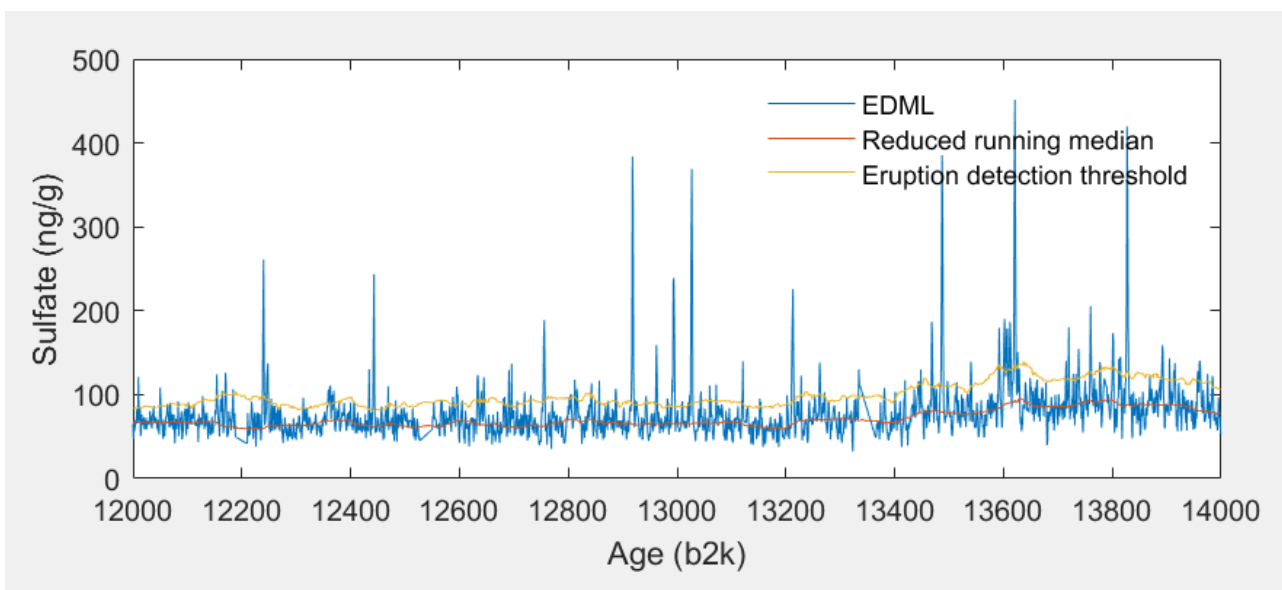


Figure 6: Sulfate record from the high-resolution EDML core, Antarctica, spanning 12000 b2k – 14000 b2k. The red line is the reduced running median while the yellow is the eruption detection threshold, both with a window width of 91 years.

Table 3: The ice cores and the applied criteria and the data references

Core	Years	S or SO4 record	Background window length*	MAD window length**	Size of MAD	Thinning function ref.
NGRIP	12000-60000 b2k	SO4 (Bigler, 2004)	51 years Best fit and width possible to catch DO events	51 years To follow the background	3X Same method used by Sigl et al., (2013). Good fit applied on the variable MAD	(Johnsen <i>et al.</i> , 2001)
NEEM	12000-60000 b2k	SO4 (Schüpbach <i>et al.</i> , 2018)	181 years Best fit on low resolution	181 years To follow the background	3X Same method used by Sigl et al., (2013). Good fit applied on the variable MAD	(Rasmussen <i>et al.</i> , 2013)
GISP2	12000-60000 b2k	SO4 (Mayewski <i>et al.</i> , 1997)	181 years Best fit on low resolution	181 years To follow the background	3X Same method used by Sigl et al., (2013). Good fit applied on the variable MAD	No thinning corrections yet exist. As a substitute, thinning corrections from the nearby GRIP core are used. (Johnsen <i>et al.</i> , 2001)
WD/WDC	12000-60000 b2k	S, but converted into SO4 in the volcano list (multiplying S with 3) (Fudge <i>et al.</i> , 2013)	91 years Best fit	91 years To follow the background	3X Same method used by Sigl et al., (2013). Good fit applied on the variable MAD	(Fudge <i>et al.</i> , 2016)
EDML	12000-60000 b2k	SO4 (Severi <i>et al.</i> , 2007)	91 years Best fit	91 years To follow the background	3X Same method used by Sigl et al.,	(Bazin <i>et al.</i> , 2013; Veres <i>et al.</i> , 2013)

					(2013). Good fit applied on the variable MAD	
EDC	12000-60000 b2k	SO4 (Severi <i>et al.</i> , 2007)	91 years Best fit	91 years To follow the background	3X Same method used by Sigl <i>et al.</i> , (2013). Good fit applied on the variable MAD	(Bazin <i>et al.</i> , 2013; Veres <i>et al.</i> , 2013)
NEEM (Sigl <i>et al.</i> , 2013)	78-1997AC	NssS, but converted into SO4 in the volcano list (multiplying S with 3)	31 years Following Sigl's methods	Set MAD Following Sigl's methods	3X Following Sigl's methods	-
WAIS (Sigl <i>et al.</i> , 2013)	408BC-2007AC	NssS, but converted into SO4 in the volcano list (multiplying S with 3)	31 years Following Sigl's methods	Set MAD Following Sigl's methods	3X Following Sigl's methods	-
*Calculation	$RM_i = \text{median}(x_i - n, \dots, x_i + n)$ Where i=sulfate and n = the width of the window					
** Calculation	SK used to mad-function is Matlab to calculate the MAD					

5. Results

Figure 5 and Figure 6 show sulfate concentration (blue line), the reduced running median (red line) and the eruption detection threshold (yellow line) in NEEM and EDML respectively spanning 12000-14000 b2k. If the sulfate concentration exceeds the eruption detection threshold, the origin is most likely from a volcano and thus registered as an eruption. The records also reveal that the background signal increases at the onset of colder periods where it shows bigger fluctuations compared to the warmer periods where the sulfate background signal decreases and the fluctuations are smaller. A signal like that clearly shows in the Greenland sulfate records at approx. 14700 b2k which coincides with an increase in NGRIP $\delta^{18}\text{O}$ (Andersen *et al.*, 2004) (Figure 7) that marks the termination of the warmer Greenland Interstadial 1 (GI-1) (Svensson *et al.*, 2020). Additionally, the records also reveal that the Greenland sites in general show increased amounts of sulfate compared to the Antarctic sites. This can be explained by Greenland on average receives

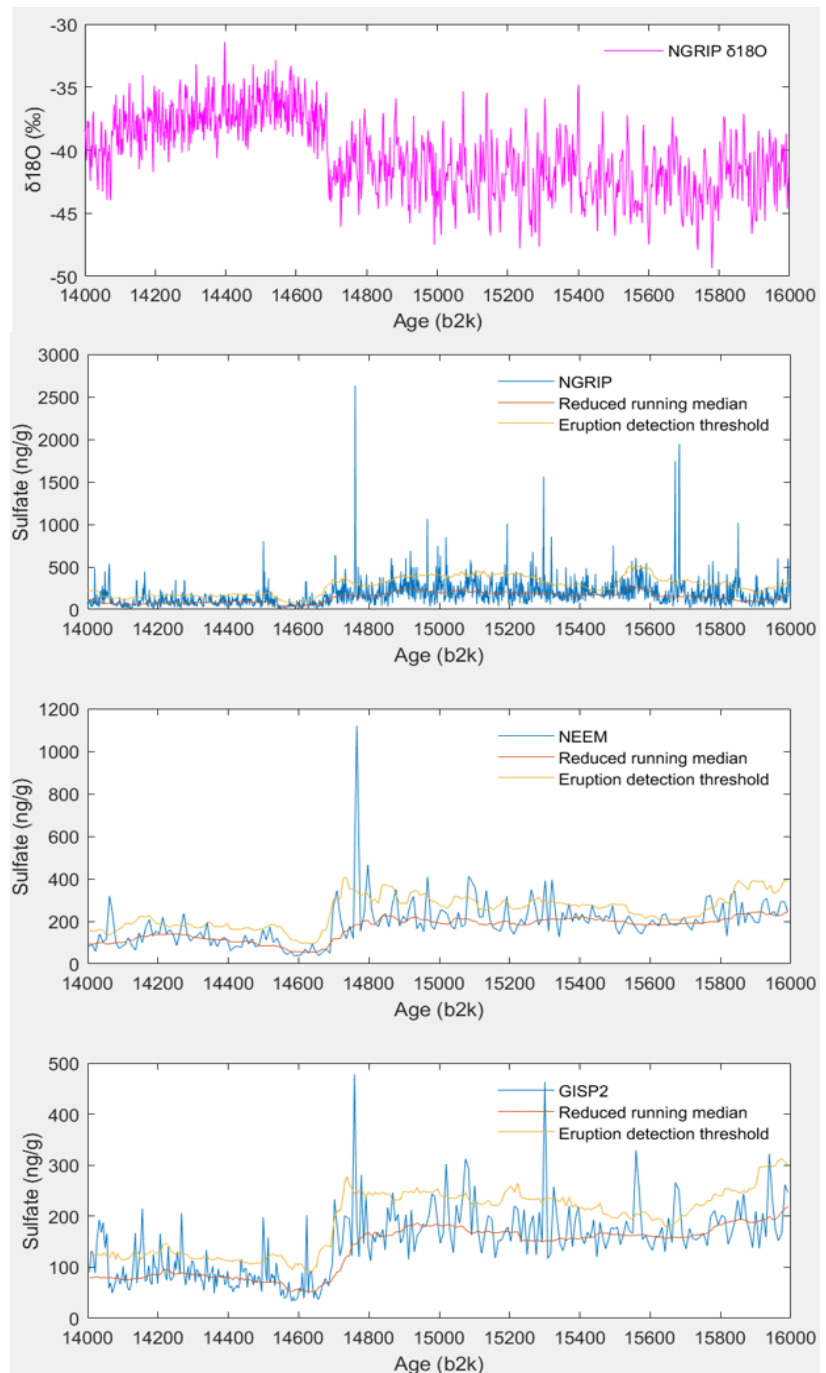


Figure 7: The Greenland sulfate records spanning 14000-16000 b2k. A change in the sulfate background signal is clearly visible at approx. 14700 b2k which coincides with the onset of GI 2.1 seen in the $\delta^{18}\text{O}$ records.

more precipitation than Antarctica (Matsuura Kenji & National Center for Atmospheric Research Staff (Eds), 2020). Additionally, peaks occurring at the same time in both the Greenland and the Antarctic records such as the 13027 b2k peak are registered as being bipolar. Sulfate records for all six cores spanning the whole 12000-60000 b2k period are found in Appendix B.2. (Figure 30 to Figure 53).

5.1. Bipolar eruptions

This study investigates bipolar eruptions synchronized by Svensson *et al.* (2020). A table of all the registered eruptions is found in Appendix A.4. and A.5. for Greenland and Antarctica, respectively. Figure 8 shows the average of the NH eruptions (blue) and SH eruptions (red, negative scale). A dashed green line marks the Tambora, 1815 CE, sulfate deposition found by Sigl *et al.* (2013) and later refined by Sigl *et al.* (2015) on Greenland and Antarctica respectively. Plots marked with an x-head marks eruptions which simultaneously exceeds the Tambora threshold on Greenland and Antarctica. Tambora has been chosen as a reference point due to the fact that it is the biggest eruption (VEI 7) in recent history (Robock, 2000; Sigl *et al.*, 2015). It is noteworthy that, even though an eruption shows high sulfate values in one of the hemispheres, it is not necessarily so in the opposing hemisphere. The NAAZ II eruption (55383 b2k) shows such a clear signal with a vast Greenland signal and an almost non-existent Antarctic signal. Hence, an eruption like that is likely not to have had a global Tambora-like impact. Instead, the 45555 b2k eruption, which shows the second biggest global average sulfate deposition (after NAAZ II), also shows large signals in both hemispheres and the global impact is more likely to have been Tambora-like or bigger. The same applies to e.g. the 25460 b2k, 29678 b2k and 52302 b2k which by far exceeds the Tambora thresholds on both hemispheres (Figure 8 and Appendix A.7.)

A trend towards Greenland eruptions being bigger is visible in Figure 8. The trend is visualized in Figure 9 which shows a histogram of the average hemispheric sulfate deposition values distributed in bars with a bin width of 10 SO₄ (kg/km²). It is evident that both hemispheres show many smaller eruptions and that the bigger the eruptions are less frequent. However, Antarctic records reveal that the frequency of eruptions between 0 and 90 SO₄ (kg/km²) is approx. >50% bigger than the Greenland frequency for the same size distribution. Greenland furthermore shows more bigger eruptions; while the biggest eruption in Antarctica is 301 SO₄ (kg/km²), Greenland has 11 eruptions surpassing that value (Appendix A.7.). Greenland also reveals a rare eruption that is almost off the charts – the NAAZ II (55383 b2k) eruption with 1283.99 SO₄ (kg/km²). Second to that in

Greenland, is the 45555 b2k eruption which, while the histogram reveals the rarity of it, only is about half the size ($685.39 \text{ SO}_4 \text{ (kg/km}^2\text{)}$).

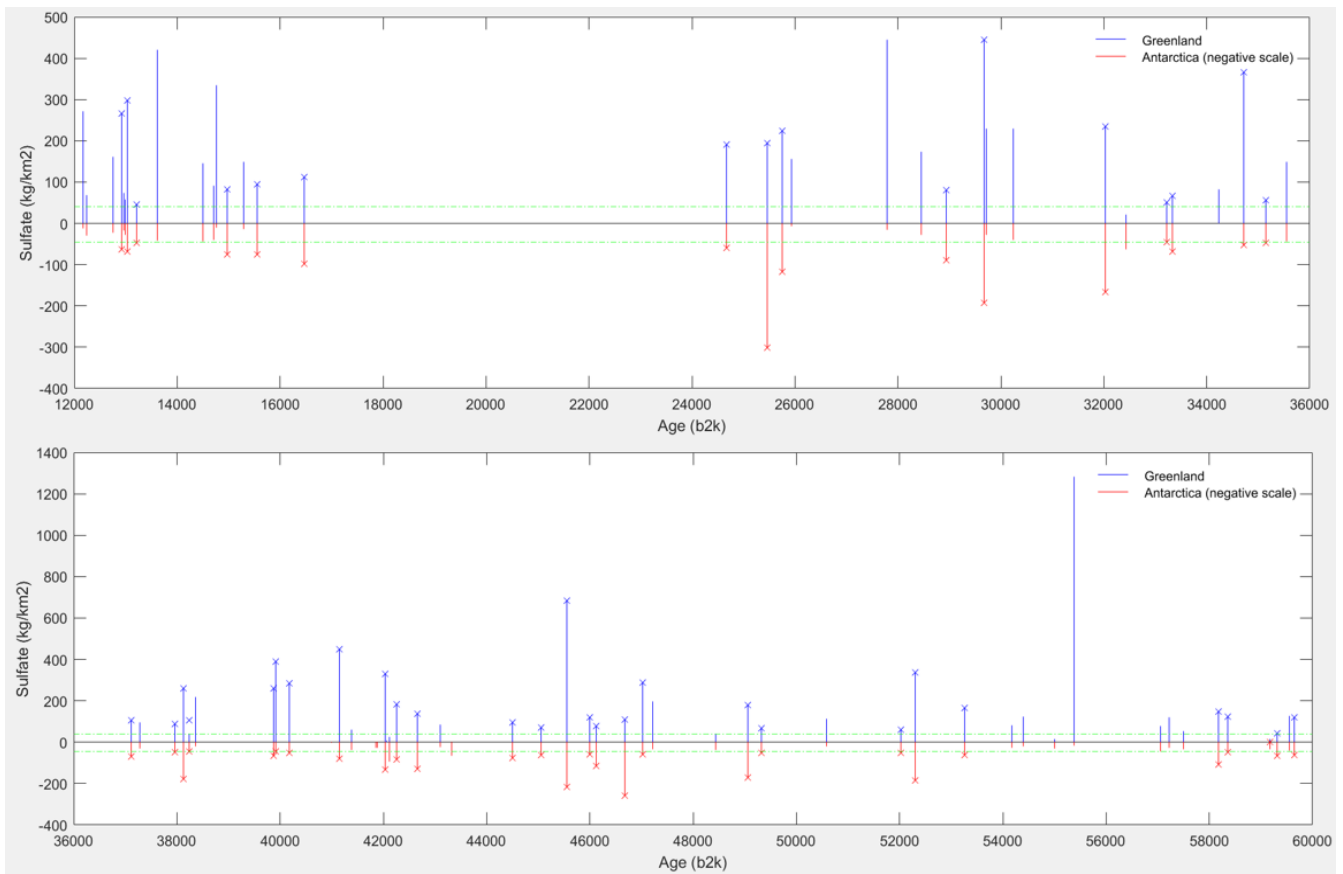


Figure 8: All registered bipolar eruptions from 12000 b2k to 60000 b2k. Blue shows the average of NH bipolar eruption, red shows the average of the SH bipolar eruptions. Dashed green line is SO_4 -values (Sigl et al., (2015)) from Tambora, 1815 CE eruption. Bipolar eruptions simultaneously exceeding the Tambora threshold are marked with an x. The lag of registered eruptions between 16500 and 24500 b2k is due to missing synchronization between Greenland and Antarctica.

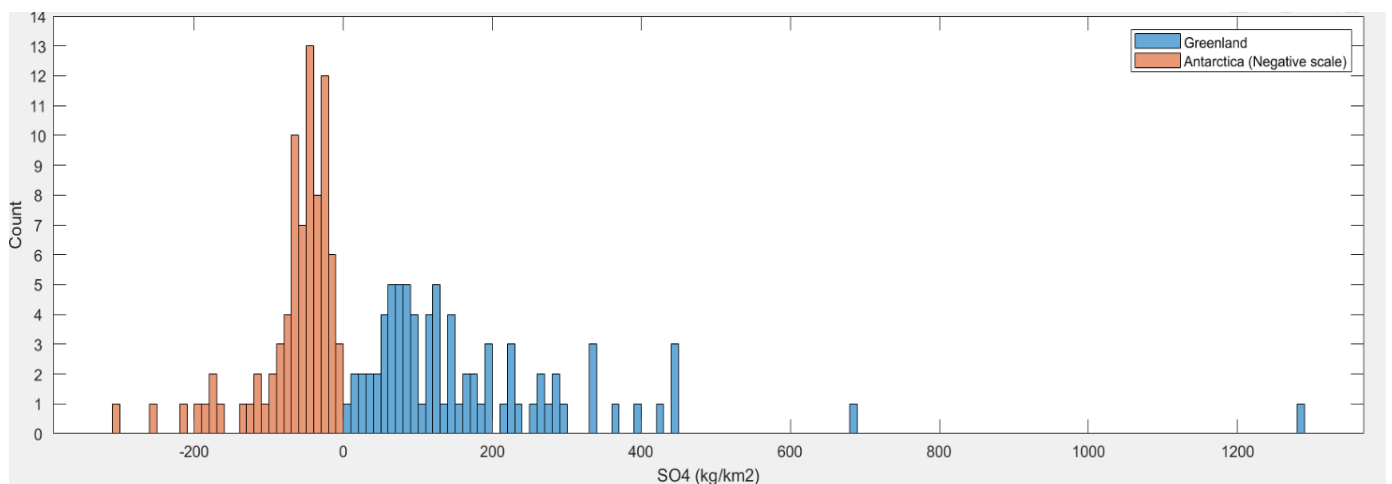


Figure 9: Histogram of the hemispheric sulfate deposition averages from glacial bipolar eruptions with a bin width of 10 kg/km^2 . NH values are in blue and SH values are in orange (negative scale).

5.2. Sulfate concentration vs. latitude

In order to check whether or not there is a trend in the amount of deposited sulfate and latitudinal origin of eruption, latitudes from 19 known historical (last 2500 years) and last glacial (12000-60000 b2k) eruptions (Lavigne *et al.*, 2013; Sigl *et al.*, 2013, 2015; Giaccio *et al.*, 2017; Guillou *et al.*, 2019; Svensson *et al.*, 2020) have been plotted against the difference between Greenland sulfate and Antarctic sulfate (Figure 10). Latitudes are found using Smithsonian Institute's volcano database (Smithsonian Institution, National Museum Of Natural History, no date). The NAAZ II eruption (Icelandic origin, 1267.38 SO₄ (kg/km²) difference) has been excluded from the plot to better show the sizes of the other eruptions. If a trend exists, the NH eruptions should plot positive sulfate values and SH eruptions negative and hence, latitudinal bands origin can be applied to eruptions which origin is unknown. Figure 10 reveals that such an overall trend is current, and not only can the eruptions be divided into which hemisphere they originate. A further tropics category is visible too. Dividing the latitude axis into NH (>30°N), tropical (30°N-30°S) and SH (>30°S), further shows that the NH and SH eruptions are >±100 SO₄ (kg/km²) difference while the tropical

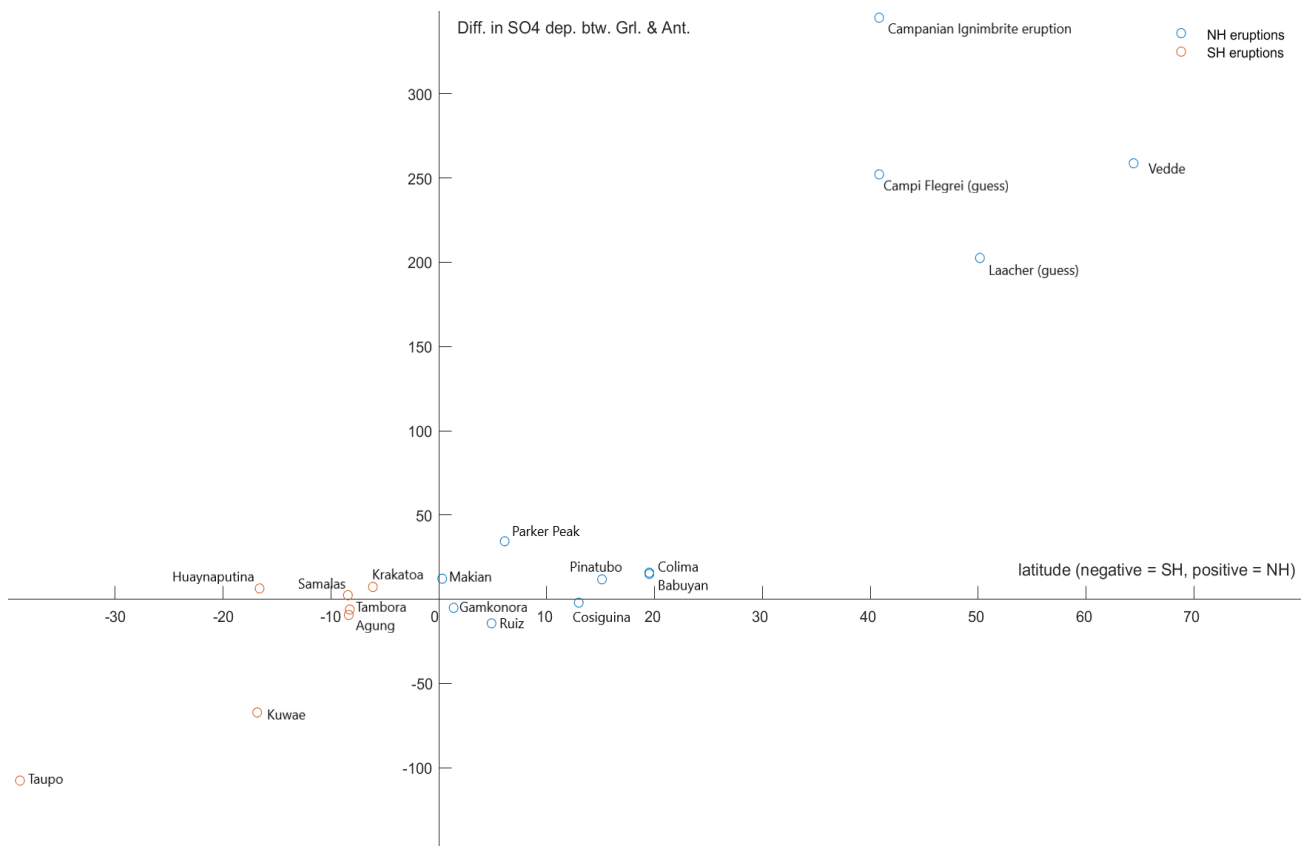


Figure 10: Scatterplot of the known origins of historical (last 2500 years) and glacial (12000-60000 b2k) eruptions. Two of the eruptions (Laacher and Campi Flegrei) are probable locations. The NAAZ II eruption has been excluded to make the size of the other eruptions more visible.

eruptions are $<\pm 100$ SO₄ (kg/km²) difference. For sulfate deposition values, ages (b2k and AD/BC) and references for the used eruptions, see Appendix A.6.

6. Discussion

The sulfate records (Appendix B.2.) show plenty of volcanic peaks through the last glacial with some being more distinct than others. Among the most distinct peaks are the three biggest eruptions on global average scale – the 55383 b2k NAAZ II eruption (Appendix B.2, Figure 51), the 45555 b2k eruption (Appendix B.2, Figure 46) and the 29678 b2k eruption (Appendix B.2, Figure 38). However, while all three of them on average are the biggest ones on global scale, the peaks show different fluctuations in the cores. The NAAZ II eruption is very distinct in all three Greenland cores while it in the three Antarctic cores barely is noticeable. Second to the NAAZ II eruptions is the 45555 b2k eruption which shows a very distinct peak in all cores except EDC. In the bipolar eruption list with global averages (Appendix A.7.), this is also the eruption that shows largest sulfate deposition values in both hemispheres that both exceed the Tambora threshold with a large margin. Since both hemispheric sulfate deposition values surpass this margin, the eruption is likely to have been one of the most globally impactful during the last glacial. The 29678 b2k is the fourth biggest eruption of global average which shows three very distinct peaks in the Antarctic cores. The Greenland signal is less prominent; however, the signals are still distinguishable from the background.

6.1. Data resolution and window width

The resolution of the data is different from ice core to ice core. The two Greenland cores (NEEM and GISP2) are the two with the lowest resolutions which is also clearly visible when comparing the sulfate plots (Figure 11). The resolution influences how many eruptions are being detected by the threshold. In the higher resolution cores, more eruptions are registered while the lower resolution cores show fewer. As an example, in NEEM, 297 eruptions have been registered throughout the 48000 years, while NGRIP has 2680 eruptions registered in the same period. This is among others because of the higher resolution capturing more detailed sulfate variations and thus, the risk of not capturing a sulfate fluctuation that is big enough to surpass the eruptions threshold is smaller. Choosing the window width of the RM/RRM and the detection threshold, was done by trying and finding the best fit. For the two low-resolution cores, the best fit was decided to be a window width of 181 years while the high-resolution cores had the best fit with a width of 91 years. To be able to

detect possible eruption-induced DO-events, the window width on the Greenland NGRIP core was lowered to 51 years. Slight variations in the applied window width, can have implications in registering eruptions. The low-resolution data is especially sensible to that. Hence, even though the 181 years were chosen as the best fit, wrong detections might show up. An example of this can be seen in the GISP2-plot at 38232 b2k (Figure 43,

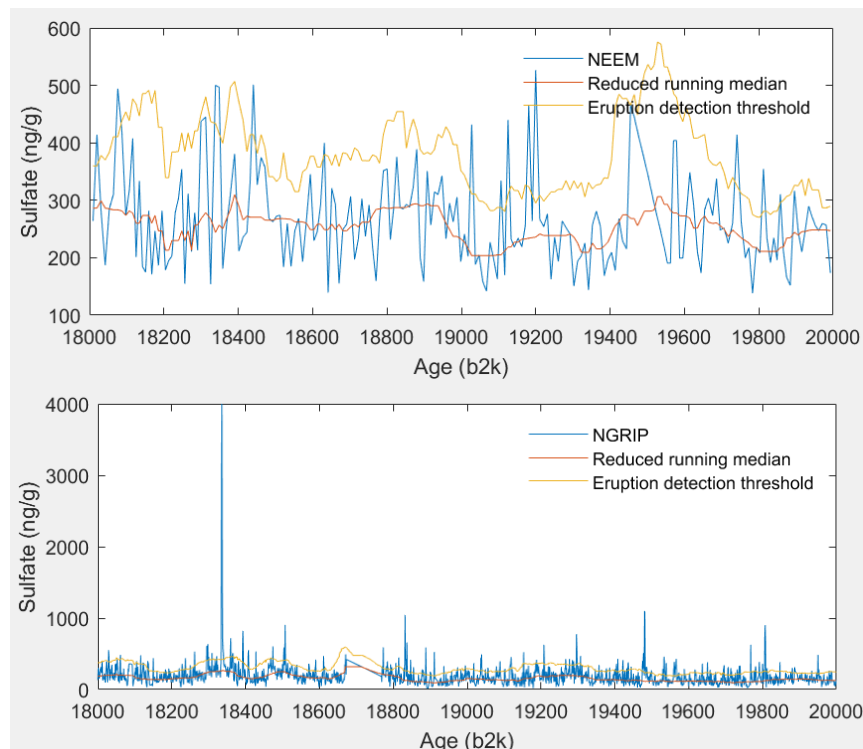


Figure 11: Record showing the Greenland cores NEEM and NGRIP. The blue curve is the sulfate concentration, the red is the reducing running median and the yellow is the eruption detection threshold. NEEM has low resolution while NGRIP has high resolution.

Appendix B.2. . The period marks the termination of GS-9 (Svensson *et al.*, 2020) and the background changes from high values to lower values. The low resolution makes the change in sulfate background very abrupt; a change that the long window width has troubles following, and thus, an eruption is registered. However, the registered eruption might not be an eruption at all; instead, it is likely that it is the background changing too fast. One could argue that a different window width could have helped in this case, however, it would likely have resulted in problems in other places. Furthermore, the thinning data also have implicated the eruption deposition results. Especially the thinning data used on WD can have caused implications in the outcome. Two different datasets have been used, and below approx. 2800 m, the resolution in the thinning data is lower than above, hence difference in the applied thinning correction within the same core exist.

Furthermore, the low resolution in the NEEM and GISP2 ice cores also impacts the amount of registered sulfate values. With fewer data points, only small changes in the background and eruptions threshold are needed in order to alter the sulfate values. Hence, this can affect the outcome, and especially when using the ice core sulfate values to calculate the hemispheric values. Thus, using averages in the data might not be the most precise, but as sulfate is the only factor to be used in the quantification of the bipolar eruptions, calculating and using an average from the three

Greenland and Antarctic cores has been necessary. Additionally, the low resolution also adds to the uncertainty in terms of the eruption age. While uncertainty in the higher resolution cores is about ± 5 years, it increases to about ± 10 years in the cores with the low resolution.

6.2. Size of glacial eruptions compared to historical

In recent history, the Tambora 1815 CE eruption is the biggest occurring eruption and according to Sigl *et al.* (2015) it is the eruption within the last 2500 years that produced the biggest cooling in Europe/Arctic and the sixth biggest global forcing. In sulfate deposition values, during the last 2500 years, only four eruptions have simultaneously surpassed the Tambora values on each hemisphere (Figure 12). The glacial period looked at in the project spans 48000 years, hence approx. 20 times the length and by directly upscaling the frequency of eruptions bigger than Tambora, around 80 such eruptions should be expected. An examination of the glacial eruption frequency that simultaneously exceeds Tambora reveals 43 such eruptions (Figure 8), thus about half the amount that would be expected. However, excluding the gap of 8000 years with no synchronized bipolar eruptions (16500-24000 b2k) in the frequency upscaling, the amount of expected bipolar eruptions bigger than Tambora decreases to 64. Hence, even though the gap is excluded from the calculations, the last glacial show a lower frequency, but with bigger deposition values. I should however also be noted that Svensson *et al.* (2020) in finding the bipolar eruptions have focused on periods with abrupt climate changes and thus, not all occurring bipolar eruptions during the last glacial are accounted for. A more comprehensive synchronization will with great certainty reveal more bipolar eruptions and hence, the actual frequency of Tambora-sized bipolar eruptions will reach closer to the direct upscaled number. Comparing the size and frequency of glacial bipolar eruptions with

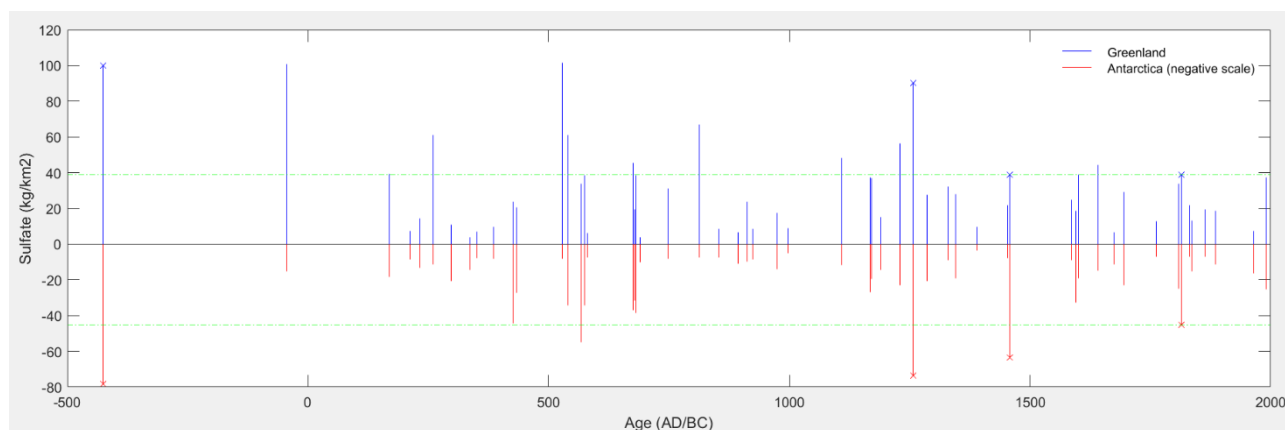


Figure 12: Sulfate deposition values for bipolar eruptions throughout the last 2500 years (Sigl *et al.*, (2013, 2015)). The blue stems are Greenland, the red is Antarctica (negative scale). The dashed green line is the Tambora sulfate deposition value on each hemisphere. The eruption that on both hemispheres simultaneously exceed Tambora is marked with an x.

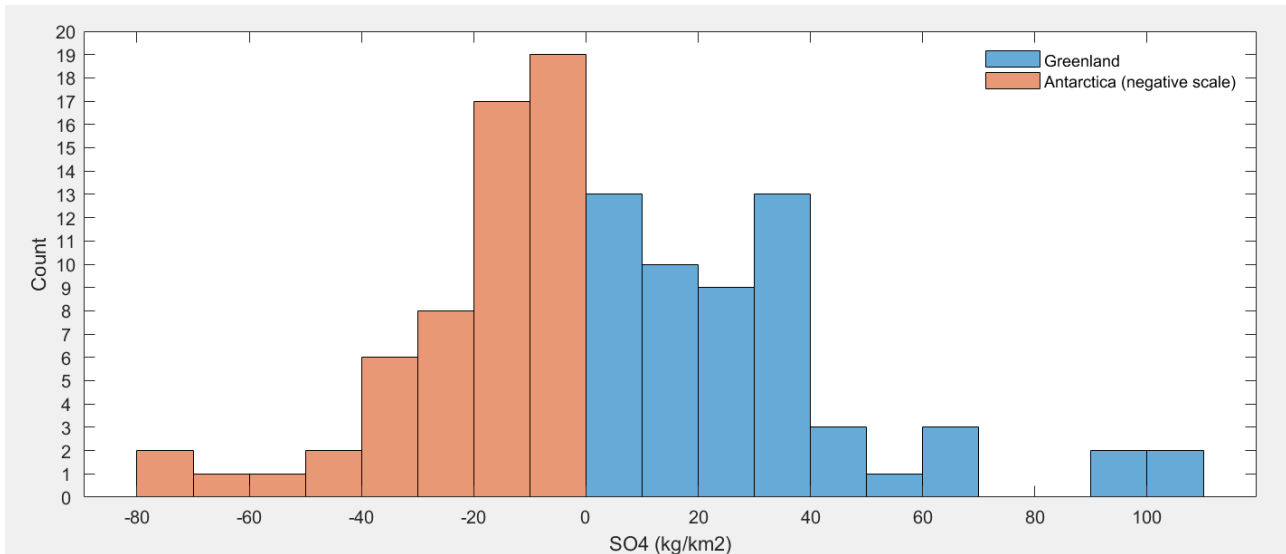


Figure 13: Histogram of bipolar eruptions during the last 2500 years (Sigl *et al.*, 2013, 2015) with a bin width of 10 kg/km². Blue is Greenland eruptions and orange (negative scale) is Antarctic eruptions.

bipolar eruptions during the last 2500 years (Sigl *et al.*, 2013, 2015), further reveals a glacial with eruptions with bigger sulfate deposition values. While the last 2500 years do not show eruptions bigger than between 100 and 110 kg/km² on the NH and between 70 and 80 kg/km² on the SH (Figure 13) the glacial has several eruptions above those values. So, while the direct upscaling of eruptions that simultaneously exceed Tambora is bigger than what is found, the last glacial conversely shows more and bigger sulfate deposition values than the last 2500 years that only exceeds the Tambora limit on one of the hemispheres.

The Tambora 1815 CE eruptions was a VEI 7 (Robock, 2000) and thus, accepting a direct upscaling of frequency, the last glacial period, should, in terms of VEI 7 eruptions be half as active as expected. Checking for even bigger eruptions, the VEI 8 Taupo eruption at 25460 b2k is used using the same approach as for Tambora. An examination of data shows, that this eruption has an average of 193.78 SO₄ (kg/km²) in Greenland and 301.41 SO₄ (kg/km²) in Antarctica (Appendix A.4. and A.5. . Figure 14 reveals, that while 22 eruptions exceed the Taupo value in Greenland, no such eruptions exists in the Antarctic records. Thus, no eruptions during last glacial show values that on both hemispheres simultaneously surpass Taupo in size. Hence, using the Taupo sulfate deposition as a threshold for a VEI 8 eruption shows that Taupo was the only eruption of that size to occur during the last glacial. This fits well with the Taupo eruption being the second biggest eruption in terms of erupted volume during the last 100000 years only surpassed by the 74000 years Toba super eruption (Wilson, 2001). However, approaching it in a different way by looking at the global averages and hemispheric sulfate values together, it could be argued that five eruptions (29678 b2k,

41144 b2k, 45555 b2k, 52302 b2k and 55383 b2k (NAAZ II)) are bigger than Taupo and thus five VEI 8 eruptions could potentially have occurred. Though, including the hemispheric values in the calculation, 41144 b2k and the NAAZ II eruptions show small sulfate values in the Antarctic records, while the eruptions heavily influence the Greenland cores with the latter increasing the global averages to exceed Taupo. The big difference in hemispheric values and vast Greenland values indicate that these eruptions are of NH origin, and while they might have been VEI 8 eruptions, their global impact probably have not been as big as Taupo's, even though Taupo is hemispheric eruption too. Guillou *et al.* (2019) findings of NAAZ II being of Icelandic origin is also in agreement with that. The vast sulfate deposition values could conversely also be explained by the proximal location to Greenland. Under the right atmospheric circulation patterns, huge amounts of sulfate can have been transported from Iceland to Greenland, and thus making the eruption occurring bigger than it is. The same argument can be applied to the other eruptions that shows huge sulfate deposition values on one hemisphere only. Sigl *et al.* (2015) also lists two Icelandic eruptions occurring over the last 2500 years (Laki and Eldgja). Here, the same pattern with great Greenland sulfate deposition is visible too. The three remaining eruptions (29678 b2k, 45555 b2k and 52302 b2k) also show bigger Greenland values than Taupo does; the Antarctic values are smaller than Taupo in all three cases. However, while being smaller than Taupo on Antarctica, the three eruptions show much greater values than the 41444 b2k and NAAZ II eruptions, hence it could be argued that they have been bigger than those. The 45555 b2k stands out from the three eruptions. The sulfate deposition is second and third most in Greenland and Antarctica respectively and the global average exceeds the Taupo eruptions with approx. a factor 1.8. With Taupo being an SH eruption, the Antarctic deposition is naturally larger there, however, the difference in Antarctic deposition between the two eruptions is much smaller than the difference between the two eruptions in the Greenland deposition. Hence, while it based on the 45555 b2k Greenland deposition can be argued that this is a NH eruption, the overall picture is an eruption that probably could have exceeded Taupo in size and impact. It should here be noted, that the deposition value for Taupo in the EDC core has been manually discarded due to an unrealistically small value compared to the other Antarctic cores (approx. 8 kg/km² compared to 263 kg/km² and 339 kg/km² in EDML and WD respectively) Including the registered EDC value would lower the Antarctic deposition with approx. 100 kg/km². The changes in the Antarctic values would thus also alter the global average lowering it to approx. 198 kg/km² which puts the Taupo eruption further down on the global average list.

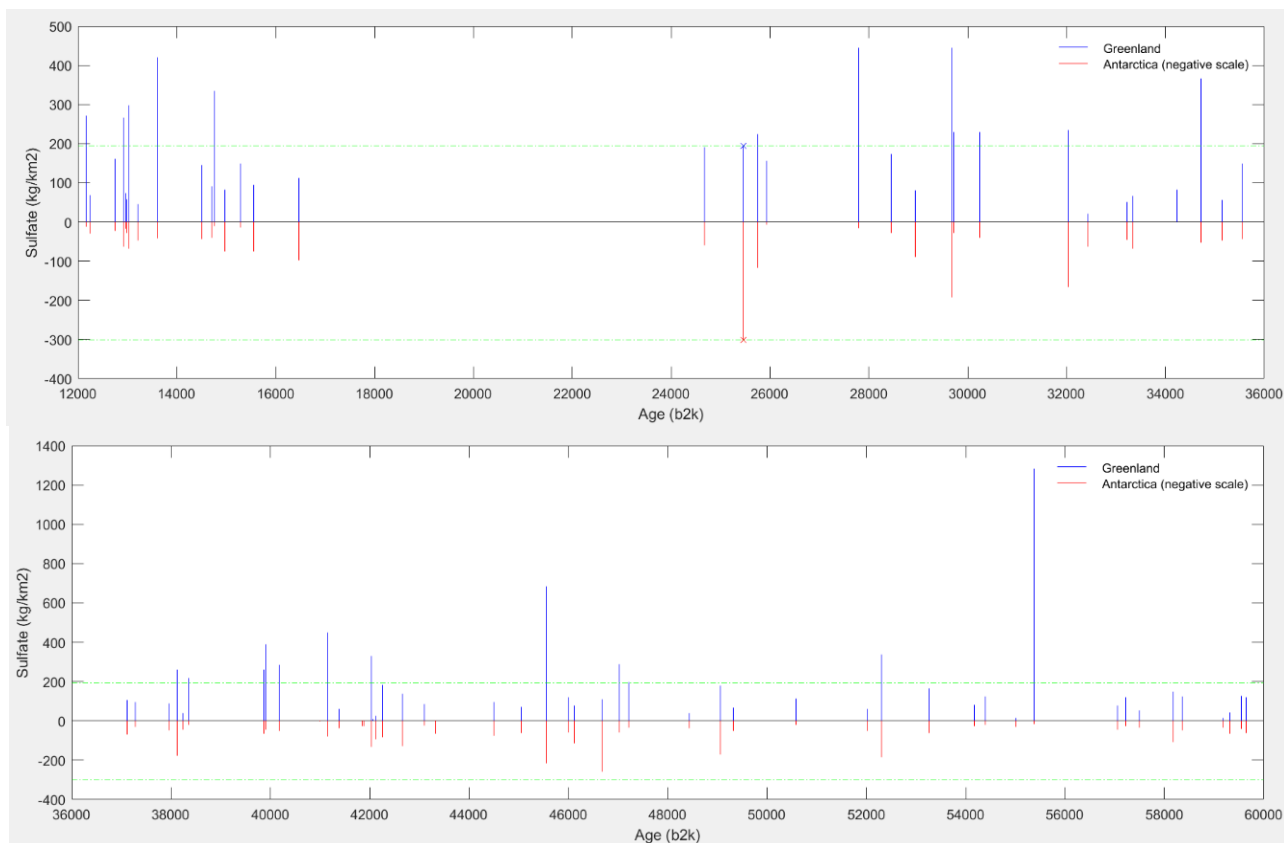


Figure 14: Stem diagram of bipolar eruptions compared to the size of the 25460 b2k Taupo eruption spanning 12000-60000 b2k. The blue marks Greenland sulfate values, the red marks Antarctic sulfate values (negative scale) and the dashed green line marks the Taupo threshold on each hemisphere. The eruptions that on both hemispheres simultaneously exceed Taupo is marked with an x.

6.2.1. Sulfate concentration during the glacial and last 2500 years

A comparison of the sulfate concentration between the glacial and the last 2500 years, reveals that both the background levels and eruptions show higher values in the glacial. In Greenland, the present-day sulfate mainly comes from marine biogenic and non-eruptive volcanic emissions with terrestrial sources being very small, while the Antarctic sources are mainly marine and biogenic (Legrand, 1997; Schüpbach *et al.*, 2018). Legrand (1997) backs up that the glacial levels are higher than the modern values. As Table 4 shows, the average background sulfate (nssS) levels in Summit, Greenland lies in the hundreds, while it during Holocene has dropped below 30 ng/g (excluding the uncertainty). Hence, during cold periods, the sulfate content in the ice increases. During the glacial, the marine and biogenic sources in the NH are likely depressed why the sulfate content should then decrease and not increase. However, the increase in sulfate coincides with a remarkably similar increase in dust concentrations which is represented by the calcium records (Figure 15). It is

suggested that the increased sulfate signal in the glacial is caused by enhanced terrestrial sources from e.g. direct gypsum emissions (Legrand, 1997).

Table 4: Average background levels of sulfate (nssS) in Summit (Legrand, 1997).

Depth (m)	Age (kyr)	SO ₄ ²⁻ (nssS) (ng/g)
0 – 1450	0 – 9	27 ± 10
1450 – 1617	9 – 11.5	55 ± 19
1628 – 1673	11.7 – 12.9	108 ± 55
1683 – 1750	13.1 – 14.4	78 ± 37
1800 – 2000	15.0 – 25.0	243 ± 84
2000 – 2585	25.0 – 72.5	146 ± 99
2585 – 2740	72.5 – 100.0	54 ± 31

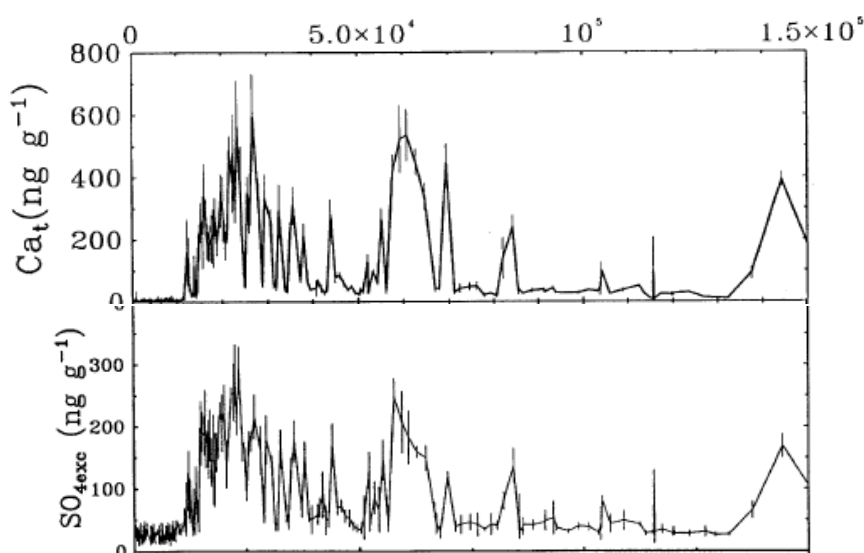


Figure 15: Calcium and sulfate (nssS) records from the GRIP core, Greenland (Legrand, 1997).

Schüpbach *et al.* (2018) has further applied an aerosol transport model in which the loss of aerosols from the source to the ice is controlled by the precipitation. Using the changes in precipitation patterns could thus also explain the increase in sulfate concentration during the glacial. With higher aridity during cold stages, besides the increased terrestrial source, the atmospheric residence time in the atmosphere would increase due to less precipitation. The more arid conditions during the glacial could thus also be a reason why the volcanic eruptions also show increased amounts of sulfate in the glacial compared to eruptions during the last 2500 years found by Sigl *et al.* (2013, 2015). Furthermore, the more arid conditions could also explain the increased volcanic signals. With less precipitation, the volcanic stratospheric fallout would accumulate in less snow, hence increasing the

concentration. This also applies to the interstadials, but with opposite sign where the decrease in concentration could be explained by an increase in snow accumulation. Additionally, changes in the atmospheric circulation could also have an impact on the deposition patterns. Since the dust and sulfate concentration show great coincidence, changes in the wind patterns that brings dust to the ice sheet might also explain the increase in sulfate. However, some models show that while the jet stream might have split in two around the Laurentide Ice Sheet during the last glacial maximum, the changes in general wind speed have been insignificant (Schüpbach *et al.*, 2018).

6.3. Latitudinal origin

By plotting the latitude for known and speculated origin of eruptions for both historical and glacial, against the difference in sulfate deposition between the two hemispheres, Figure 10 revealed that the eruptions can be divided into three categories. NH eruptions ($>30^{\circ}\text{N}$) which all show a difference deposition value greater than 100 kg/km^2 , tropical eruptions ($30^{\circ}\text{N} - 30^{\circ}\text{S}$) which all show a difference deposition value lower than 100 kg/km^2 and bigger than -100 kg/km^2 and SH eruptions ($>30^{\circ}\text{S}$) which show a difference deposition value $<-100 \text{ kg/km}^2$. The data is highly influenced by NH and tropical eruptions which show the clear trend. The SH is unfortunately only represented by the Taupo eruption which naturally brings uncertainties into the plot. However, only looking at the NH and tropical eruptions, none of them exceed the above listed limits and accepting that the SH hemisphere is following the same pattern, a band of latitudinal origin can be applied to the unknown eruptions. Appendix A.8. shows the glacial bipolar eruptions sorted high to low after the difference in sulfate deposition between Greenland and Antarctica. Like the data in Figure 10, the glacial shows a clear overweight of NH and tropical eruptions with only two occurring in the SH. Table 5 shows the amount of NH, tropical and SH eruptions during the last glacial which also includes the eruptions of known and suspected origin used to create Figure 10. Hence one of the two occurring SH eruptions is the Taupo eruption. Thus, following this, only Taupo and one other SH bipolar eruption has occurred during the last glacial. A reason for this overweight in NH and tropical eruptions could probably be due to the distribution of Earth's landmasses and volcanic zones where both the NH and tropics have more landmass and more volcanoes than the SH. The only landmasses with volcanoes on latitudes lower than 30°S are New Zealand, the southern part of South America and Antarctica (Figure 16) (Decker and Decker, 2020) and hence, the likelihood of an eruption being detected on both the NH and the SH is smaller compared to that of a NH or tropical eruption.

Table 5: Number of glacial bipolar eruptions pr. latitudinal band.

Latitudinal band origin		
NH eruptions(>30°N)	Tropical eruptions (30°N - 30°S)	SH eruptions (>30°S)
35	45	2

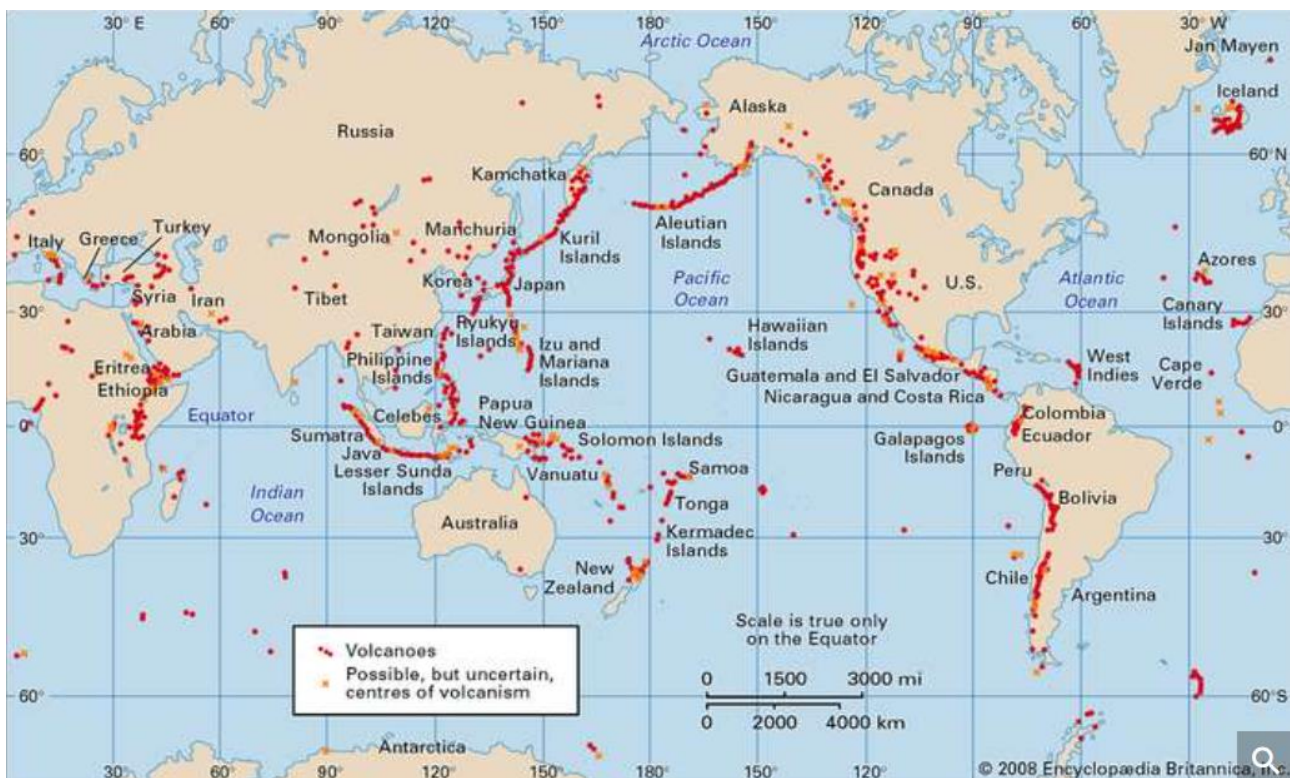


Figure 16: Earth and its volcanoes. Most landmasses and volcanoes are situated in the tropics and the NH. (Decker and Decker, 2020)

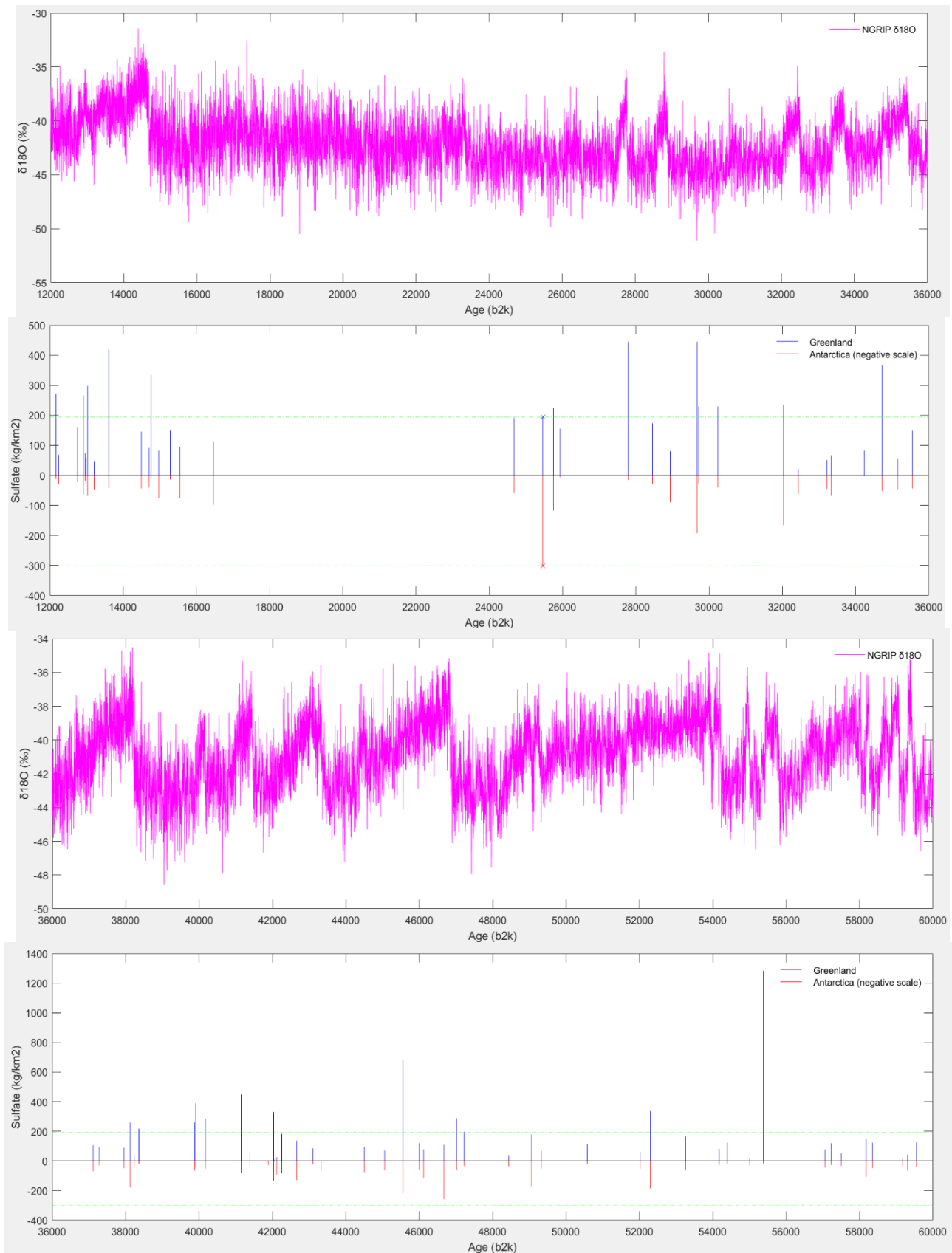


Figure 17: The glacial bipolar eruptions (Greenland blue, Antarctica red (negative scale) and the Taupo limit on each hemisphere (dashed horizontal line) plotted with $\delta^{18}\text{O}$ from NGRIP (magenta). The $\delta^{18}\text{O}$ shows fluctuations in temperature during the glacial.

6.4. The $\delta^{18}\text{O}$ -temperature relationship

If the eruptions coincide with a cooling, the relationship between $\delta^{18}\text{O}$ and temperature can be used in order to estimate the resulted change in temperature. The connection is unfortunately not straight forward and different papers give different relationship values. The relationship is e.g. determined by the precipitation rates, and thus various ice cores show differences in the relationship which on longer timescales also means that modern day values are not the same as the glacial values.

Furthermore, the glacial also shows great climate variability (the DO-events). Thus, it is difficult to determine a perfect

relationship (Johnsen *et al.*,

2001; Guillevic *et al.*,

2013; Kindler *et al.*, 2014).

Using the NGRIP ice core,

Kindler *et al.* (2014) has

reconstructed the

temperature from 10 to 120

kyr b2k hence covering the

period investigated in this

paper. Figure 18 shows the

relationship between $\delta^{18}\text{O}$

and the temperature during

the last glacial and reveals

that the $\delta^{18}\text{O}$ -temperature

relationship has a mean value of $0.52 \text{ ‰ } ^\circ\text{C}^{-1}$. However, the mean annual temperature is not the

only factor of which the relationship is dependent on. The changes in seasonal precipitation also has

an influence which further adds to the complexity.

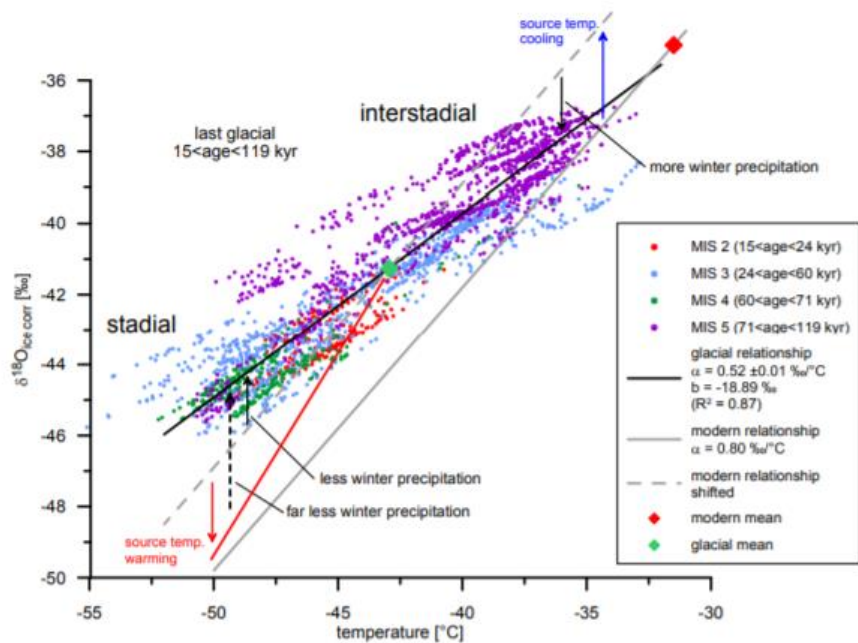


Figure 18: The relationship between the $\delta^{18}\text{O}$ and the temperature during the glacial. The data is color-coded depending on the state of the climatic background (MIS). The relationship for the glacial is represented by the black regression line, and the modern-day relationship is represented by the grey line (Kindler *et al.*, 2014).

6.5. Bipolar eruptions and climatic changes

To see if there is any link between the glacial bipolar eruptions and the temperature, the registered eruptions are plotted with the NGRIP $\delta^{18}\text{O}$ which works as temperature proxy for Greenland

(Figure 17). The NGRIP $\delta^{18}\text{O}$ shows clear variations with more than 10 visible DO-events.

However, the timescale is too long in order to see a more detailed picture, and it does not reveal if

any of the eruptions have resulted in any coolings. To check whether some of the eruptions coincide

with a long-term cooling or short-lived masked cooling, the five big eruptions that have been mentioned in section 6.2 (29678 b2k, 41144 b2k, 45555 b2k, 52302 b2k and 55383 b2k (NAAZ II)) are looked at in more detail. The resolution in the NGRIP ice core is 2 - 5 years which means that apart from long-term climatic changes, possible short-term changes theoretically could be visible in the records.

6.5.1. The 29678 b2k eruption (Campi Flegrei)

According to Albert *et al.* (2019), the eruption produced a widespread $> 150,000 \text{ km}^2$ volcanic ash layer in the Mediterranean. Their model suggests a volume of approx. 16 km^3 . The dispersion area and the volume indicate an VEI 6 eruption. Hence the likelihood of stratospheric injection is significant (Newhall and Self, 1982). Additionally, looking only at the sulfate deposition values, the eruption exceeds the VEI 8 Taupo eruption which indicates an eruption bigger than VEI 6. With significant injection, the eruption should have the ability to impact climate and with it being a NH eruption, a possible climatic impact could be seen as a cooling in Greenland. Figure 19 reveals that the $\delta^{18}\text{O}$ does not indicate a cooling following the eruption. Instead, the records show that the eruption happened close to a $\delta^{18}\text{O}$ minimum at 29586 b2k. Hereafter, the $\delta^{18}\text{O}$ increases quickly, where the eruption happens approx. in the mist of the warming.

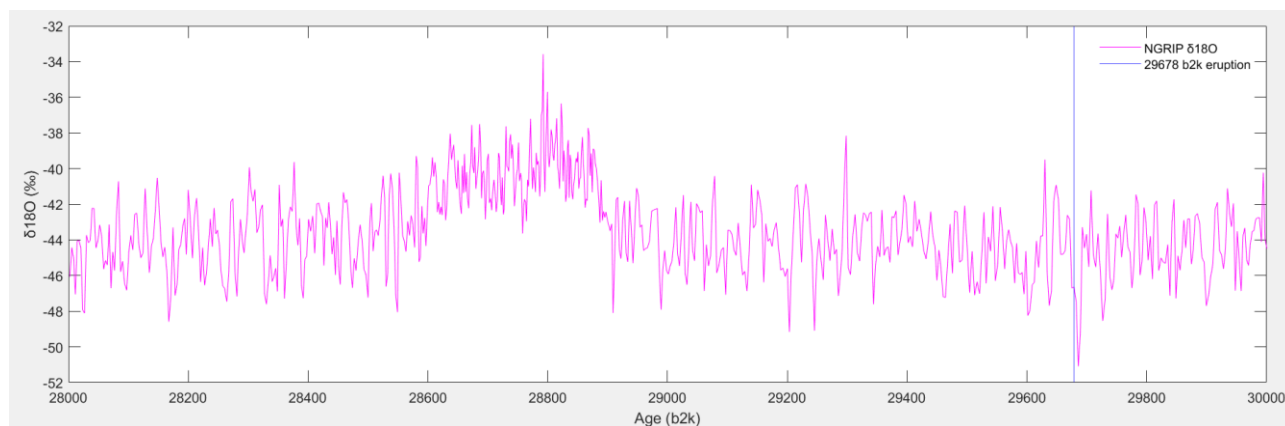


Figure 19: NGRIP $\delta^{18}\text{O}$ variations (magenta) spanning 28000 - 30000 b2k. The 29678 b2k eruption is represented by the blue, vertical line.

6.5.2. The 41444 b2k eruption

Unfortunately, no known origin of this eruption is available and only the sulfate deposition values can indicate the size of the eruption. As for the possible Campi Flegrei eruption, the average global sulfate deposition value exceeds the Taupo values and hence, the eruption might be close to that in size. However, it is noticeable that the Greenland sulfate deposition value is much bigger than the Antarctic value, and thus, the eruption is likely to be of NH origin and perhaps, as is the case with NAAZ II, the eruption can appear bigger due to a geographical position close to Greenland. Figure 20 reveals that the eruption occurs just as the Greenland temperature has increased and entered a rather stable period of around 200 years. Any small-scale changes are barely distinguishable from the background fluctuations and can therefore be counted as negligible. It could however be argued that a slow decreasing trend is visible, however, the most apparent cooling trend first begins about 200 years after the eruptions at around 41200 b2k

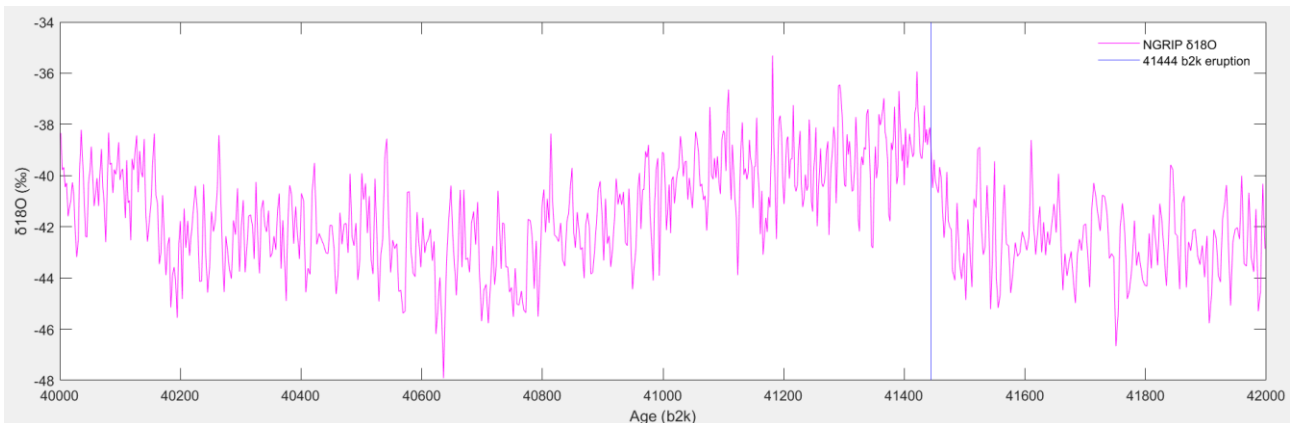


Figure 20: NGRIP $\delta^{18}O$ variations (magenta) spanning 40000 - 42000 b2k. The 41444 b2k eruption is represented by the blue, vertical line.

6.5.3. The 45555 b2k eruption

Here, no known origin of the eruption is available, and again only the sulfate deposition values can indicate the size. The difference between the Greenland and the Antarctic sulfate deposition values also indicates a NH eruption, however, the SH value is much bigger compared to the two previous eruptions. Thus, this eruption might be bigger and hence also is more likely to show a climatic impact, but as Figure 21 shows, no clear trend is visible. As the eruption is dated, it occurs exactly at a minimum in the $\delta^{18}\text{O}$ record that over a two-year period between 45555 b2k and 45553 b2k increases approx. 4‰. Expanding the period to 10 years, the increase is approx. 7‰. However, the age uncertainty is only ± 5 years, the eruption would coincide with abrupt decrease in $\delta^{18}\text{O}$ beginning in 45560 b2k and ending in 45555 b2k. However, the variability in the $\delta^{18}\text{O}$ is big in this period, and it is difficult to tell if the decrease is only due to the variability. Without plotting the eruption line, the decrease would not be one to take notice of and would just stand out as a coincidental variability.

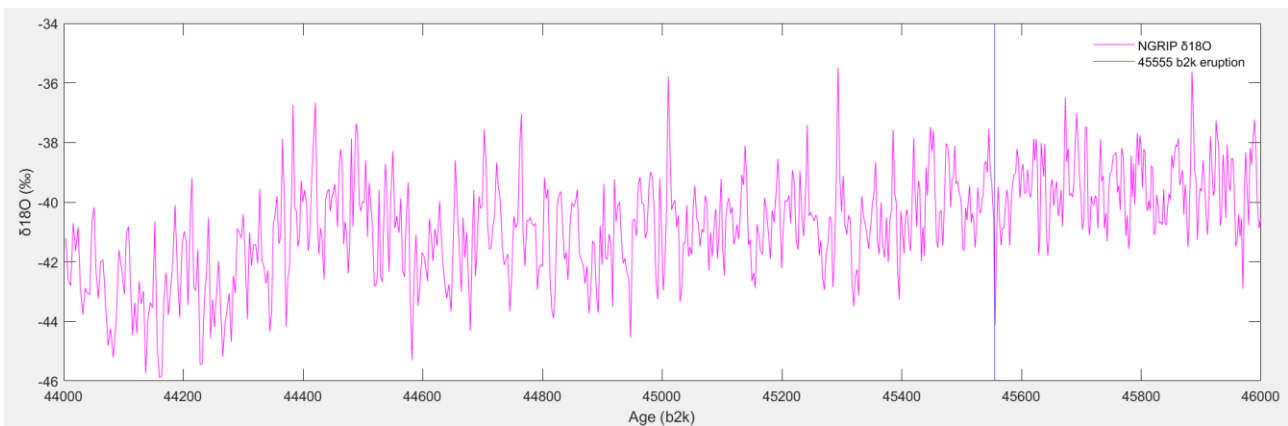


Figure 21: NGRIP $\delta^{18}\text{O}$ variations (magenta) spanning 44000 - 46000 b2k. The 45555 b2k eruption is represented by the blue, vertical line

6.5.4. The 52302 b2k eruption

Unfortunately, no known origin of this eruption is available and only the sulfate deposition values can indicate the size of the eruption. The difference in sulfate deposition values between Greenland and Antarctica also here indicates an NH eruption, but as for the 45555 b2k eruption, the SH value is rather big and thus it is likely, the impact has been bigger than the 41444 b2k and 29678 b2k eruptions. Figure 22 shows that the eruption occurred in the middle of a rather stable period. A long-term cooling is only evident around 300 years after the eruption and thus a small-scale cooling is the only possible climatic fingerprint due to this eruption. However, the small-scale trend after the eruption shows an increase in $\delta^{18}\text{O}$ and hence no cooling. As it is the case with the 45555 b2k eruption, the variability is also great in the period surrounding the eruption why the increase likely is due to natural occurring background variations.

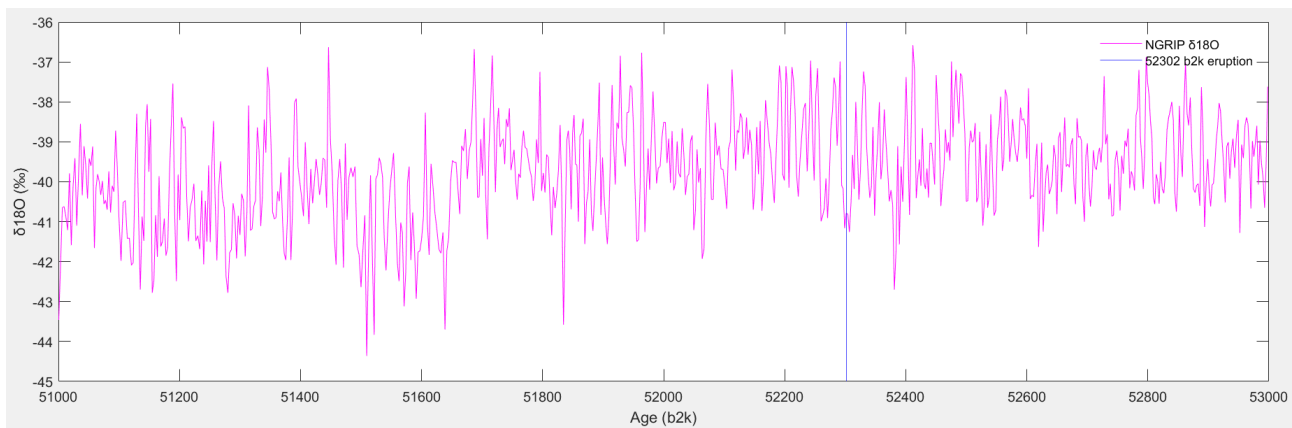


Figure 22: NGRIP $\delta^{18}\text{O}$ variations (magenta) spanning 51000 -536000 b2k. The 52302 b2k eruption is represented by the blue, vertical line

6.5.5. The 55383 b2k eruption (NAAZ II)

The NAAZ II eruption shows by far the biggest sulfate deposition values in Greenland while the Antarctic fingerprint is negligible. Hence, the sulfate deposition difference between the two hemispheres strongly suggests that the eruption is of NH origin. This has also been confirmed by Guillou *et al.* (2019) who has correlated that NAAZ II with the Thorsmark ignimbrite located in Iceland. The small Antarctic deposition indicates that the eruption probably not had a big global impact, but a NH impact might be possible. Figure 23 reveals that the eruption occurred in an intermediate period located in between two distinct decreases in temperature. While the eruption did not play a role in the prior temperature decrease, it could be argued that it might have played a role in the extra decrease in temperature following about 50 years after due to possible positive feedback mechanisms induced by the eruption following ideas published by Baldini, Brown and Mawdsley

(2018). Using the $\delta^{18}\text{O}$ -temperature relationship mean of $0.52 \text{ ‰ } ^\circ\text{C}^{-1}$ the approx. decrease of 4 ‰ in $\delta^{18}\text{O}$ would correspond to an approx. 8°C temperature decrease. Compared to Kindler *et al.* (2014) this temperature decrease is exaggerated as according to them, the complete cooling from approx. 55500 to 55300 b2k is $<10^\circ\text{C}$.

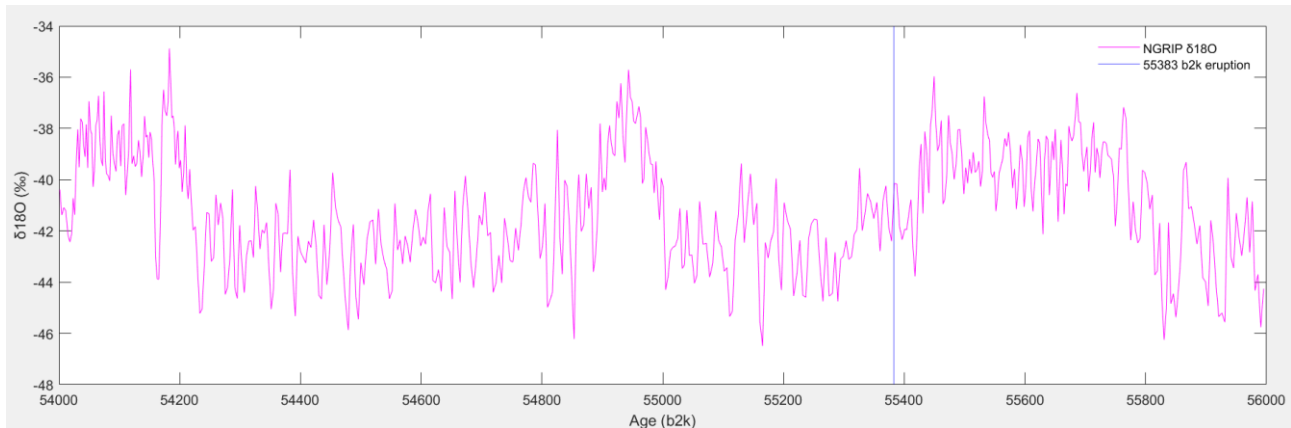


Figure 23: NGRIP $\delta^{18}\text{O}$ variations (magenta) spanning 54000 - 56000 b2k. The 45555 b2k eruption is represented by the blue, vertical line

6.5.6. Other eruptions of interest

While the four of the eruptions do not correlate with any visible short-term climatic changes in the NGRIP $\delta^{18}\text{O}$ records and with NAAZ II might having an influence about 50 years later due to feedback mechanisms, two other eruptions are of interest. Following Wilson (2001) that the Taupo (25460 b2k) was the biggest eruptions in terms of ejected volume during the last 100,000 years, an eruption this size could also likely affect the $\delta^{18}\text{O}$ records. Second, Baldini, Brown and Mawdsley (2018) has proposed that the 12917 b2k Laacher eruption played a role in the initiation of the Younger Dryas.

6.5.6.1. Taupo (25460 b2k)

The Taupo eruption is the only of the eruption which are known to be in the SH – more specifically, New Zealand. It has been classified as a super-eruption producing approx. 1100 km^3 of tephra during a period of weeks to months. The deposits are due to the eruption's explosivity widely spread stretching from New Zealand down southeast over the southern Pacific (Figure 24)(Dunbar *et al.*, 2017). An eruption this size would be likely to show up in the $\delta^{18}\text{O}$ records, however plotting the eruption with the $\delta^{18}\text{O}$ records, from Antarctica (EDC and WD) reveals that no climatic changes are present (Figure 25). Figure 25a shows records from the EDC ice core and the next 5000 years

after the eruption, the climate exhibits stable conditions. For WD (Figure 25b), the eruption occurs following a warming which slows down just prior to the eruption and enters a stable state over the next approx. 1000 years after which the climate warms again. Hence, no overall clear cooling is apparent in Antarctica. To check if the eruption could have had a global impact that somehow does not show in Antarctica, the eruption has also been plotted on the NGRIP $\delta^{18}\text{O}$ (Figure 26) which shows somewhat the same stable climatic trend following the eruption. With no long-term climatic impacts on either hemisphere, the possible climatic fingerprints would have occurred on timescales too short for the resolutions to register.

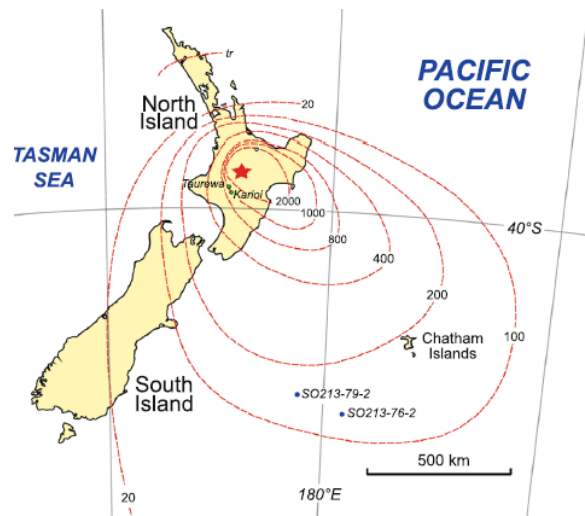


Figure 24: The location of the Taupo volcano (red star). The isopachs are tephra deposits in mm (Dunbar et al., 2017)

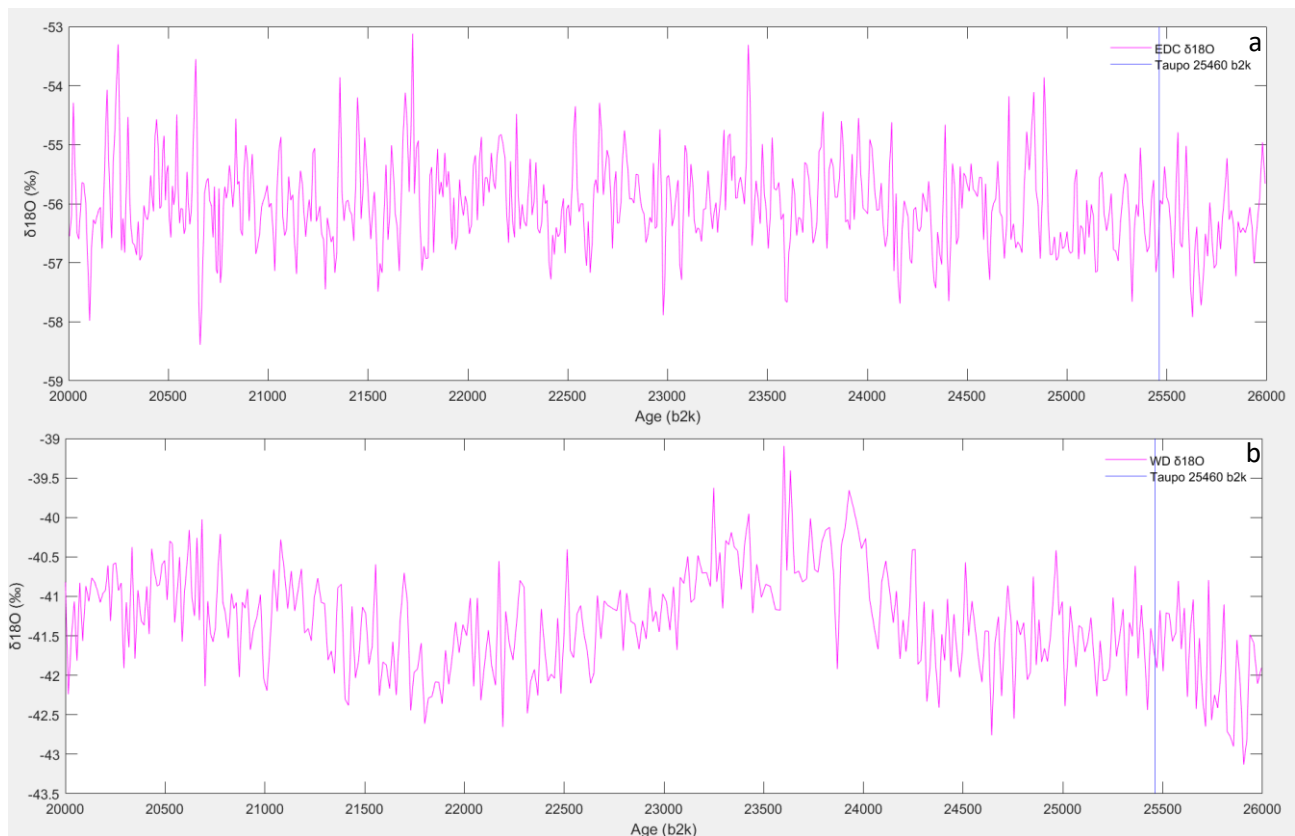


Figure 25: EDC (a) and WD (b) $\delta^{18}\text{O}$ variations (magenta) spanning 20000 - 26000 b2k. The 25460 Taupo eruption is represented by the blue, vertical line

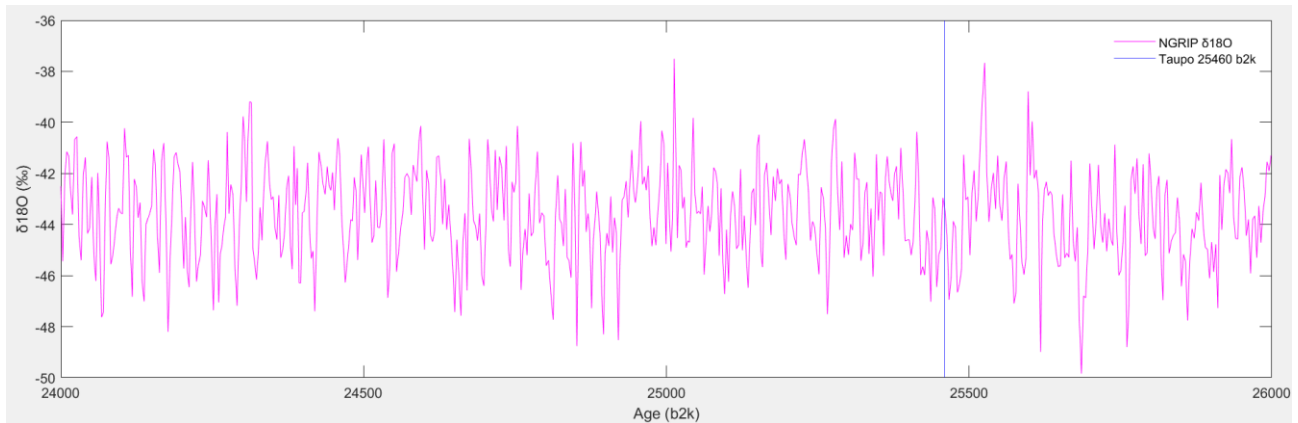


Figure 26: NGRIP $\delta^{18}\text{O}$ variations (magenta) spanning 24000 - 26000 b2k. The 25460 b2k Taupo eruption is represented by the blue, vertical line

6.5.6.2. Laacher (12917 b2k)

According to Graf and Timmreck (2001), the Laacher (12917 b2k) eruption located in Germany (Figure 27), produced aerosols that were mostly restricted to the NH that lead to a strong stratospheric cooling which disproportionately affected the NH. And in line with that, Baldini, Brown and Mawdsley (2018) proposes that it could have triggered the initiation of the Younger Dryas which was an abrupt climatic change of the NH lasting about 1000 years seeing a temperature decrease of about 10°C in Greenland (NOAA, no date). Figure 28 also reveals that the eruption is occurring just prior to a decrease in NGRIP $\delta^{18}\text{O}$ lasting approx. 200 years from where it enters a steady level. However, other causes such as meltwater pulses or changes in orographic winds have through time also been proposed as possible triggers. But among the other investigated eruptions, the Laacher eruption is the only where a long-term decrease in $\delta^{18}\text{O}$ is apparent succeeding the eruption, and thus, among the eruptions, it is the most possible to have triggered or added to a long-term climatic cooling.

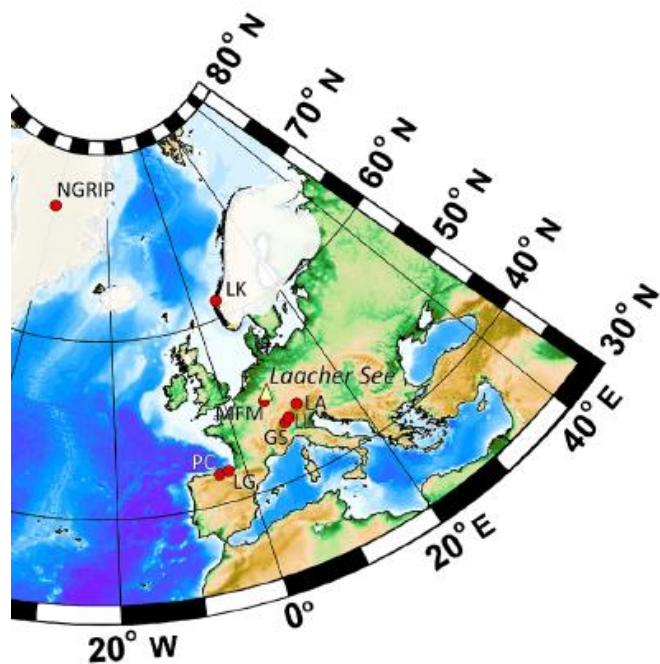


Figure 27: Map showing the location of the Laacher volcano (yellow triangle) (Baldini, Brown and Mawdsley, 2018)

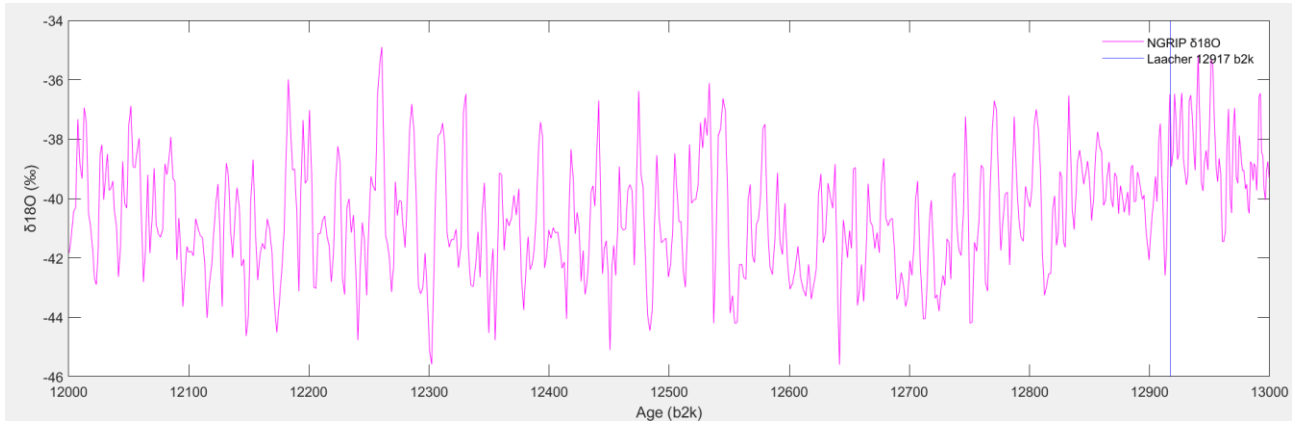


Figure 29: NGRIP $\delta^{18}\text{O}$ variation (magenta) spanning 12000 - 13000 b2k. The 12917 b2k Laacher eruption is represented by the blue vertical line.

However, while the Laacher eruption is coinciding well with the relative abrupt cooling in the NGRIP core, it is not necessarily so when looking at other Greenland ice cores. Figure 28 reveals that the NGRIP core appears to show the steepest transition in the $\delta^{18}\text{O}$ to the onset of YD while especially NEEM and GISP2 shows a delay in the $\delta^{18}\text{O}$ maximum which hence does not correlate as well with the Laacher eruption. Further, the transition in GISP2 is not as pronounced compared to the three other cores.

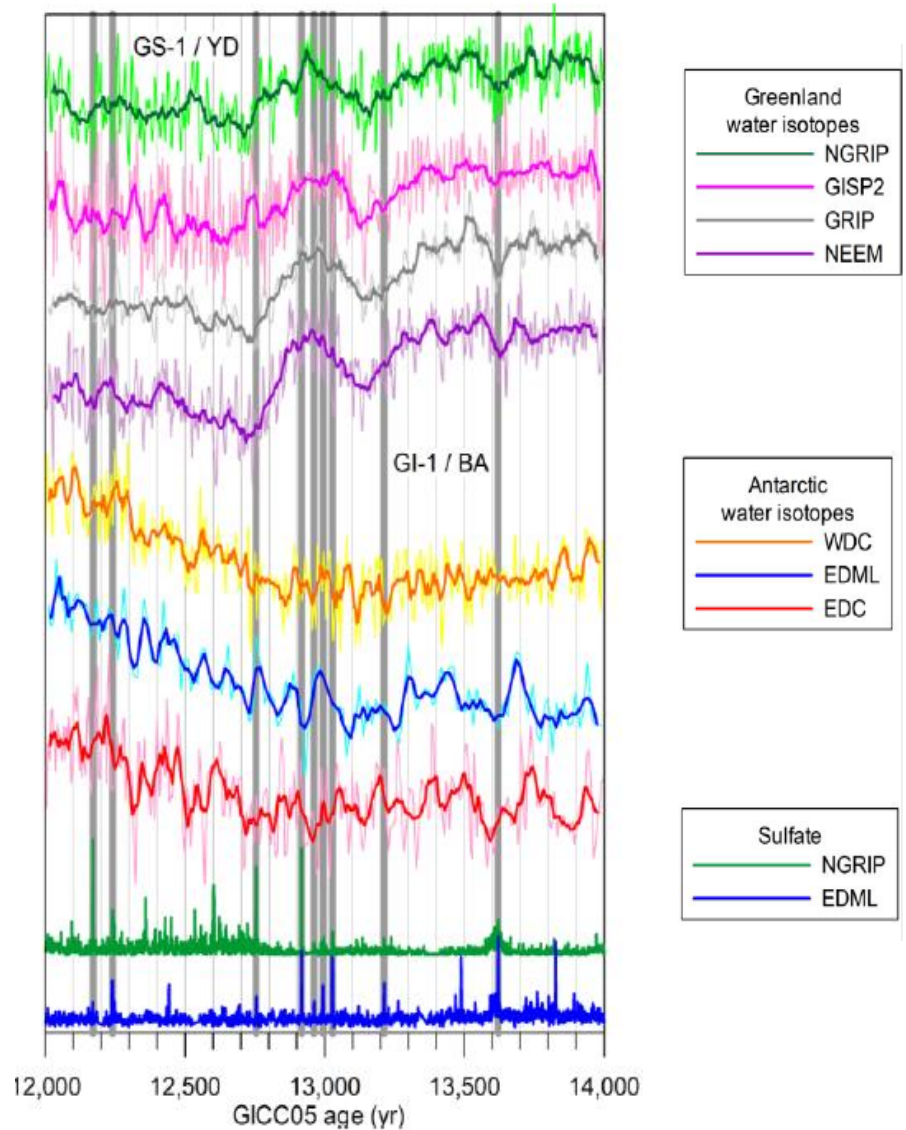


Figure 28: The four top curves show the water isotopes from the four Greenland cores NGRIP, GISP2, GRIP and NEEM. The center three curves show the water isotopes from the three Antarctic cores WD(C), EDML and EDC. The bottom two curves show the sulfate in from the Greenland cores NGRIP and EDML (Svensson et al., 2020)

Conclusion

From the ice core records, it is evident that sulfate peaks can be used to identify volcanic eruptions. This study used sulfate and sulfur (converted to sulfate) records from three Greenland and three Antarctic ice cores to quantify bipolar volcanic eruptions during the last glacial (12000 – 60000 b2k) identified and synchronized by Svensson *et al.* (2020). Furthermore, the size and frequency of the glacial eruptions have been compared to eruptions during the last 2500 years found by Sigl *et al.* (2013, 2015).

The ice cores have different resolutions which influence the data. With low resolution, the error margin should be expected to be greater compared to the high-resolution cores. In order to compare the NH and SH eruptions with eruptions during the last 2500 years, it has further been necessary to quantify using averages which also affect the data. However, even with potential error margins in mind, it is clear that the glacial shows bigger sulfate values compared to the last 2500 years. A trend is visible in both the background levels and eruption deposition values. Besides the change of the eruptions for no current known reason being bigger, this apparent difference can also be explained with an enhanced terrestrial sulfate origin and increased aridity during glacial conditions. Additionally, changes in wind patterns might have had an influence too.

Using known and probable known latitudinal locations of eruptions plotted against the deposition difference between Greenland and Antarctica, reveals that known NH eruptions ($>30^{\circ}\text{N}$) show a sulfate deposition difference $>100 \text{ kg/km}^2$ with the same applying to SH eruptions, but with opposite sign. Tropical eruptions (30°N - 30°S) all lie within a sulfate deposition difference of $\pm 100 \text{ kg/km}^2$. This trend has been applied to the bipolar eruptions in the glacial which shows a large overweight of NH and tropical eruptions which is explained by the distribution of Earth's landmasses and volcanic zones.

In order to investigate if some of the bipolar eruptions have had a climatic influence, seven of the eruptions showing the biggest sulfate deposition values have been examined using $\delta^{18}\text{O}$ records from both Greenland and Antarctica. Out of the eruptions, only the, on Greenland, immensely big NAAZ II (55383 b2k) and the Laacher (12917 b2k) eruptions could coincide with any clear climatic changes. However, even with a coincidence of eruption and climatic change it is difficult to estimate whether the eruptions have played a role in the climatic changes or if the eruptions just coincidentally have happened close to a change in climate. To further estimate the climatic impacts, more temperature proxies are needed.

Outlook

Research has revealed that melting of the glaciers during the last deglaciation caused an enhanced Icelandic volcanic activity approx. 600 years after a climatic change caused by changes in the surface pressure (Tuffen, 2010; Swindles *et al.*, 2018). Applying this to the glacial data with several DO-events, additional research could reveal if the same pattern shows after warmings and further investigation could also tell whether it is a Icelandic phenomenon or if it applies to all volcanic zones.

7. Bibliography

- Albert, P. *et al.* (2019) 'Evidence for a large magnitude eruption from Campi Flegrei caldera (Italy) at 29 ka', *Geology*, 47(7), pp. 595–599.
- Alley, R. B. *et al.* (1997) 'Visual-stratigraphic dating of the GISP2 ice core: Basis, reproducibility, and application', *Journal of Geophysical Research: Oceans*. Blackwell Publishing Ltd, 102(C12), pp. 26367–26381. doi: 10.1029/96JC03837.
- Alley, R. B. (2000) 'Ice-core evidence of abrupt climate changes', *Proceedings of the National Academy of Sciences of the United States of America*, 97(4), pp. 1331–1334. doi: 10.1073/pnas.97.4.1331.
- Andersen, K. K. *et al.* (2004) 'High-resolution record of Northern Hemisphere climate extending into the last interglacial period', *Nature*, 431(7005), pp. 147–151. doi: 10.1038/nature02805.
- Baldini, J. U. L., Brown, R. J. and Mawdsley, N. (2018) 'Evaluating the link between the sulfur-rich Laacher See volcanic eruption and the Younger Dryas climate anomaly', *Climate of the Past*, 14(7), pp. 969–990. doi: 10.5194/cp-14-969-2018.
- Baldini, J. U. L., Brown, R. J. and McElwaine, J. N. (2015) 'Was millennial scale climate change during the Last Glacial triggered by explosive volcanism?', *Scientific Reports*. Nature Publishing Group, 5, pp. 1–9. doi: 10.1038/srep17442.
- Bazin, L. *et al.* (2013) 'An optimized multi-proxy, multi-site Antarctic ice and gas orbital chronology (AICC2012): 120–800 ka', *Climate of the Past*, 9(4), pp. 1715–1731. doi: 10.5194/cp-9-1715-2013.
- Bigler, M. (2004) *Hochauflösende Spurenstoffmessungen an polaren Eisbohrkernen: Glazio-chemische und klimatische Prozessstudien*.
- Bradley, R. S. (2015) 'Ice Cores', in *Paleoclimatology*. Elsevier Inc., pp. 137–194. doi: 10.4135/9781446216187.n162.
- Brauer, A., Endres, C. and Negendank, K. F. W. (1999) 'Lateglacial calendar year chronology based on annually laminated sediments from Lake Meerfelder Maar, Germany', *Quaternary International*, 61(1), pp. 17–25.
- Cadoux, A. *et al.* (2015) 'Stratospheric Ozone destruction by the Bronze-Age Minoan eruption (Santorini Volcano, Greece)', *Scientific Reports*. Nature Publishing Group, 5(November 2014), pp. 1–12. doi: 10.1038/srep12243.
- Cole-Dai, J. (2010) 'Volcanoes and climate', *Wiley Interdisciplinary Reviews: Climate Change*, 1(6), pp. 824–839. doi: 10.1002/wcc.76.
- Cooper, C. L. *et al.* (2018) 'Evaluating the relationship between climate change and volcanism', *Earth-Science Reviews*. Elsevier, 177(September 2017), pp. 238–247. doi: 10.1016/j.earscirev.2017.11.009.
- Decker, B. B. and Decker, R. W. (2020) *Volcano*, *Britannica*. Available at: <https://www.britannica.com/science/volcano> (Accessed: 6 June 2020).
- Dunbar, N. W. *et al.* (2017) 'New Zealand supereruption provides time marker for the Last Glacial Maximum in Antarctica', *Scientific Reports*. Springer US, 7(1), pp. 3–10. doi: 10.1038/s41598-017-11758-0.
- European Science Foundation (no date) *European Project for Ice Coring in Antarctica (EPICA)*. Available at: <http://archives.esf.org/coordinating-research/research-networking-programmes/life-earth-and-environmental-sciences-lee/completed-esf-research-networking-programmes-in-life-earth-and-environmental-sciences/european-project-for-ice-coring-in-antarctica-epic> (Accessed: 12 May 2020).

- Fitzpatrick, J. J. *et al.* (2014) 'Physical properties of the WAIS divide ice core', *Journal of Glaciology*, 60(224), pp. 1140–1154. doi: 10.3189/2014JoG14J100.
- Franklin, B. (1784) 'Meteorological Imaginations and Conjectures', in *Memoirs of the Literary and Philosophical Society of Manchester vol. II*, p. 373.
- Fudge, T. J. *et al.* (2013) 'Onset of deglacial warming in West Antarctica driven by local orbital forcing', *Nature*, 500(7463), pp. 440–444. doi: 10.1038/nature12376.
- Fudge, T. J. *et al.* (2016) 'Variable relationship between accumulation and temperature in West Antarctica for the past 31,000 years', *Geophysical Research Letters*, 43(8), pp. 3795–3803. doi: 10.1002/2016GL068356.
- Geology In (2015) *Volcanic eruptions found to durably impact climate through alterations to Ocean circulation*. Available at: <http://www.geologyin.com/2015/03/volcanic-eruptions-found-to-durably.html> (Accessed: 24 March 2020).
- Giaccio, B. *et al.* (2017) 'High-precision ^{14}C and $^{40}\text{Ar}/^{39}\text{Ar}$ dating of the Campanian Ignimbrite (Y-5) reconciles the time-scales of climatic-cultural processes at 40 ka', *Scientific Reports*. Nature Publishing Group, 7(April), pp. 1–10. doi: 10.1038/srep45940.
- Graf, H. F. and Timmreck, C. (2001) 'A general climate model simulation of the aerosol radiative effects of the Laacher See eruption (10,900 B.C.)', *Journal of Geophysical Research Atmospheres*, 106(D14), pp. 14747–14756. doi: 10.1029/2001JD900152.
- Grönvold, K. *et al.* (1995) 'Ash layers from Iceland in the Greenland GRIP ice core correlated with oceanic and land sediments', *Earth and Planetary Science Letters*, 135(1–4), pp. 149–155. doi: 10.1016/0012-821X(95)00145-3.
- Guillevic, M. *et al.* (2013) 'Spatial gradients of temperature, accumulation and $\delta^{18}\text{O}$ - ice in Greenland over a series of Dansgaard-Oeschger events', *Climate of the Past*, 9(3), pp. 1029–1051. doi: 10.5194/cp-9-1029-2013.
- Guillou, H. *et al.* (2019) '40 Ar/ 39 Ar dating of the Thorsmork ignimbrite and Icelandic sub-glacial rhyolites', *Quaternary Science Reviews*, 209, pp. 52–62. doi: 10.1016/j.quascirev.2019.02.014.
- Holm, P. M. (2012) *Vulkaner - varme hilsner fra Jordens indre*. 1st edn. Copenhagen: Gyldendal.
- Johansen, S. J. *et al.* (2001) 'Oxygen isotope and palaeotemperature records from six Greenland ice-core stations: Camp Century, Dye-3, GRIP, GISP2, Renland and NorthGRIP', *Journal of Quaternary Science*, 16(4), pp. 299–307. doi: 10.1002/jqs.622.
- Kindler, P. *et al.* (2014) 'Temperature reconstruction from 10 to 120 kyr b2k from the NGRIP ice core', *Climate of the Past*, 10(2), pp. 887–902. doi: 10.5194/cp-10-887-2014.
- Kirchner, I. *et al.* (1999) 'Climate model simulation of winter warming and summer cooling following the 1991 Mount Pinatubo volcanic eruption', *Journal of Geophysical Research Atmospheres*, 104(D16), pp. 19039–19055. doi: 10.1029/1999JD900213.
- Lane, C. S. *et al.* (2012) 'Was the 12.1ka Icelandic Vedde Ash one of a kind?', *Quaternary Science Reviews*. Elsevier Ltd, 33, pp. 87–99. doi: 10.1016/j.quascirev.2011.11.011.
- Lavigne, F. *et al.* (2013) 'Source of the great A.D. 1257 mystery eruption unveiled, Samalas volcano, Rinjani Volcanic Complex, Indonesia', *Proceedings of the National Academy of Sciences of the United States of America*, 110(42), pp. 16742–16747. doi: 10.1073/pnas.1307520110.

- Legrand, M. (1997) 'Ice-core records of atmospheric sulphur', *Philosophical Transactions of the Royal Society B: Biological Sciences*, 352(1350), pp. 241–250. doi: 10.1098/rstb.1997.0019.
- Mason, B. G., Pyle, D. M. and Oppenheimer, C. (2004) 'The size and frequency of the largest explosive eruptions on Earth', *Bulletin of Volcanology*, 66(8), pp. 735–748. doi: 10.1007/s00445-004-0355-9.
- Matsuura Kenji & National Center for Atmospheric Research Staff (Eds) (2020) *The Climate Data Guide: Global (land) precipitation and temperature: Willmott & Matsuura, University of Delaware, The Climate Data Guide*. Available at: <https://climatedataguide.ucar.edu/climate-data/global-land-precipitation-and-temperature-willmott-matsuura-university-delaware> (Accessed: 22 May 2020).
- Mayewski, P. A. *et al.* (1997) 'Major features and forcing of high-latitude northern hemisphere atmospheric circulation using a 110,000-year-long glaciochemical series', *Journal of Geophysical Research: Oceans*, 102(C12), pp. 26345–26366. doi: 10.1029/96JC03365.
- McCormick, M. P., Thomason, L. W. and Trepte, C. R. (1995) 'Atmospheric effects of the Mt Pinatubo eruption', *Nature*, 373(6513), pp. 399–404. doi: 10.1038/373399a0.
- Newhall, C. G. and Self, S. (1982) 'The volcanic explosivity index (VEI): an estimate of explosive magnitude for historical volcanism.', *Journal of Geophysical Research*, 87(C2), pp. 123–1238. doi: 10.1029/jc087ic02p01231.
- NOAA (no date) *The Younger Dryas | National Centers for Environmental Information (NCEI) formerly known as National Climatic Data Center (NCDC)*. Available at: <https://www.ncdc.noaa.gov/abrupt-climate-change/The Younger Dryas> (Accessed: 5 June 2020).
- Rasmussen, S. O. *et al.* (2013) 'A first chronology for the North Greenland Eemian Ice Drilling (NEEM) ice core', *Climate of the Past*, 9(6), pp. 2713–2730. doi: 10.5194/cp-9-2713-2013.
- Robock, A. (2000) 'Volcanic eruptions and climate', *Reviews of Geophysics*, 38(2), pp. 191–219.
- Robock, A. and Mao, J. (1992) 'Winter warming from large volcanic eruptions', *Geophysical Research Letters*, Vol. 12(24), pp. 2405–2408.
- Schüpbach, S. *et al.* (2018) 'Greenland records of aerosol source and atmospheric lifetime changes from the Eemian to the Holocene', *Nature Communications*. Springer US, 9(1). doi: 10.1038/s41467-018-03924-3.
- Severi, M. *et al.* (2007) 'Synchronisation of the EDML and EDC ice cores for the last 52 kyr by volcanic signature matching', *Climate of the Past*, 3(3), pp. 367–374. doi: 10.5194/cp-3-367-2007.
- Sigl, M. *et al.* (2013) 'A new bipolar ice core record of volcanism from WAIS Divide and NEEM and implications for climate forcing of the last 2000 years', *Journal of Geophysical Research Atmospheres*, 118(3), pp. 1151–1169. doi: 10.1029/2012JD018603.
- Sigl, M. *et al.* (2015) 'Timing and climate forcing of volcanic eruptions for the past 2,500 years', *Nature*, 523(7562), pp. 543–549. doi: 10.1038/nature14565.
- Smithsonian Institution, National Museum Of Natural History, G. V. P. (no date) *Global Volcanism Program | Database Search*. Available at: https://volcano.si.edu/search_volcano.cfm (Accessed: 24 May 2020).
- Stenchikov, G. L. *et al.* (1998) 'Radiative forcing from the 1991 Mount Pinatubo volcanic eruption', *Journal of Geophysical Research Atmospheres*, 103(D12), pp. 13837–13857. doi: 10.1029/98JD00693.
- Stothers, R. B. (1984) 'Mystery cloud of AD 536', *Nature*, Vol. 307, pp. 9–10.
- Stothers, R. B. (1996) 'Major optical depth perturbations to the stratosphere from volcanic eruptions :

Pyrheliometric period , 1881-1960', *Journal of Geophysical Research*, Vol. 101(No. D2), pp. 3901–3920.

Svensson, A. *et al.* (2005) 'Visual stratigraphy of the North Greenland Ice Core Project (NorthGRIP) ice core during the last glacial period', *Journal of Geophysical Research D: Atmospheres*, 110(2), pp. 1–11. doi: 10.1029/2004JD005134.

Svensson, A. *et al.* (2020) 'Bipolar volcanic synchronization of abrupt climate change in Greenland and Antarctic ice cores during the last glacial period', *Climate of the Past*, (April), pp. 1–28. Available at: <https://www.clim-past-discuss.net/cp-2020-41/cp-2020-41.pdf>.

Swindles, G. T. *et al.* (2018) 'Climatic control on Icelandic volcanic activity during the mid - Holocene', *Geology*, 46(1), pp. 47–50.

Textor, C. *et al.* (2003) 'Emissions from volcanoes', in *Emissions of Chemical Compounds and Aerosols in the Atmosphere*, pp. 1–32.

The University of Maine (no date) *Greenland Ice Sheet Project 2 - GISP2*. Available at: <https://climatechange.umaine.edu/gisp2/> (Accessed: 11 May 2020).

Traufetter, F. *et al.* (2004) 'Spatio-temporal variability in volcanic sulphate deposition over the past 2 kyr in snow pits and firn cores from Amundsenisen, Antarctica', *Journal of Glaciology*, 50(168), pp. 137–146. doi: 10.3189/172756504781830222.

Tuffen, H. (2010) 'How will melting of ice affect volcanic hazards in the twenty-first century?', *Philosophical Transactions of the Royal Society*, 368, pp. 2535–2558. doi: 10.1098/rsta.2010.0063.

University of Copenhagen (no date a) *NEEM*. Available at: <https://neem.dk/> (Accessed: 11 May 2020).

University of Copenhagen (no date b) *The search for Eemian ice*. Available at: http://www.iceandclimate.nbi.ku.dk/research/drill_analysing/history_drilling/search_eemian/ (Accessed: 11 May 2020).

Veres, D. *et al.* (2013) 'The Antarctic ice core chronology (AICC2012): An optimized multi-parameter and multi-site dating approach for the last 120 thousand years', *Climate of the Past*, 9(4), pp. 1733–1748. doi: 10.5194/cp-9-1733-2013.

Wilson, C. J. . (2001) 'The 26.5 ka Oruanui eruption, New Zealand: an introduction and overview', *Journal of Volcanology and Geothermal Research*, 112(1–4), pp. 133–174.

Zielinski, G. A. (2002) 'Climatic Impact of Volcanic Eruptions', *The Scientific World JOURNAL*, 2, pp. 869–884. doi: 10.1100/tsw.2002.83.

Appendix A

A.1.

Annual averaging

```
WAIS_ANN = (-407:2000)';  
for i=1:size(WAIS_ANN)  
    idx = find(WAIS(:,1)>WAIS_ANN(i,1)-1  
& WAIS(:,1)<WAIS_ANN(i,1)+0);  
    WAIS_ANN(i,2) = mean(WAIS(idx,2));  
end
```

Interpolating sulfur values

```
idx = ~isnan(WAIS_ANN(:,2));  
WAIS_ANN(:,5) =  
interp1(WAIS_ANN(idx,1),  
WAIS_ANN(idx,2), WAIS_ANN(:,1));
```

31-year running median (RM)

```
for i=1:size(WAIS_ANN,1)  
    idx =  
find(WAIS_ANN(:,1)>WAIS_ANN(i,1)-16  
& WAIS_ANN(:,1)<WAIS_ANN(i,1)+16 &  
~isnan(WAIS_ANN(:,2)));  
    WAIS_ANN(i,3) =  
median(WAIS_ANN(idx,2));  
end
```

3xMAD

```
MADWAIS = mad(WAIS_ANN(:,2),1);  
WAIS_ANN(:,4)=3*MADWAIS+WAIS_ANN(:,3);
```

Excluding volcanic signals

```
WAIS_ANN(:,7) = WAIS_ANN(:,5);  
idx =  
find(WAIS_ANN(:,5)>WAIS_ANN(:,4));  
WAIS_ANN(idx,7) = nan;
```

31-year reduced running median (RRM)

```
for i=1:size(WAIS_ANN,1)  
    idx =  
find(WAIS_ANN(:,1)>WAIS_ANN(i,1)-16  
& WAIS_ANN(:,1)<WAIS_ANN(i,1)+16 &  
~isnan(WAIS_ANN(:,7)));  
    WAIS_ANN(i,8) =  
median(WAIS_ANN(idx,7));  
end
```

Finding the annual layer depth

```
WAIS_ANN(:,6) =  
interp1(WAIS(:,1),WAIS(:,4),WAIS_ANN(:,1));
```

Eruption detection list

```
while(i < size(WAIS_ANN,1))  
    i = i+1;  
    if (WAIS_ANN(i,5) > WAIS_ANN(i,9))  
        j = j+1;  
        Volcano_RRM(j,1) = WAIS_ANN(i,1);  
        Volcano_RRM(j,3) = 0;  
        while (WAIS_ANN(i,5) >  
WAIS_ANN(i,9))
```

```
Volcano_RRM(j,3)=Volcano_RRM(j,3)+3*(  
WAIS_ANN(i-1,6)-  
WAIS_ANN(i,6))*(WAIS_ANN(i,5)-  
WAIS_ANN(i,8));  
        i = i+1;  
    end  
    Volcano_RRM(j,2) = WAIS_ANN(i-1,1);  
end  
end
```

A.2.

INTERPOLATING WHERE THERE ARE NAN'S

```
idx = ~isnan(EDML(:,2));
EDML(:,4) = interp1(EDML(idx,3),
EDML(idx,2), EDML(:,3));
```

ANNUALIZED

```
EDML_ANN = (11999:60004)';
for i=1:size(EDML_ANN)
    EDML_ANN(:,2) =
interp1(EDML(:,3),EDML(:,1),EDML_ANN(
:,1));
    EDML_ANN(:,3) =
interp1(EDML(:,3),EDML(:,4),EDML_ANN(
:,1));
end
```

FINDING THE BACKGROUND (RUNNING
MEDIAN, RM)

```
for i=1:size(EDML_ANN,1)
    idx =
find(EDML_ANN(:,1)>EDML_ANN(i,1)-45
& EDML_ANN(:,1)<EDML_ANN(i,1)+45);
    EDML_ANN(i,4) =
median(EDML_ANN(idx,3));
end
```

FINDING THE VARIABLE THRESHOLD (MAD)

```
for i=1:size(EDML_ANN,1)
    idx =
find(EDML_ANN(:,1)>EDML_ANN(i,1)-45
& EDML_ANN(:,1)<EDML_ANN(i,1)+45);
    EDML_ANN(i,5) =
3*mad(EDML_ANN(idx,3),1)+EDML_ANN
(i,4);
end
```

PEAKS > MAD = NAN

```
EDML_ANN(:,6) = EDML_ANN(:,3);
idx =
find(EDML_ANN(:,3)>EDML_ANN(:,5));
EDML_ANN(idx,6) = nan;
```

REDUCED RUNNING MEDIAN (RRM)

```
for i=1:size(EDML_ANN,1)
    idx =
find(EDML_ANN(:,1)>EDML_ANN(i,1)-45
& EDML_ANN(:,1)<EDML_ANN(i,1)+45 &
~isnan(EDML_ANN(:,6)));
    EDML_ANN(i,7) =
median(EDML_ANN(idx,6));
end
```

FINDING THE VARIABLE MAD on RRM

```
for i=1:size(EDML_ANN,1)
    idx =
find(EDML_ANN(:,1)>EDML_ANN(i,1)-45
& EDML_ANN(:,1)<EDML_ANN(i,1)+45 &
~isnan(EDML_ANN(:,6)));
    EDML_ANN(i,8) =
3*mad(EDML_ANN(idx,6),1)+EDML_ANN
(i,7);
end
```

VOLCANO ERUPTION LIST

```
i = 1;
j = 0;
```

```
while(i < size(EDML_ANN,1))
    i = i+1;
    if (EDML_ANN(i,3) > EDML_ANN(i,8))
        j = j+1;
        Volcano(j,1) = EDML_ANN(i,1);
        Volcano(j,3) = EDML_ANN(i,2);
        Volcano(j,5) = 0;
        while (EDML_ANN(i,3) >
EDML_ANN(i,8))
```

```
Volcano(j,5)=Volcano(j,5)+(EDML_ANN(i,2)
)-EDML_ANN(i-1,2))*(EDML_ANN(i,3)-
EDML_ANN(i,7));
        i = i+1;
    end
    Volcano(j,2) = EDML_ANN(i-1,1);
    Volcano(j,4) = EDML_ANN(i-1,2);
end
```

end

THINNING CORRECTION (INTERPOLATING
THINNING WITH DEPTH)

```
Volcano(:,6) =  
interp1(EDML_thinning(:,1),EDML_thinning  
(:,7),Volcano(:,3));
```

TOTAL SO4 DEPOSITION INCL. THINNING
CORRECTION AND WATER EQ. DEPTH
CORREC.

```
Volcano(:,7) =  
(Volcano(:,5)./Volcano(:,6))*0.917;
```

REMOVING ERUPTIONS < 2 KG/KM2

```
Volcano = Volcano(Volcano(:,7) >=2,:);
```

A.3.

INTERPOLATING WHERE THERE ARE NAN'S

```
idx = ~isnan(NEEM(:,11));
NEEM(:,14) = interp1(NEEM(idx,13),
NEEM(idx,11), NEEM(:,13));
```

LOW RESOLUTION, THUS NO ANNUALIZED

```
NEEM_ANN(:,1) = NEEM(:,13);
NEEM_ANN(:,2) = NEEM(:,3);
NEEM_ANN(:,3) = NEEM(:,14);
```

FINDING THE BACKGROUND (RUNNING MEDIAN, RM)

```
for i=1:size(NEEM_ANN,1)
    idx =
    find(NEEM_ANN(:,1)>NEEM_ANN(i,1)-90
& NEEM_ANN(:,1)<NEEM_ANN(i,1)+90);
    NEEM_ANN(i,4) =
    median(NEEM_ANN(idx,3));
end
```

FINDING THE VARIABLE THRESHOLD (MAD)

```
for i=1:size(NEEM_ANN,1)
    idx =
    find(NEEM_ANN(:,1)>NEEM_ANN(i,1)-90
& NEEM_ANN(:,1)<NEEM_ANN(i,1)+90);
    NEEM_ANN(i,5) =
    3*mad(NEEM_ANN(idx,3),1)+NEEM_ANN
(i,4);
end
```

PEAKS > MAD = NAN

```
NEEM_ANN(:,6) = NEEM_ANN(:,3);
idx =
find(NEEM_ANN(:,3)>NEEM_ANN(:,5));
NEEM_ANN(idx,6) = nan;
```

REDUCED RUNNING MEDIAN (RRM)

```
for i=1:size(NEEM_ANN,1)
```

```
    idx =
    find(NEEM_ANN(:,1)>NEEM_ANN(i,1)-90
& NEEM_ANN(:,1)<NEEM_ANN(i,1)+90 &
~isnan(NEEM_ANN(:,6)));
    NEEM_ANN(i,7) =
    median(NEEM_ANN(idx,6));
end
```

FINDING THE VARIABLE MAD on RRM

```
for i=1:size(NEEM_ANN,1)
    idx =
    find(NEEM_ANN(:,1)>NEEM_ANN(i,1)-90
& NEEM_ANN(:,1)<NEEM_ANN(i,1)+90 &
~isnan(NEEM_ANN(:,6)));
    NEEM_ANN(i,8) =
    3*mad(NEEM_ANN(idx,6),1)+NEEM_ANN
(i,7);
end
```

VOLCANO ERUPTION LIST

```
i = 1;
j = 0;
```

```
while(i < size(NEEM_ANN,1))
    i = i+1;
    if (NEEM_ANN(i,3) > NEEM_ANN(i,8))
        j = j+1;
        Volcano(j,1) = NEEM_ANN(i,1);
        Volcano(j,3) = NEEM_ANN(i,2);
        Volcano(j,5) = 0;
        while (NEEM_ANN(i,3) >
NEEM_ANN(i,8))
```

```
Volcano(j,5)=Volcano(j,5)+(NEEM_ANN(i,2)
)-NEEM_ANN(i-1,2))*(NEEM_ANN(i,3)-
NEEM_ANN(i,7));
```

```
        i = i+1;
        end
        Volcano(j,2) = NEEM_ANN(i-1,1);
        Volcano(j,4) = NEEM_ANN(i-1,2);
    end
end
```

THINNING CORRECTION (INTERPOLATING
THINNING WITH DEPTH)

```
Volcano(:,6) =  
interp1(NEEM_thinning(:,1),NEEM_thinning  
(:,2),Volcano(:,3));
```

TOTAL SO4 DEPOSITION INCL. THINNING
CORRECTION AND WATER EQ. DEPTH
CORREC.

```
Volcano(:,7) =  
(Volcano(:,5)./Volcano(:,6))*0.917;
```

REMOVING ERUPTIONS LOWER THAN 25
KG/KM2

```
Volcano = Volcano(Volcano(:,7) >=25,:);
```

A.4.

PERIOD	NGRIP DEPTH(M)	NGRIP SO4	NEEM DEPTH(M)	NEEM SO4	GISP2 DEPTH(M)	GISP2 SO4	AVG. SO4 (KG/KM2)	GICC05 AGE(B2K)
GREENLAND								
GS-1	1506.11	228.63	1429.08	411.66	1692.25	172.83	271.04	12170
	1508.05	70.74	1430.56		1694.24	65.10	67.92	12241
	1522.20	210.96	1441.43		1708.64	111.49	161.22	12755
GI-1	1527.31	340.21	1445.01	218.88	1713.92	237.95	265.68	12917
	1529.05	73.49	1446.09		1715.71		73.49	12961
	1530.49	65.81	1447.06		1717.29	50.29	58.05	12995
	1531.78	69.00	1447.94	437.21	1718.67	387.83	298.01	13028
	1538.35	54.09	1452.02		1725.74	38.68	46.39	13212
	1555.52	265.40	1462.37	473.84	1744.25	522.41	420.55	13620
	1595.04	160.42	1484.04		1787.32	129.33	144.88	14500
GS-2.1	1605.00	55.43	1489.47	120.29	1798.17	99.09	91.60	14705
	1606.52	268.82	1490.35	516.84	1799.77	220.44	335.37	14761
	1611.97	72.62	1493.30	92.81	1805.39		82.71	14966
	1619.54	152.47	1497.56	85.93	1812.80	210.60	149.66	15296
	1625.57	17.73			1818.88	172.67	95.20	15559
	1645.85	97.85			1838.60	126.70	112.28	16469
LGM								
GS-3	1814.92	204.98	1610.35	175.29	2006.76		190.13	24669
	1827.21	166.44	1617.11	221.12			193.78	25460
	1831.58	143.41	1619.60	119.12	2022.74	408.03	223.52	25759
	1834.25	103.30	1621.00	207.57			155.44	25940
GI-3/GS-4	1869.52	114.80	1641.23	399.61	2057.05	818.79	444.40	27797
	1880.00	78.18	1647.55	203.42	2066.17	240.21	173.93	28454
GS-5.1	1892.34	79.98					79.98	28942
	1902.84	547.72			2086.38	342.31	445.02	29678
	1903.45	224.68	1661.59	234.15			229.41	29722
	1910.97	61.62	1665.98	360.19	2092.92	265.63	229.15	30244

GI-5.2/GS-5.2	1939.54	219.44	1683.32	223.29	2117.06	259.31	234.01	32032
	1949.59	20.81	1688.83		2125.72		20.81	32433
GS-6	1962.24	51.09	1696.24				51.09	33221
	1963.75	16.02			2137.48	117.42	66.72	33328
GS-7	1982.33	82.36					82.36	34227
GI-7/GS-7	1989.90	99.01	1712.05		2160.07	631.47	365.24	34718
	2000.22	30.74	1717.88	64.24	2169.35	72.22	55.74	35145
GS-8/GI-7	2010.98	74.46	1724.05	208.49	2179.13	163.45	148.80	35556
GI-8	2038.07	39.38	1740.25	157.00	2202.73	119.95	105.44	37113
	2042.28	160.54	1742.65		2206.65	32.92	96.73	37277
	2061.99	47.14	1754.19	105.51	2224.84	110.05	87.57	37965
	2067.36	262.17	1757.30	76.14	2229.71	442.29	260.20	38133
GS-9	2070.24	39.15			2232.37		39.15	38232
	2072.48	103.59	1760.39	389.37	2234.14	166.43	219.80	38366
	2094.13	165.89	1774.31	352.60			259.24	39869
	2094.88	137.07	1774.76	402.59	2252.11	634.15	391.27	39915
	2100.03	160.69	1777.73	411.48	2256.31		286.09	40183
GS-10	2106.01							40563
	2109.62							40794
	2113.22							41002
	2116.18	183.88	1786.94	760.01	2269.63	401.11	448.33	41144
	2121.86	44.01	1790.01		2274.58	76.35	60.18	41379
GS-11	2129.82							41858
	2130.21							41887
	2132.21	185.09	1796.08	477.31			331.20	42037
	2132.64	7.89					7.89	42067
	2133.28	27.06					27.06	42111
	2135.13	28.64	1797.95	339.37	2285.24		184.01	42250
	2142.36	152.28	1801.80	155.13	2291.16	104.14	137.18	42658

	2151.80	55.12	1807.00	82.34	2299.22	117.77	85.08	43104
GS-12	2157.20		1809.94		2303.70			43327
GI-12	2173.90	96.58	1819.87		2317.11		96.58	44507
	2182.77	30.98	1824.74		2324.64	113.54	72.26	45050
	2191.97	628.45	1829.66	1151.60	2332.68	276.12	685.39	45555
	2201.55	95.79	1834.82	125.68	2341.17	136.88	119.45	46002
	2204.14	41.68	1836.23	99.11	2343.48	95.68	78.82	46116
	2217.64	97.21	1843.68	68.40	2355.20	165.54	110.38	46683
	2224.62	330.88	1848.15	229.72	2360.97	300.33	286.98	47023
GS-13	2227.22	195.92			2362.94		195.92	47214
	2242.20	26.22			2374.00	49.92	38.07	48441
	2252.88	114.12	1863.15	142.25	2382.30	277.99	178.12	49065
GS-14	2257.55	67.40	1865.65		2386.05		67.40	49319
GI-14	2277.65	104.14	1876.39		2401.80	119.48	111.81	50586
	2302.75	56.87	1889.52	71.99	2421.67	56.08	61.64	52031
	2307.61	353.80	1892.00	176.58	2425.62	478.22	336.20	52302
	2326.10	144.19	1901.77	134.47	2440.00	217.55	165.40	53259
	2344.59	83.18	1911.42		2454.19		83.18	54178
GS-15.1	2347.73	123.97					123.97	54390
GS-15.2	2355.40	16.32					16.32	55005
	2359.45	887.72	1919.82	1055.10	2464.26	1909.13	1283.99	55383
GI-16.1	2382.65	61.80			2480.28	96.17	78.99	57051
	2385.25	76.00	1933.39	63.83	2482.04	225.12	121.65	57222
	2389.49	45.94			2485.05	62.76	54.35	57499
GI-16.2	2400.69	149.66	1941.27		2493.25		149.66	58182
	2403.59	123.72					123.72	58355
	2416.26	13.87					13.87	59180
GI-17.2	2417.90	41.37					41.37	59317
GS-18	2421.72	73.41			2507.702	182.52	127.96	59545
	2422.82	120.39					120.39	59647

A.5.

PERIOD	EDML DEPTH(M)	EDML SO4	EDC DEPTH(M)	EDC SO4	WDC DEPTH(M)	WDC SO4	AVG. SO4 (KG/KM2)	GICC05 AGE(B2K)
ANTARCTICA								
GS-1	700.18	6.11	370.09		2012.50	18.55	12.33	12170
	703.40	23.49	371.94		2019.07	36.79	30.14	12241
	725.83	16.67	384.13		2068.41	26.95	21.81	12755
GI-1	731.46	37.66	387.28	49.76	2082.95	102.06	63.16	12917
	732.63	7.03	388.03		2086.53	27.78	17.41	12961
	733.68	26.79	388.71	6.92	2089.55	49.77	27.83	12995
	734.77	33.40	389.36	82.02	2092.72	88.93	68.12	13028
	741.24	17.90	393.01	30.68	2111.25	94.38	47.65	13212
	754.71	35.53	400.28	8.84	2145.41	82.94	42.43	13620
	784.90	37.26	417.01		2219.81	50.76	44.01	14500
GS-2.1	793.21	38.03	421.88	7.51	2240.15	72.63	39.39	14705
	795.52	11.28	423.06	3.57	2245.21	14.67	9.84	14761
	803.86	46.96	427.11		2263.20	104.87	75.91	14966
	817.26	17.44	433.78	3.77	2290.21	21.91	14.37	15296
	826.00	32.68	438.10	82.27	2308.70	111.02	75.32	15559
	859.70	105.54	454.00	91.57	2370.00		98.55	16469
LGM								
GS-3	1051.82	79.16	553.36	23.31	2634.35	76.88	59.78	24669
	1069.72	263.43	561.38		2660.24	339.40	301.41	25460
	1076.94	146.95	564.43	31.08	2670.09	171.62	116.55	25759
	1080.83	9.00	566.21	3.08	2675.70		6.04	25940
GI-3/GS-4	1123.98	10.67	586.28	14.17	2742.86	23.24	16.02	27797
	1138.00	22.18	593.49	42.65	2768.10	20.10	28.31	28454
GS-5.1	1146.80	135.16	598.87	13.25	2784.36	119.05	89.15	28942
	1160.15	185.87	607.05		2806.62	199.90	192.89	29678
	1160.95	28.38					28.38	29722
	1170.18	31.88	613.20		2822.20	50.07	40.98	30244

GI-	1199.60	130.12	632.28	197.21	2863.15	170.04	165.79	32032
5.2/GS-								
5.2								
	1206.06	44.25	636.42	76.54	2872.32	66.45	62.41	32433
GS-6	1220.12	43.78	644.78	21.50	2890.77	73.23	46.17	33221
	1222.02	53.72	645.86		2893.14	82.00	67.86	33328
GS-7	1239.19		656.37		2915.12			34227
GI-7/GS-7	1248.00	30.77	661.85	60.16	2928.33	68.38	53.10	34718
	1254.95	34.37	666.34	22.86	2939.57	85.50	47.58	35145
GS-8/GI-7	1262.29	38.74	671.08	23.34	2951.03	70.73	44.27	35556
GI-8	1291.80	65.99	689.12	48.62	2987.25	95.82	70.14	37113
	1295.11	40.31	691.15	18.42	2991.13		29.36	37277
	1307.60	75.86	699.08	20.13	3006.32		47.99	37965
	1311.08	303.35	701.26	53.20	3010.47		178.27	38133
GS-9	1313.08	37.59	702.59	54.44	3012.89		46.01	38232
	1316.04	13.98	704.16		3016.48	26.76	20.37	38366
	1349.53	69.38	723.19		3052.10	61.26	65.32	39869
	1350.56	43.48	723.84	58.78	3053.26	36.19	46.15	39915
	1354.57	29.11	726.31	45.64	3057.95	84.29	53.01	40183
GS-10	1362.28		730.95					40563
	1366.56		733.85					40794
	1370.57		736.27	2.14			2.14	41002
	1372.72	74.97	737.50	47.62	3079.07	118.21	80.27	41144
	1376.92	40.47			3083.95	36.54	38.50	41379
GS-11	1386.61	30.36	745.98	21.94			26.15	41858
	1387.31	11.30	746.42	13.95	3095.68	59.01	28.09	41887
	1390.02	69.64	748.08	118.51	3098.61	205.92	131.36	42037
	1390.49		748.47					42067
	1391.45	52.93	748.96		3100.16	135.66	94.29	42111
	1393.78	59.44	750.33	124.71	3102.68	64.58	82.91	42250
	1400.14	152.87	754.37		3109.97	102.71	127.79	42658
	1408.04	21.80	759.53	2.08	3118.82	44.18	22.69	43104
GS-12	1411.97	24.81	762.24		3123.40	103.03	63.92	43327

GI-12	1431.27	51.75	775.02	20.84	3144.96	158.11	76.90	44507
	1439.07	41.38	780.58	33.73	3154.24	107.69	60.93	45050
	1446.26	161.47	785.97		3162.93	270.85	216.16	45555
	1452.62	55.08	790.58	41.54	3170.99	81.56	59.40	46002
	1454.36	105.69	791.88	75.46	3173.19	161.17	114.11	46116
	1462.99	121.08	798.50	129.36	3184.42	520.50	256.98	46683
	1468.91	33.87	802.87	8.95	3192.00	131.68	58.17	47023
GS-13	1472.47	29.98	805.18	33.50	3196.10	40.36	34.61	47214
	1494.11	6.29	819.25		3218.78	68.63	37.46	48441
	1503.60	157.56	826.00	49.88	3228.32	305.49	170.98	49065
GS-14	1507.33	57.36	828.55	46.85	3231.90	46.59	50.27	49319
GI-14	1526.13	21.24	841.62	26.94	3249.64	16.84	21.68	50586
	1547.79	36.95	856.76	74.68	3271.39	39.06	50.23	52031
	1551.53	149.78	859.49	169.22	3274.77	230.71	183.24	52302
	1568.29	76.36	871.41	62.90	3289.90	44.32	61.19	53259
	1583.34	33.56	882.27	17.27	3306.60		25.42	54178
GS-15.1	1587.05	17.14	884.80		3309.90	19.76	18.45	54390
GS-15.2	1596.69	30.27	891.34	28.34	3317.95	38.03	32.21	55005
	1602.80	27.33	895.60	5.89	3322.15		16.61	55383
GI-16.1	1628.50	41.58	914.18	46.26	3338.62		43.92	57051
	1630.90				3340.35	26.42	26.42	57222
	1635.13	24.96	919.15	57.32	3343.00	19.34	33.88	57499
GI-16.2	1645.95	142.94	927.11	71.44	3348.89		107.19	58182
	1648.91	63.42	929.20	40.45	3350.32	37.96	47.28	58355
	1662.73	54.13	939.54	26.81	3357.90	25.74	35.56	59180
GI-17.2	1665.24	45.94	941.30	30.80	3359.30	114.73	63.83	59317
GS-18	1670.14	36.75	944.59	54.37	3361.90	29.50	40.20	59545
	1672.31	106.50	946.10	52.66	3362.95	24.53	61.23	59647

A.6.

Bipolar glacial eruptions with known source							
<i>Eruption</i>	<i>Region</i>	<i>Age (b2k)</i>	<i>Latitude</i>	<i>VEI</i>	<i>SO₄ dep. Grl. (kg/km²)</i>	<i>SO₄ dep. Ant. (kg/km²)</i>	<i>Ref.</i>
<i>Vedde</i>	Iceland	12170	64°416'N		271.04	12.33	(Grönvold <i>et al.</i> , 1995; Lane <i>et al.</i> , 2012)
<i>Oruanui (Taupo)</i>	New Zealand	25460	38°82'S	8	193.78	301.41	(Mason, Pyle and Oppenheimer, 2004; Dunbar <i>et al.</i> , 2017)
<i>NAAZ II</i>	Iceland	55383	64°416'N		1289.99	16.61	(Grönvold <i>et al.</i> , 1995; Guillou <i>et al.</i> , 2019)
Bipolar glacial eruptions with source speculation							
<i>Laacher</i>	Germany	12917	50°17'N		265.58	63.16	(Brauer, Endres and Negendank, 1999; Baldini, Brown and Mawdsley, 2018; Svensson <i>et al.</i> , 2020)
<i>Campi Flegrei</i>	Italy	29678/29722	40°83'N	6	445.02/229.41	192.89/28.38	(Albert <i>et al.</i> , 2019; Svensson <i>et al.</i> , 2020)
<i>Campanian Ignimbrite</i>	Italy	39869/39915	40°83'N		259.24/391.27	65.32/46.15	(Giaccio <i>et al.</i> , 2017; Svensson <i>et al.</i> , 2020)
Bipolar historical eruptions with known source							
<i>Eruption</i>	<i>Region</i>	<i>Age (AD/BC)</i>	<i>Latitude</i>	<i>VEI</i>	<i>SO₄ dep. Grl. (kg/km²)</i>	<i>SO₄ dep. Ant. (kg/km²)</i>	<i>Ref.</i>
Tambora	Indonesia	1815 AD	8°25'S	7	39.7	45.8	(Sigl <i>et al.</i> , 2013, 2015)
Samalas	Indonesia	1257 AD	8°42'S	7	82.1	79.7	(Lavigne <i>et al.</i> , 2013)

A.7.

GICC05 AGE(B2K)	AVG. SO4 (KG/KM2) GREENLAND	AVG. SO4 (KG/KM2) ANTARCTICA	GLOBAL AVG.
12170	271.041781	12.33117281	141.69
12241	67.920418	30.13711913	49.03
12755	161.2248812	21.8071396	91.52
12917	265.6797202	63.15946086	164.42
12961	73.48596676	17.40760103	45.45
12995	58.04793476	27.82651031	42.94
13028	298.0128486	68.11957464	183.07
13212	46.38514051	47.65400267	47.02
13620	420.5508138	42.43375128	231.49
14500	144.8752908	44.01273354	94.44
14705	91.60318225	39.38867707	65.50
14761	335.3682976	9.837626485	172.60
14966	82.71487935	75.91457258	79.31
15296	149.6644124	14.37304853	82.02
15559	95.20363893	75.31998825	85.26
16469	112.27554	98.55146755	105.41
24669	190.1347865	59.77922398	124.96
25460	193.7795351	301.4144516	247.60
25759	223.518797	116.5502249	170.03
25940	155.4353103	6.042815908	80.74
27797	444.3987046	16.02488918	230.21
28454	173.9332046	28.31278034	101.12
28942	79.9770811	89.15132578	84.56
29678	445.0197915	192.8878899	318.95
29722	229.414236	28.37685117	128.90
30244	229.1490092	40.97868963	135.06
32032	234.0140834	165.7901317	199.90
32433	20.81079776	62.41299029	41.61
33221	51.09259437	46.16805634	48.63
33328	66.71958505	67.85867694	67.29
34227	82.3608497		
34718	365.237954	53.10302341	209.17
35145	55.73506662	47.57681216	51.66
35556	148.8006654	44.27111191	96.54
37113	105.4440885	70.14246764	87.79
37277	96.72710441	29.36427635	63.05
37965	87.5670234	47.99491929	67.78
38133	260.1988034	178.2726387	219.24
38232	39.14992224	46.01403918	42.58
38366	219.7984113	20.36894575	120.08
39869	259.2425791	65.3185581	162.28
39915	391.2722196	46.1507971	218.71
40183	286.0874515	53.01272222	169.55

40563			
40794			
41002		2.144948261	2.14
41144	448.333271	80.26512386	264.30
41379	60.17934448	38.50408429	49.34
41858		26.1480065	26.15
41887		28.08714334	28.09
42037	331.1993933	131.3556572	231.28
42067	7.889646415		7.89
42111	27.06499078	94.29072291	60.68
42250	184.0088448	82.91366239	133.46
42658	137.1842118	127.7929883	132.49
43104	85.07804231	22.68624695	53.88
43327		63.92348908	63.92
44507	96.57688167	76.89919714	86.74
45050	72.26008002	60.93340179	66.60
45555	685.3888548	216.1613426	450.78
46002	119.4483992	59.39531839	89.42
46116	78.8198972	114.1089363	96.46
46683	110.3829399	256.9808997	183.68
47023	286.9755566	58.16682871	172.57
47214	195.9223032	34.6125952	115.27
48441	38.06853771	37.46262259	37.77
49065	178.1189916	170.9766806	174.55
49319	67.40305609	50.26731529	58.84
50586	111.8142637	21.67612669	66.75
52031	61.64492433	50.22823958	55.94
52302	336.1992777	183.2390065	259.72
53259	165.4039964	61.19388221	113.30
54178	83.17856823	25.41703247	54.30
54390	123.9735233	18.44949995	71.21
55005	16.31523342	32.21103074	24.26
55383	1283.985943	16.60738873	650.30
57051	78.98517717	43.91648844	61.45
57222	121.6492344	26.42136479	74.04
57499	54.34983417	33.87613961	44.11
58182	149.6633821	107.1912895	128.43
58355	123.7189474	47.27548532	85.50
59180	13.87070173	35.56158479	24.72
59317	41.36531158	63.82510507	52.60
59545	127.9625167	40.20299981	84.08
59647	120.3862384	61.22963921	90.81

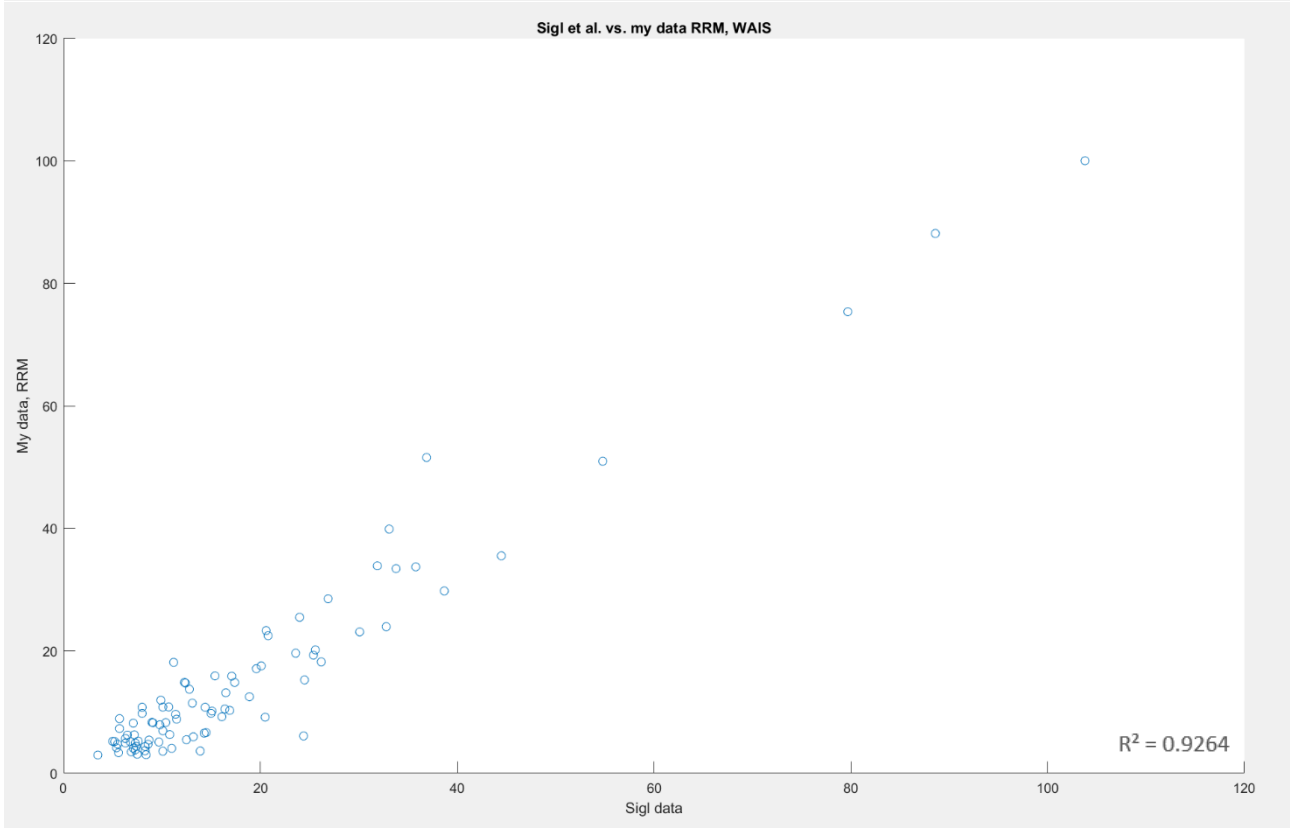
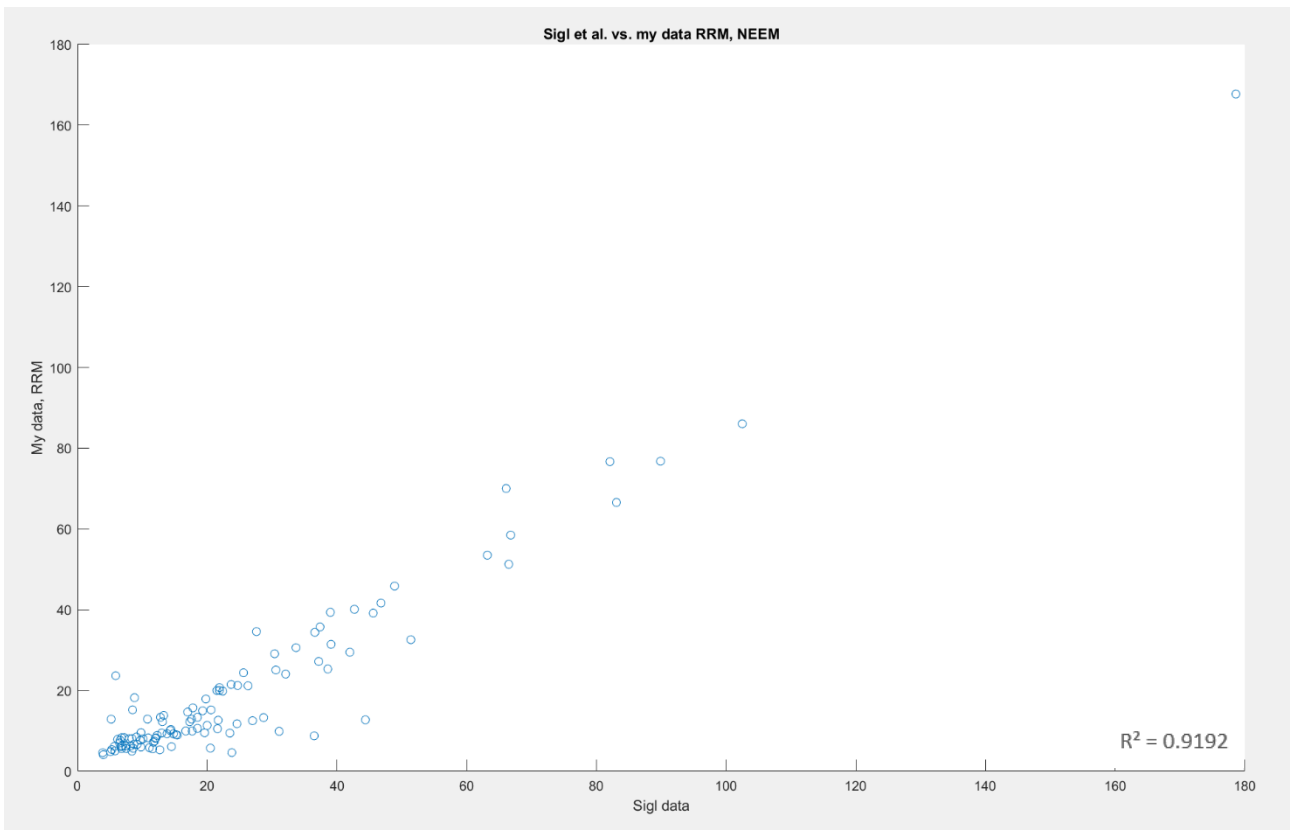
A.8.

GICC05 AGE(B2K)	AVG. SO4 (KG/KM2) GREENLAND	AVG. SO4 (KG/KM2) ANTARCTICA	HEMISPHERIC DIFFERENCE (G- A)
	NH eruptions (>30°N)		
55383	1283.985943	16.60738873	1267.378554
45555	685.3888548	216.1613426	469.2275122
27797	444.3987046	16.02488918	428.3738154
13620	420.5508138	42.43375128	378.1170625
41144	448.333271	80.26512386	368.0681472
39915	391.2722196	46.1507971	345.1214225
14761	335.3682976	9.837626485	325.5306711
34718	365.237954	53.10302341	312.1349306
41002	363.9594904	2.144948261	361.8145421
12170	271.041781	12.33117281	258.7106082
29678	445.0197915	192.8878899	252.1319016
40183	286.0874515	53.01272222	233.0747293
13028	298.0128486	68.11957464	229.893274
47023	286.9755566	58.16682871	228.8087279
12917	265.6797202	63.15946086	202.5202593
29722	229.414236	28.37685117	201.0373848
42037	331.1993933	131.3556572	199.8437362
38366	219.7984113	20.36894575	199.4294656
39869	259.2425791	65.3185581	193.924021
30244	229.1490092	40.97868963	188.1703196
41887	346.1121255	28.08714334	318.0249821
47214	195.9223032	34.6125952	161.309708
52302	336.1992777	183.2390065	152.9602713
25940	155.4353103	6.042815908	149.3924944
28454	173.9332046	28.31278034	145.6204242
12755	161.2248812	21.8071396	139.4177416
15296	149.6644124	14.37304853	135.2913639
24669	190.1347865	59.77922398	130.3555625
43327	267.9460374	63.92348908	204.0225483
25759	223.518797	116.5502249	106.9685721
54390	123.9735233	18.44949995	105.5240233
35556	148.8006654	44.27111191	104.5295534
53259	165.4039964	61.19388221	104.2101142
42250	184.0088448	82.91366239	101.0951824
14500	144.8752908	44.01273354	100.8625573
	Tropical eruptions (30°N - 30°S)		
57222	121.6492344	26.42136479	95.22786963
50586	111.8142637	21.67612669	90.13813703
59545	127.9625167	40.20299981	87.75951694
38133	260.1988034	178.2726387	81.92616464
58355	123.7189474	47.27548532	76.44346211

32032	234.0140834	165.7901317	68.22395173
37277	96.72710441	29.36427635	67.36282806
43104	85.07804231	22.68624695	62.39179536
46002	119.4483992	59.39531839	60.05308081
59647	120.3862384	61.22963921	59.15659923
54178	83.17856823	25.41703247	57.76153576
12961	73.48596676	17.40760103	56.07836573
14705	91.60318225	39.38867707	52.21450518
58182	149.6633821	107.1912895	42.47209253
37965	87.5670234	47.99491929	39.57210411
12241	67.920418	30.13711913	37.78329888
37113	105.4440885	70.14246764	35.30162081
57051	78.98517717	43.91648844	35.06868873
12995	58.04793476	27.82651031	30.22142445
41379	60.17934448	38.50408429	21.67526019
57499	54.34983417	33.87613961	20.47369456
15559	95.20363893	75.31998825	19.88365068
44507	96.57688167	76.89919714	19.67768453
49319	67.40305609	50.26731529	17.1357408
16469	112.27554	98.55146755	13.72407241
52031	61.64492433	50.22823958	11.41668475
45050	72.26008002	60.93340179	11.32667823
42658	137.1842118	127.7929883	9.39122353
35145	55.73506662	47.57681216	8.158254466
42067	7.889646415		7.889646415
49065	178.1189916	170.9766806	7.142310967
14966	82.71487935	75.91457258	6.800306772
33221	51.09259437	46.16805634	4.924538034
48441	38.06853771	37.46262259	0.605915114
33328	66.71958505	67.85867694	-1.139091895
13212	46.38514051	47.65400267	-1.268862165
38232	39.14992224	46.01403918	-6.864116935
28942	79.9770811	89.15132578	-9.174244682
55005	16.31523342	32.21103074	-15.89579731
59180	13.87070173	35.56158479	-21.69088307
59317	41.36531158	63.82510507	-22.4597935
41858		26.1480065	-26.1480065
46116	78.8198972	114.1089363	-35.28903909
32433	20.81079776	62.41299029	-41.60219253
42111	27.06499078	94.29072291	-67.22573213
	SH eruptions (>30°S)		
25460	193.7795351	301.4144516	-107.6349165
46683	110.3829399	256.9808997	-146.5979598

Appendix B

B.1.



B.2.

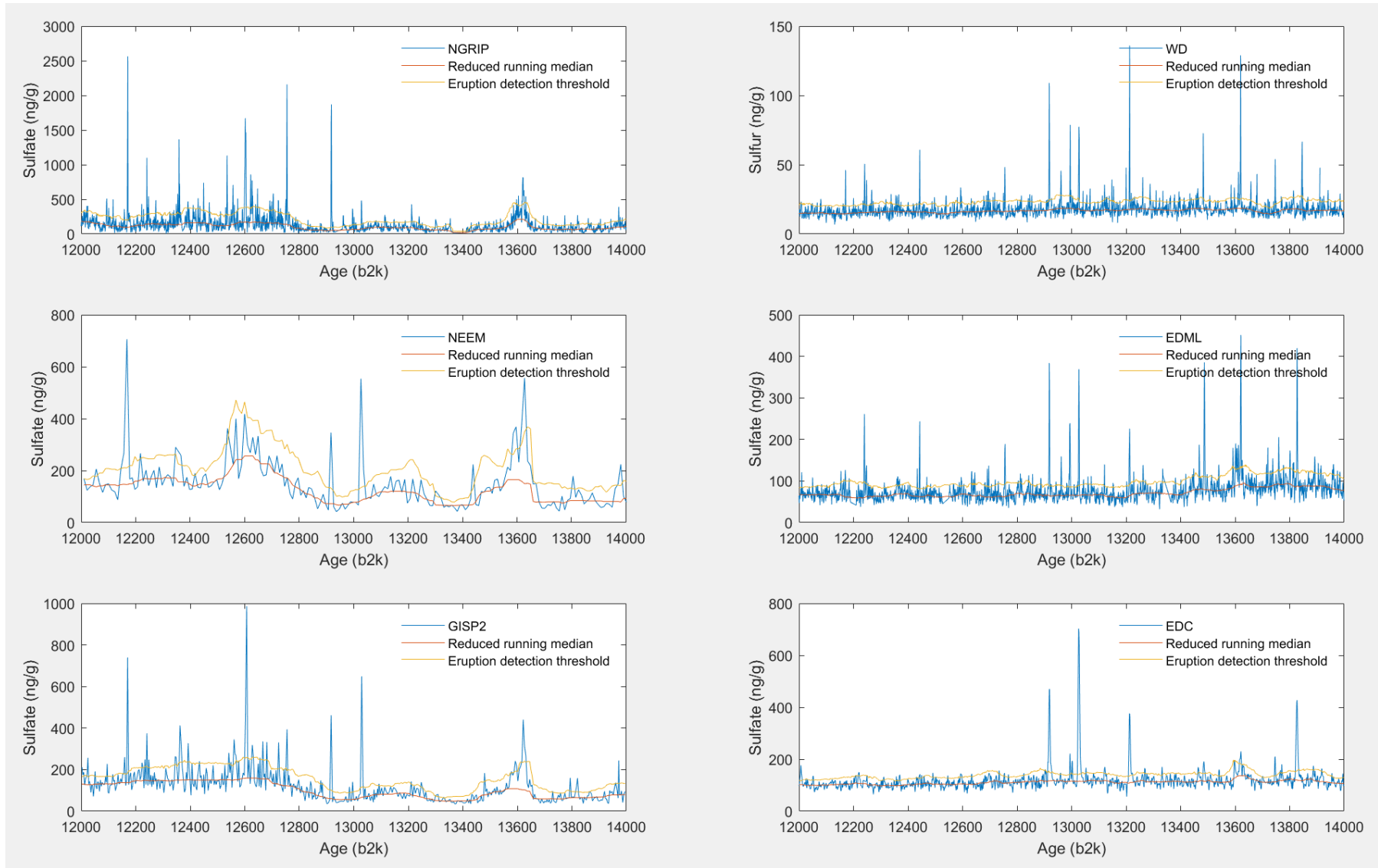


Figure 30: Record showing the sulfate concentration (WD showing sulfur) spanning 12000-14000 b2k for all six ice cores (Greenland left, Antarctica right)

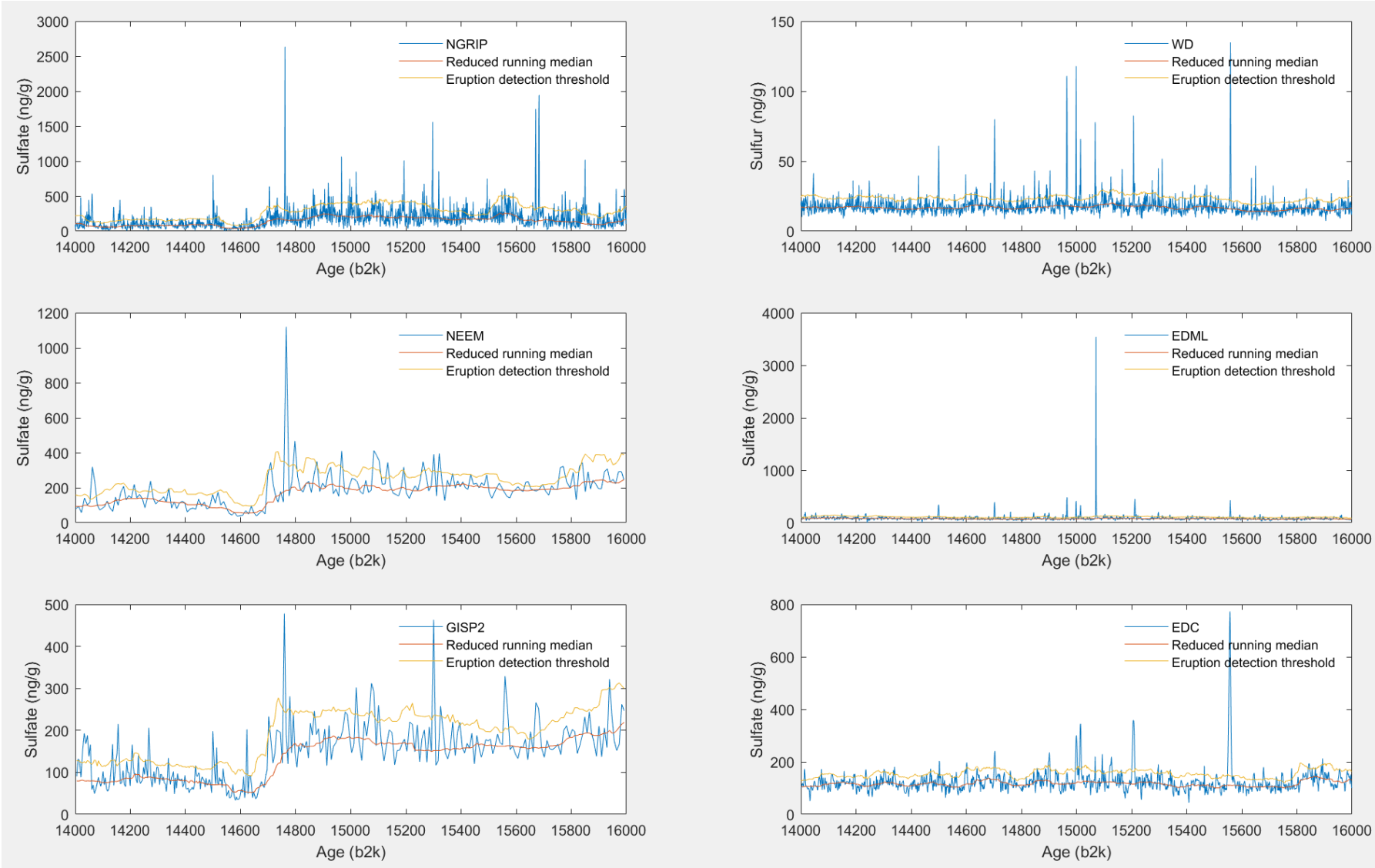


Figure 31: Record showing the sulfate concentration (WD showing sulfur) spanning 14000-16000 b2k for all six ice cores (Greenland left, Antarctica right)

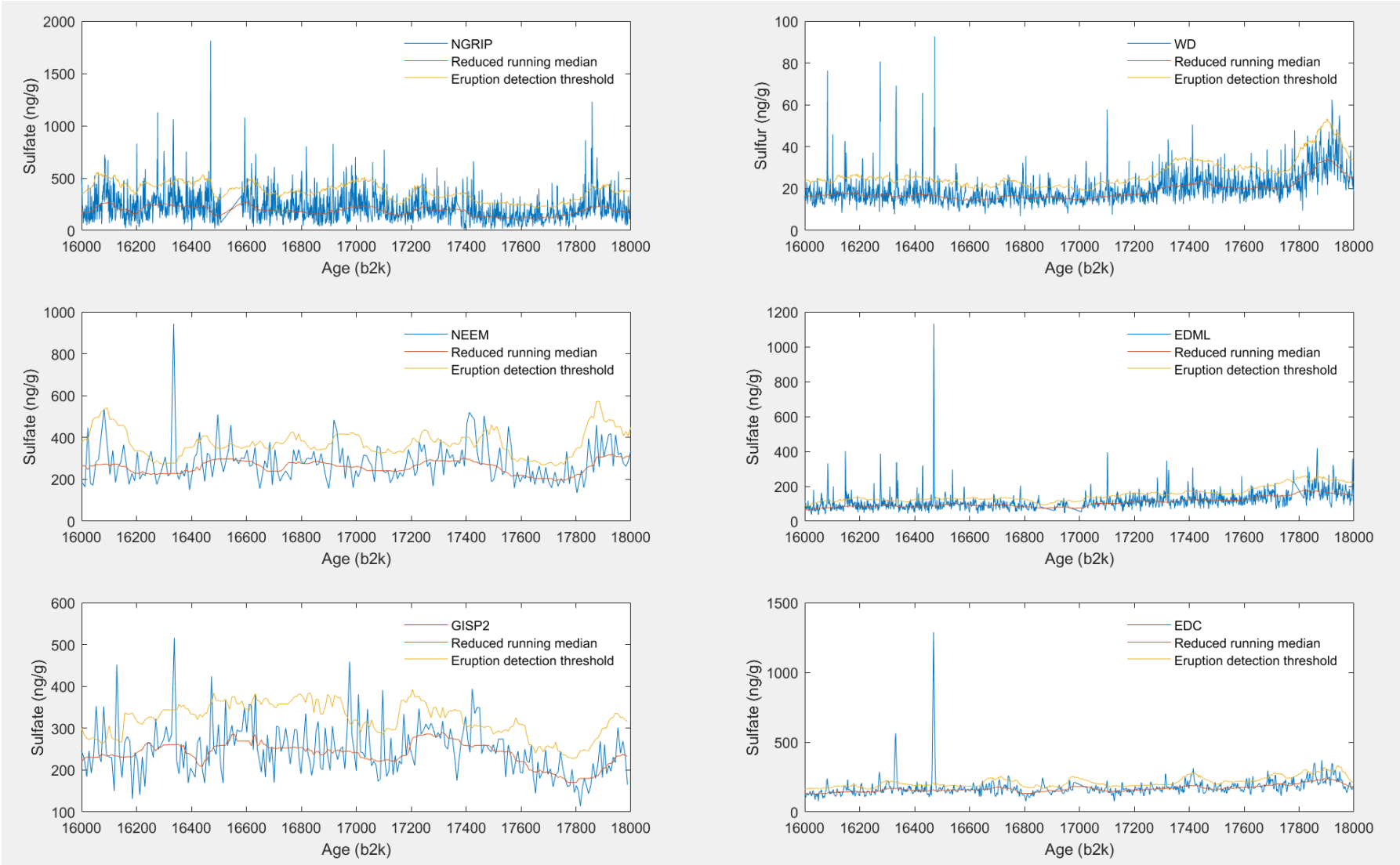


Figure 32: Record showing the sulfate concentration (WD showing sulfur) spanning 16000-18000 b2k for all six ice cores (Greenland left, Antarctica right)

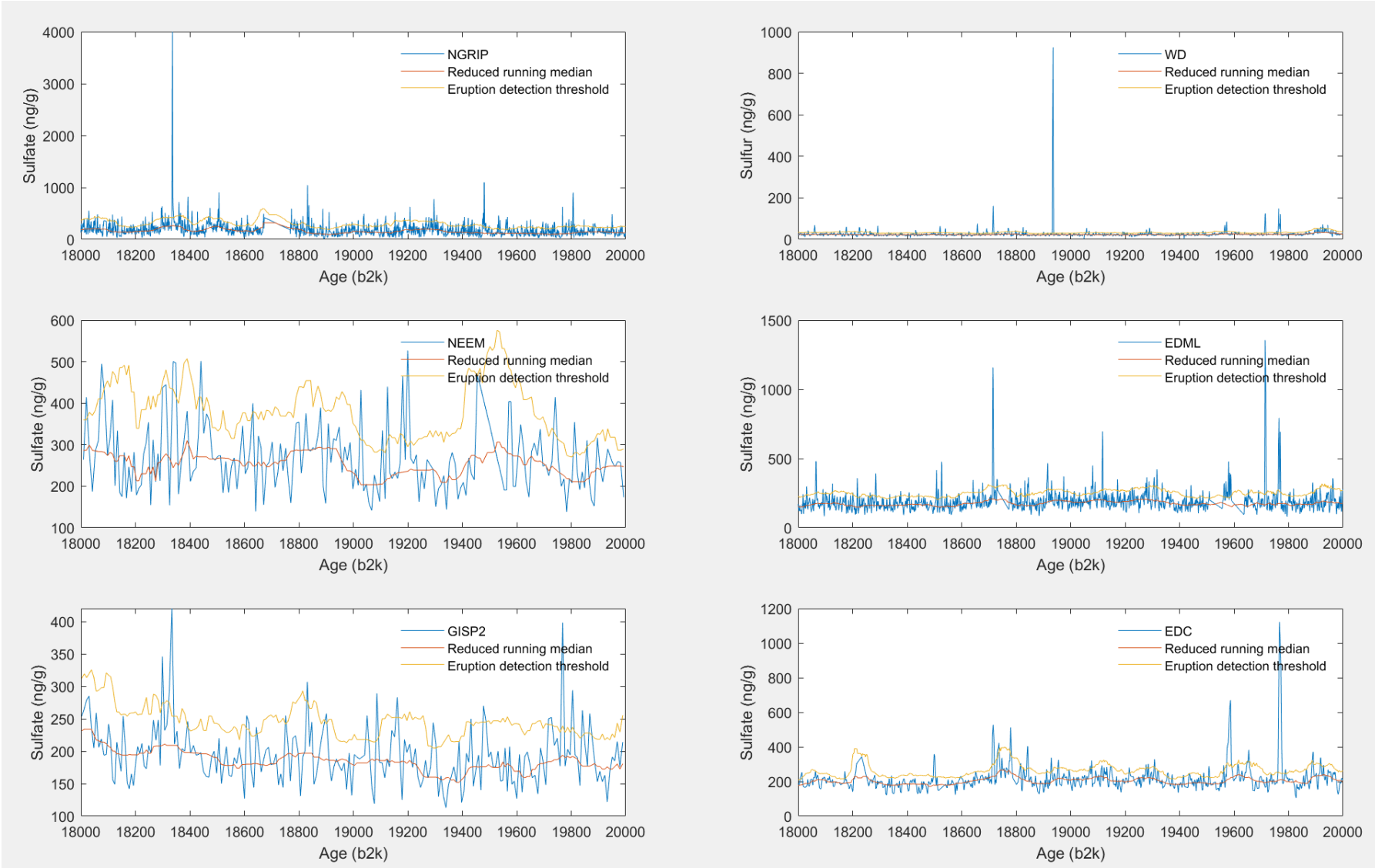


Figure 33: Record showing the sulfate concentration (WD showing sulfur) spanning 18000-20000 b2k for all six ice cores (Greenland left, Antarctica right)

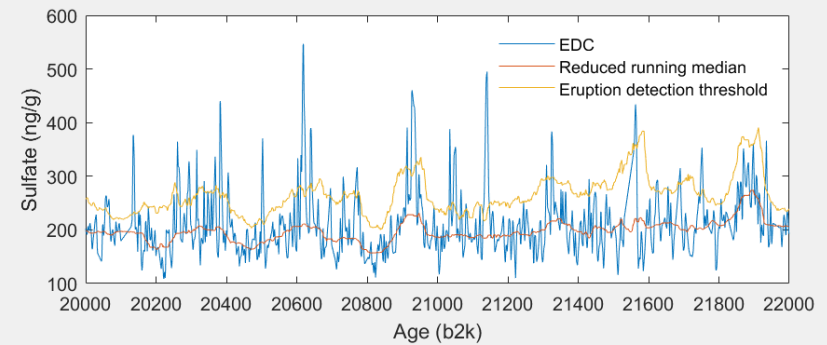
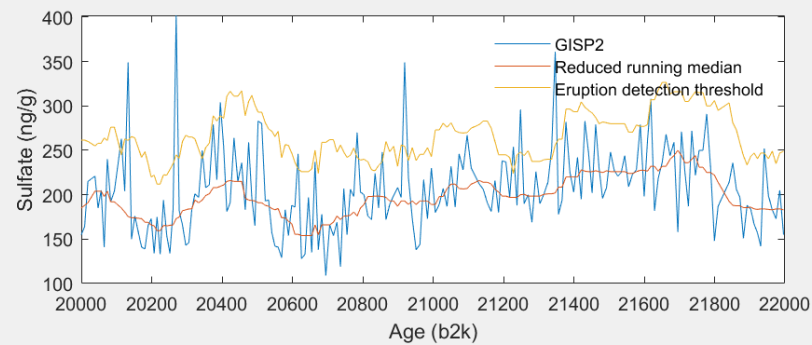
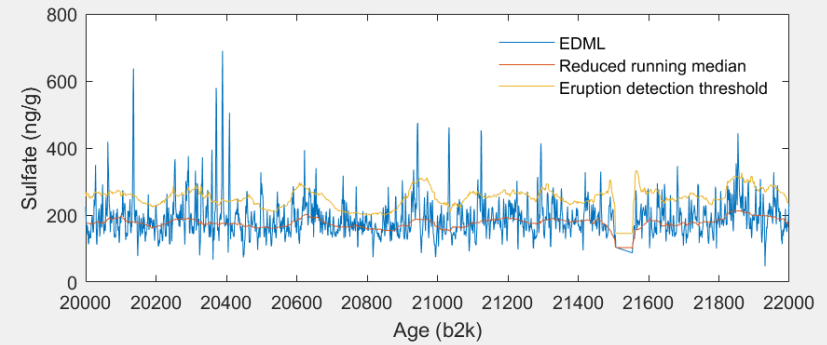
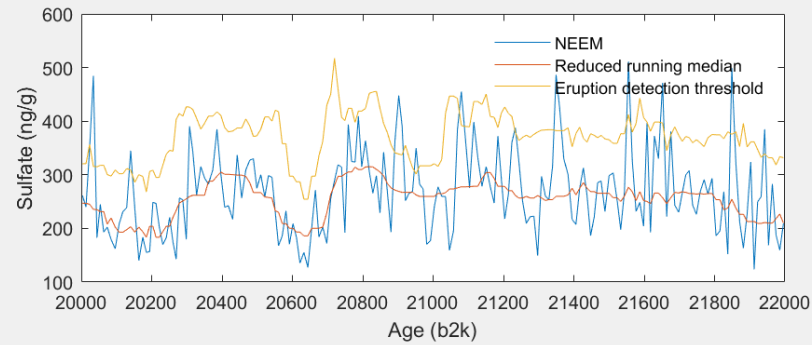
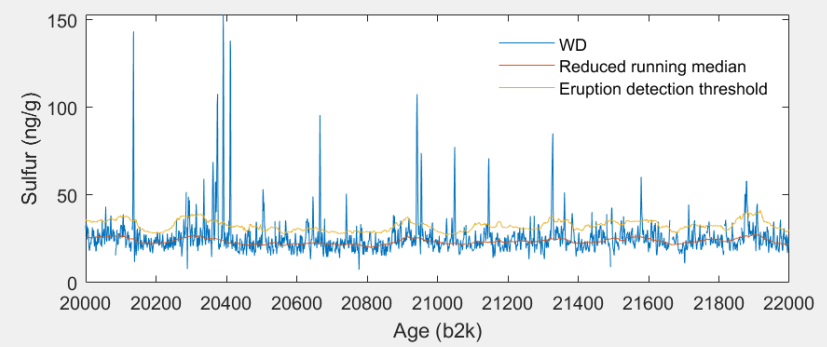
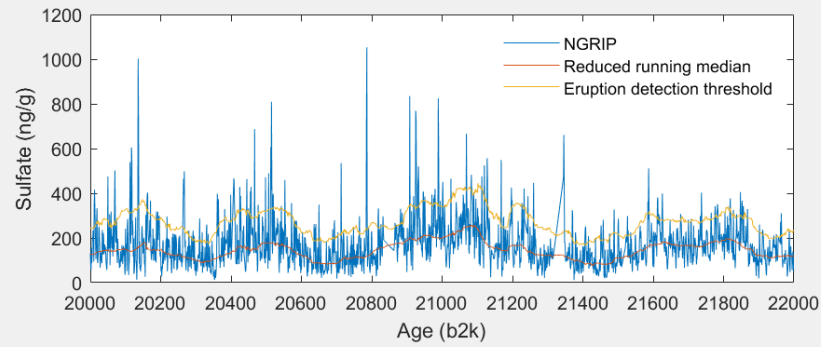


Figure 34: Record showing the sulfate concentration (WD showing sulfur) spanning 20000-22000 b2k for all six ice cores (Greenland left, Antarctica right)

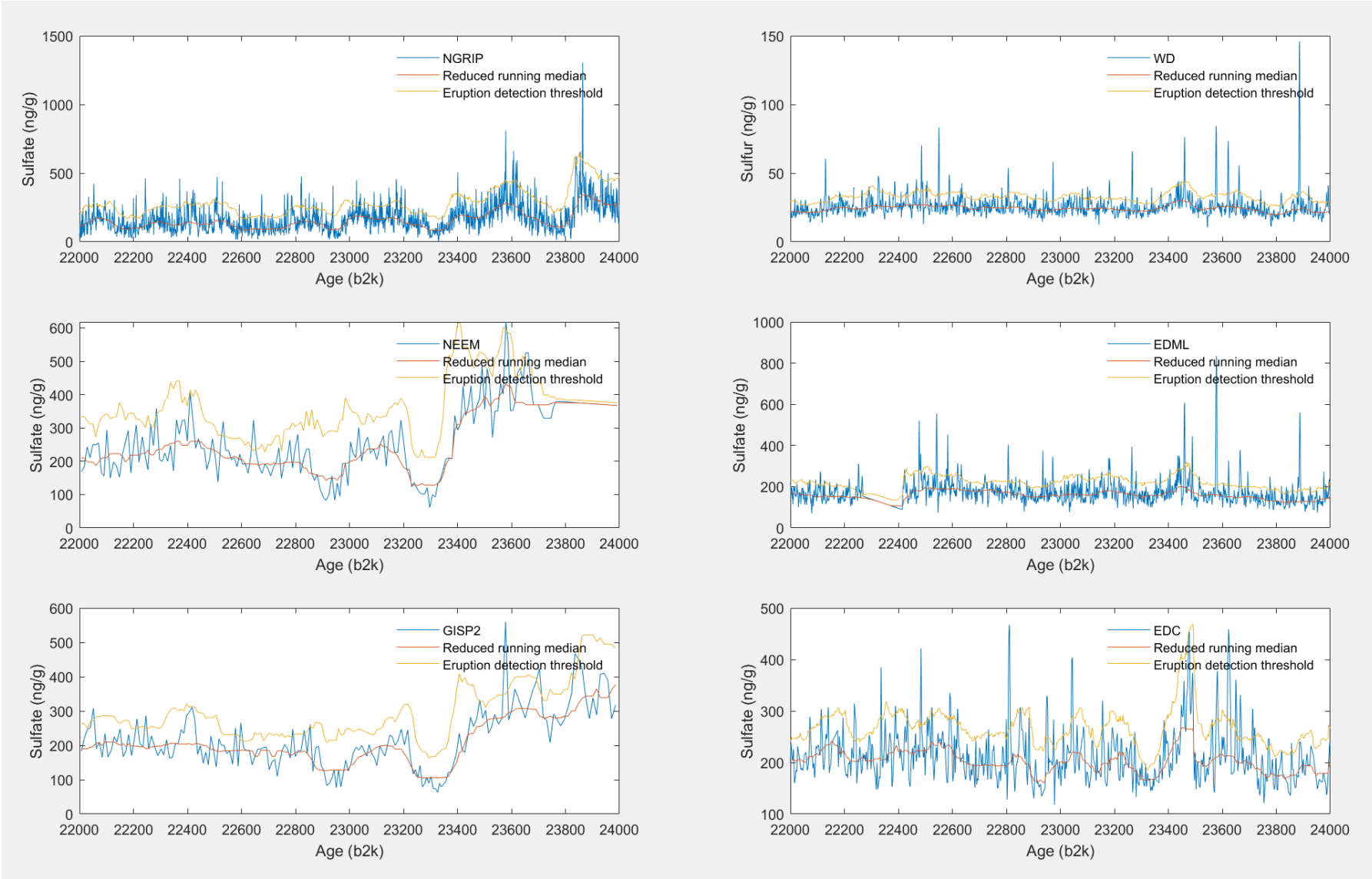


Figure 35: Record showing the sulfate concentration (WD showing sulfur) spanning 22000-24000 b2k for all six ice cores (Greenland left, Antarctica right)

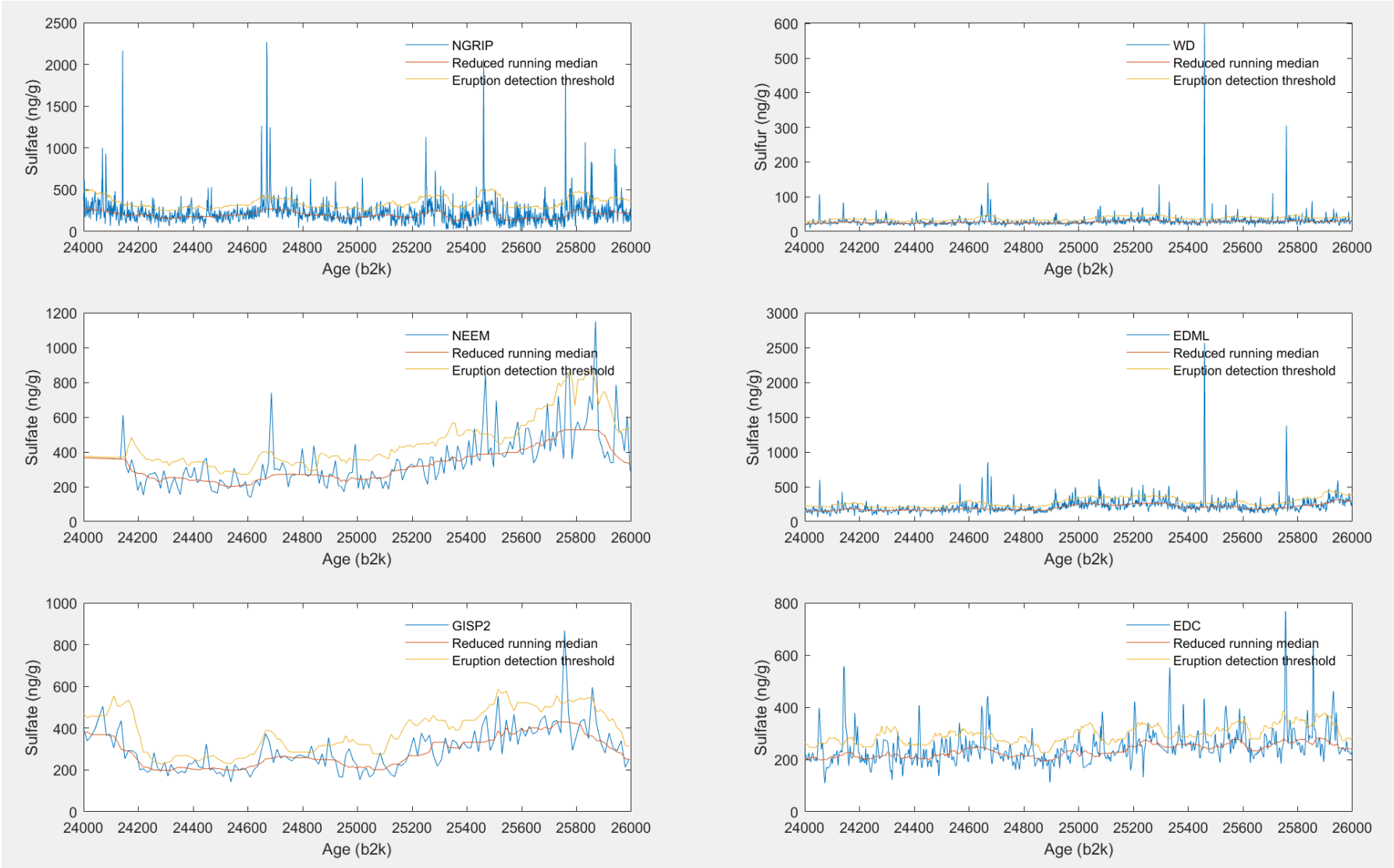


Figure 36: : Record showing the sulfate concentration (WD showing sulfur) spanning 24000-26000 b2k for all six ice cores (Greenland left, Antarctica right)

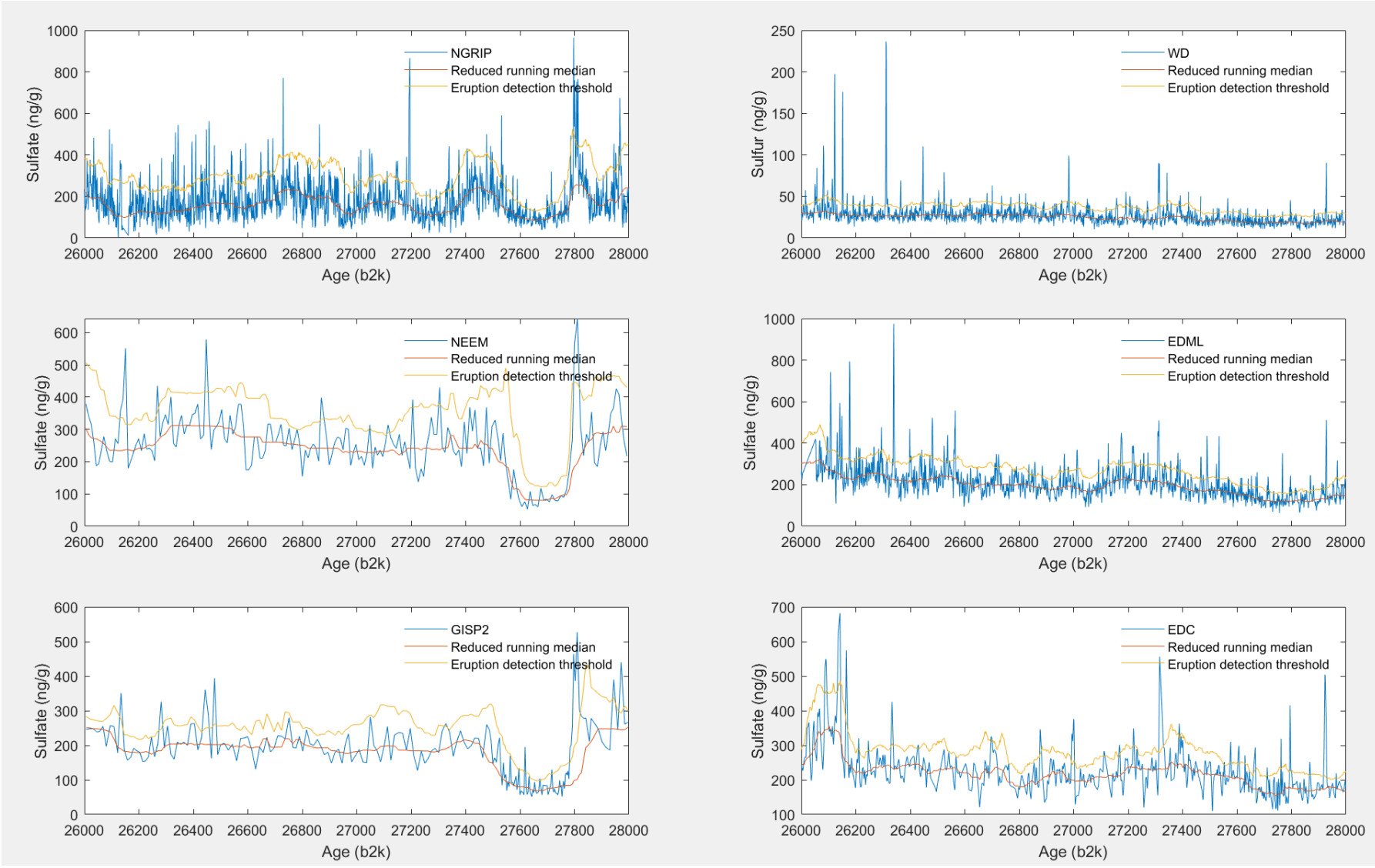


Figure 37: Record showing the sulfate concentration (WD showing sulfur) spanning 26000-28000 b2k for all six ice cores (Greenland left, Antarctica right)

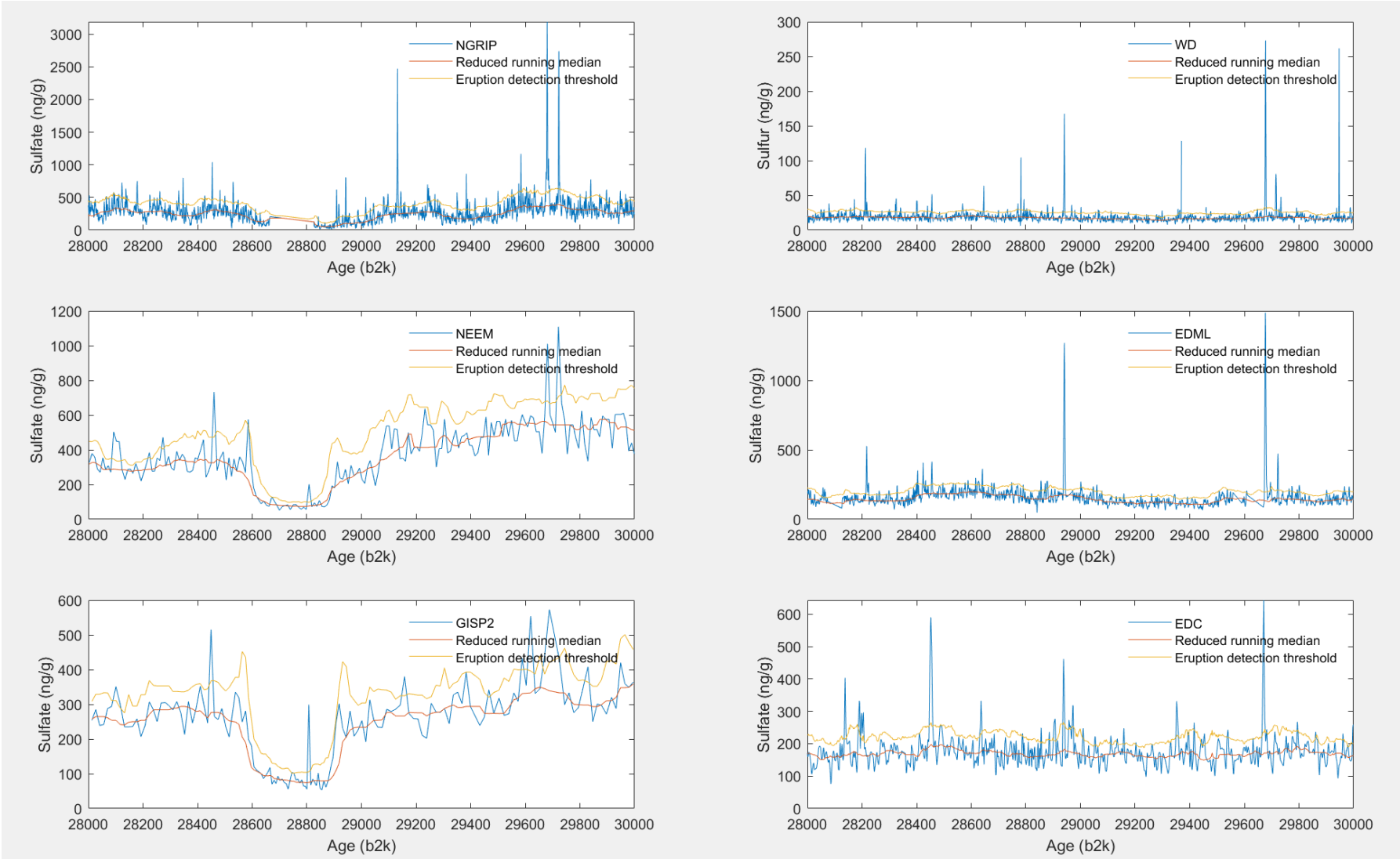


Figure 38: Record showing the sulfate concentration (WD showing sulfur) spanning 28000-30000 b2k for all six ice cores (Greenland left, Antarctica right)

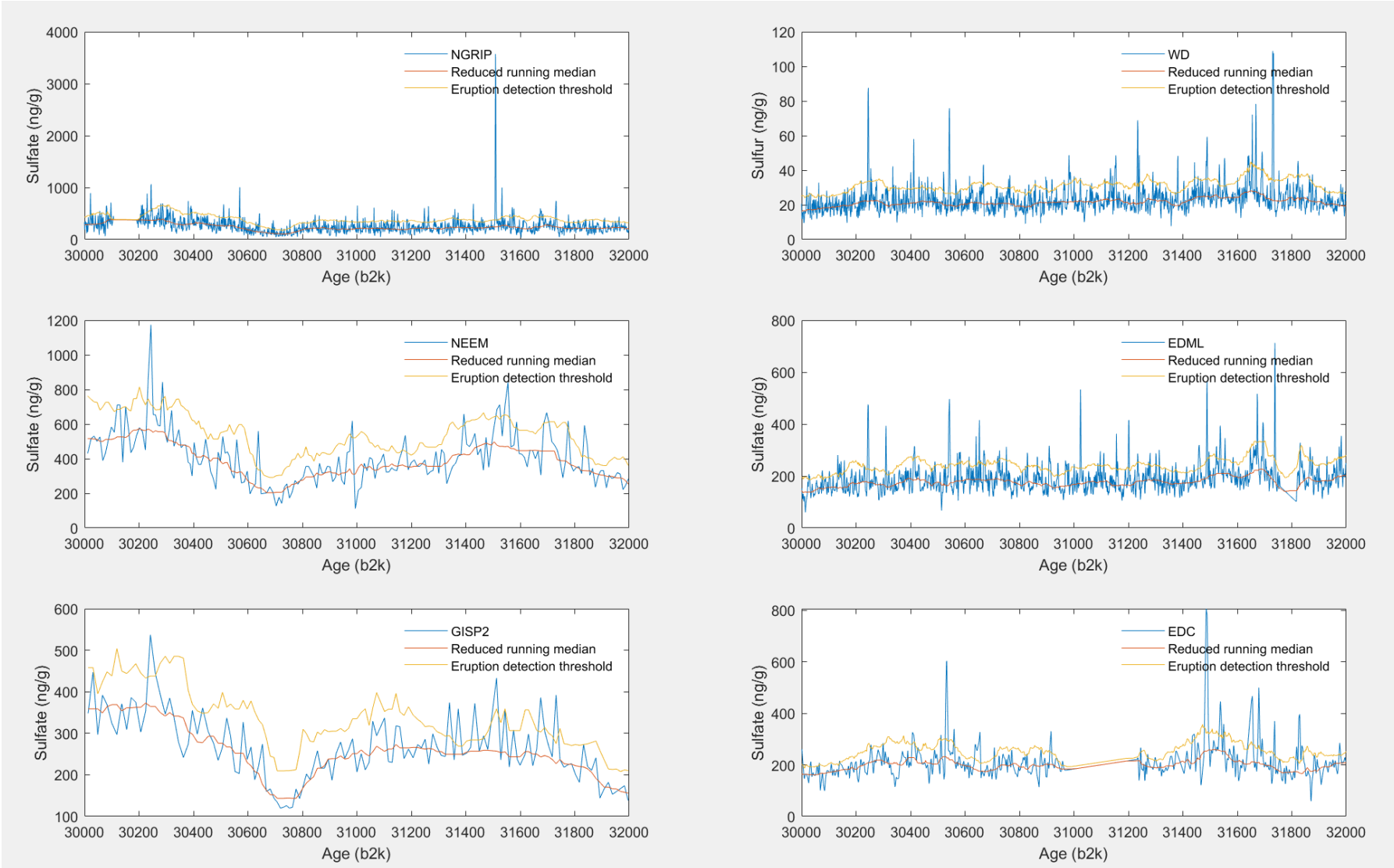


Figure 39: Record showing the sulfate concentration (WD showing sulfur) spanning 30000-32000 b2k for all six ice cores (Greenland left, Antarctica right)

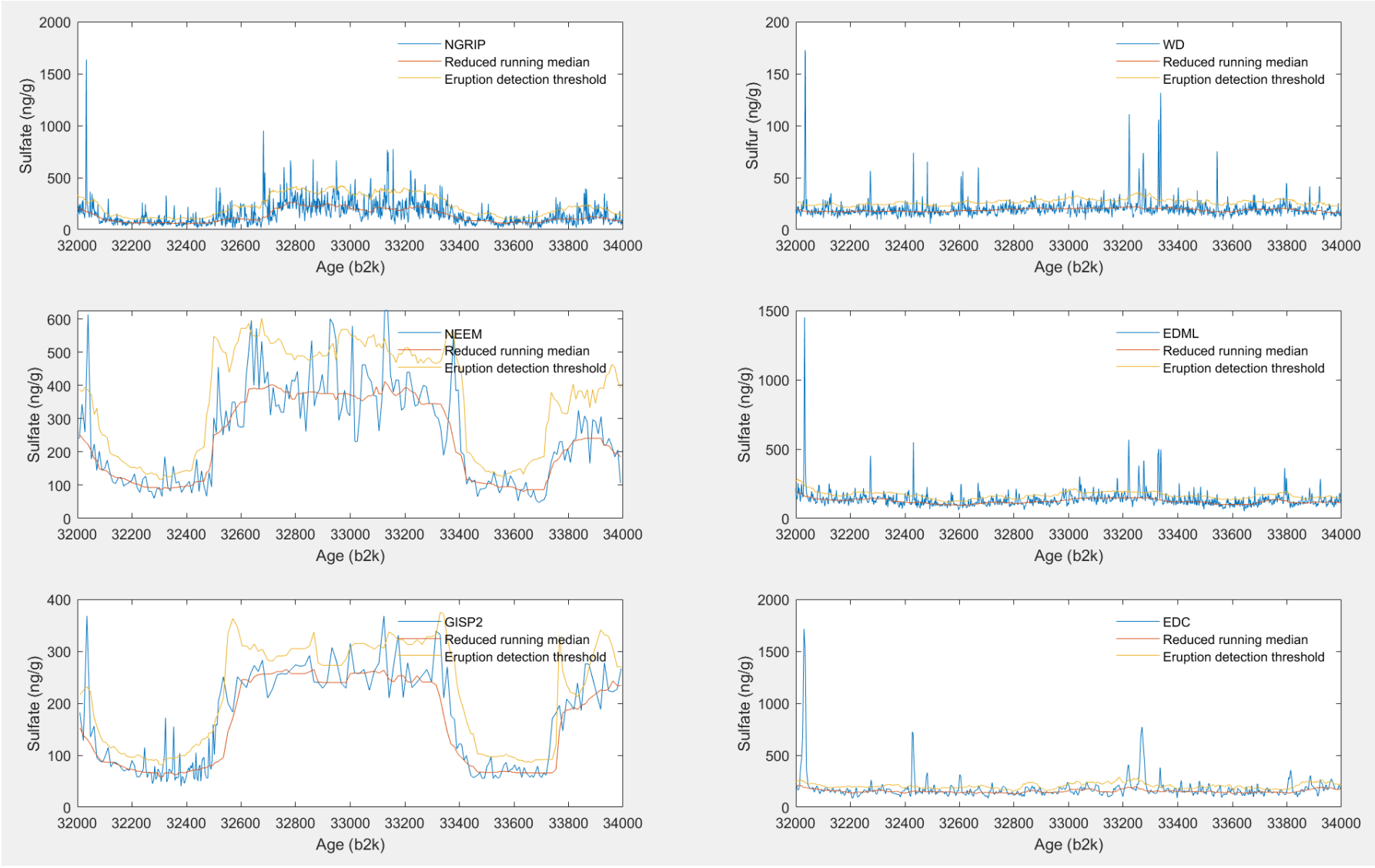


Figure 40: Record showing the sulfate concentration (WD showing sulfur) spanning 32000-34000 b2k for all six ice cores (Greenland left, Antarctica right)

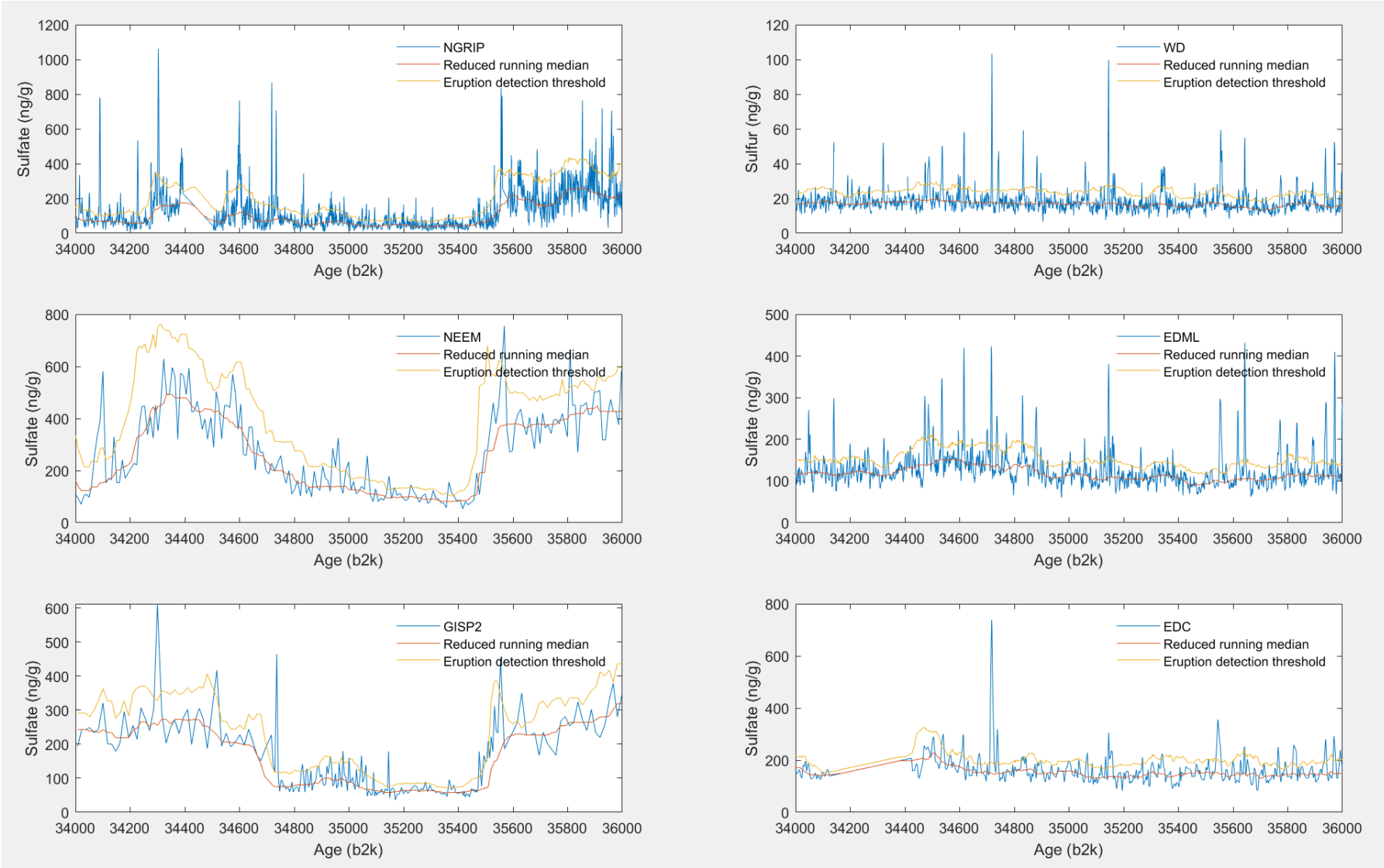


Figure 41: Record showing the sulfate concentration (WD showing sulfur) spanning 34000-36000 b2k for all six ice cores (Greenland left, Antarctica right)

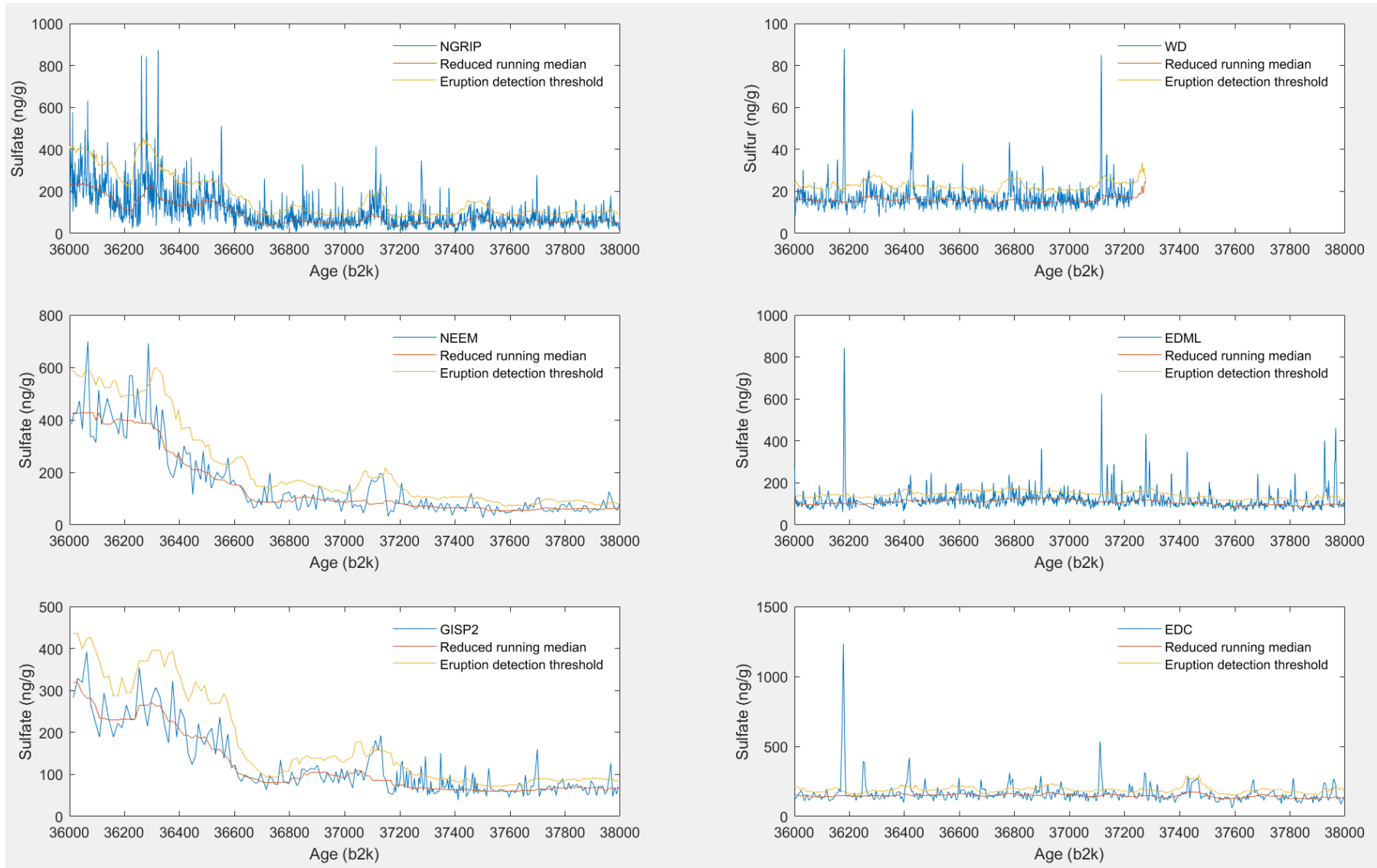


Figure 42: Record showing the sulfate concentration (WD showing sulfur) spanning 36000-38000 b2k for all six ice cores (Greenland left, Antarctica right)

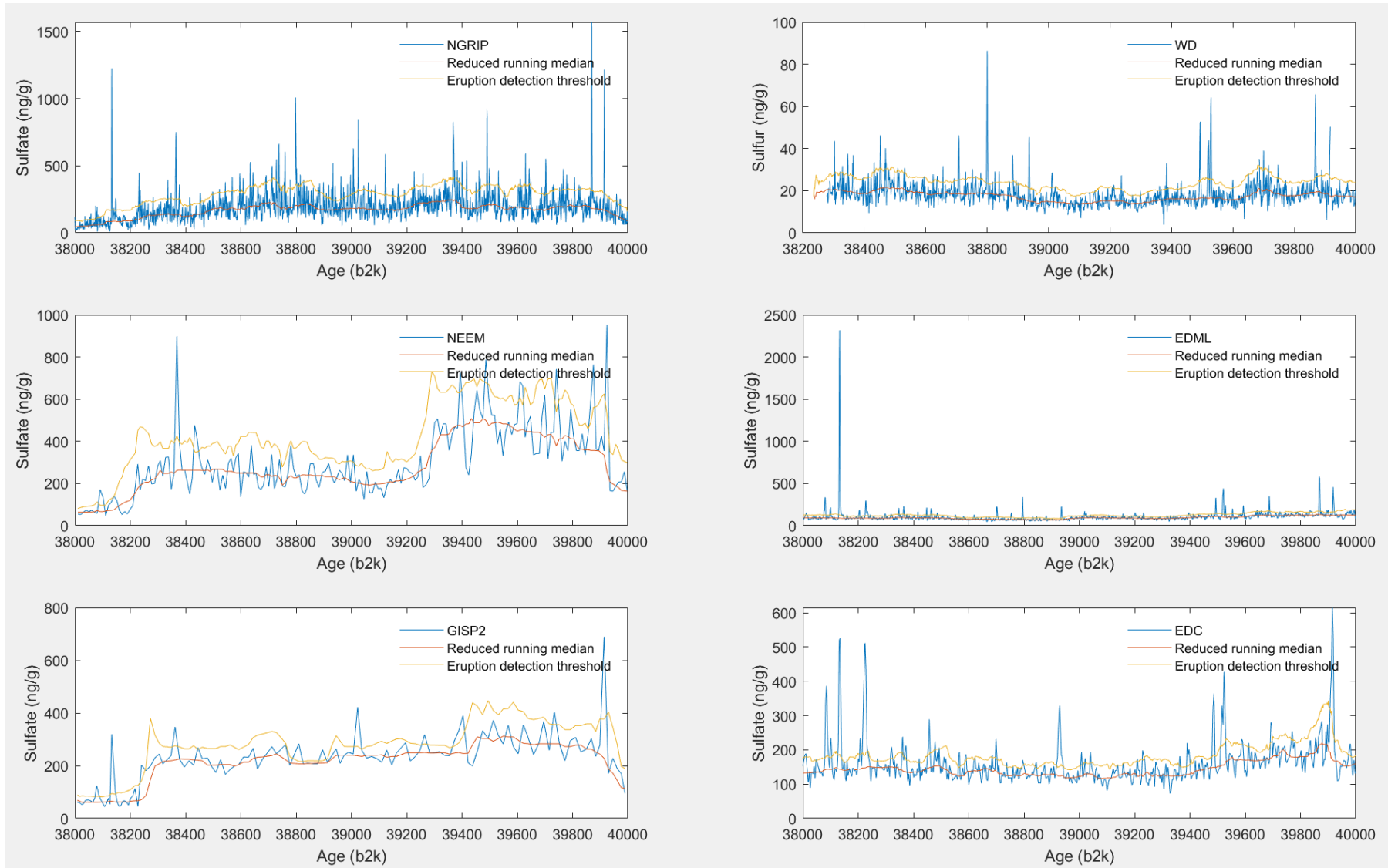


Figure 43: Record showing the sulfate concentration (WD showing sulfur) spanning 38000-40000 b2k for all six ice cores (Greenland left, Antarctica right)

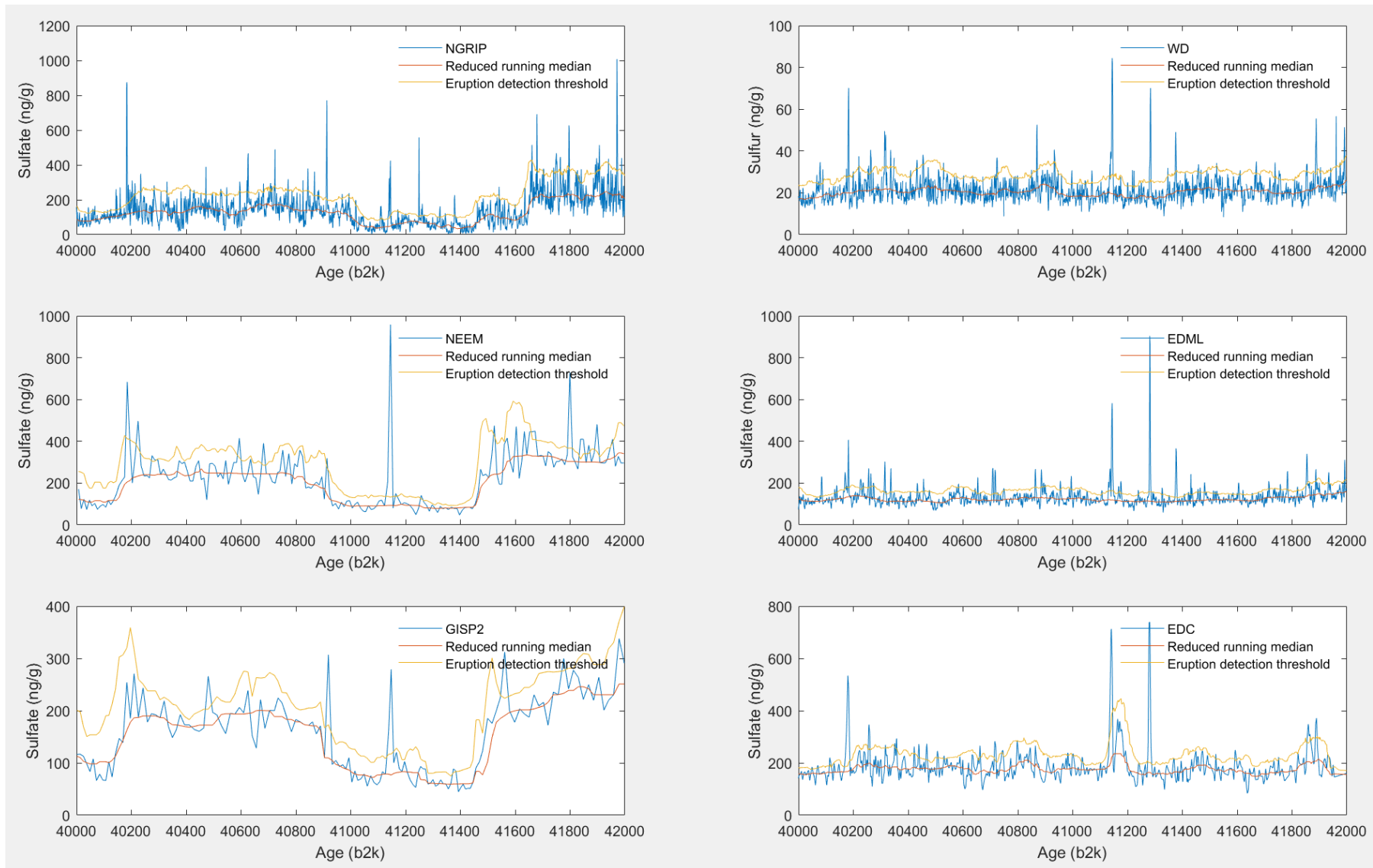


Figure 44: Record showing the sulfate concentration (WD showing sulfur) spanning 40000-42000 b2k for all six ice cores (Greenland left, Antarctica right)

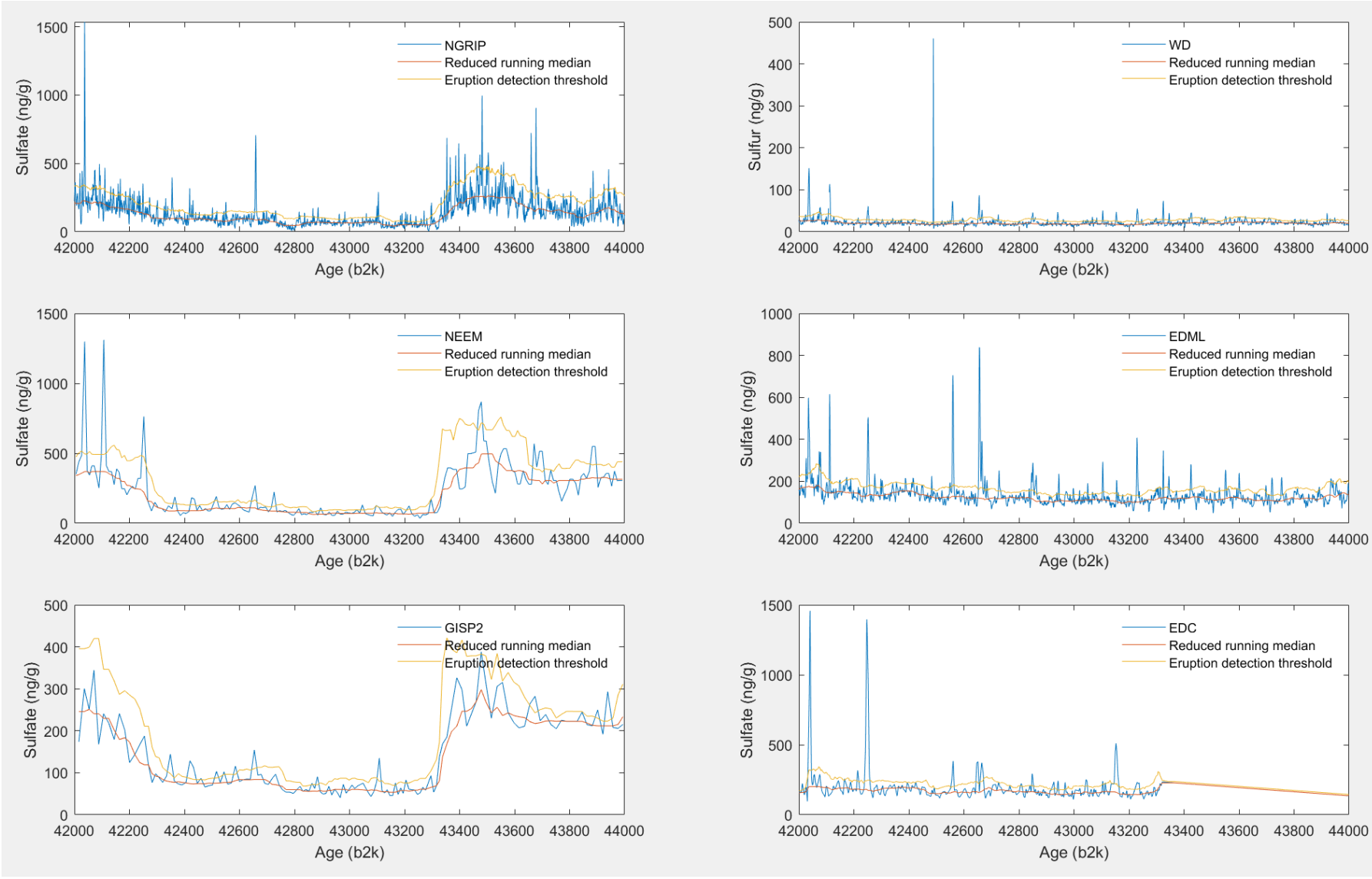


Figure 45: Record showing the sulfate concentration (WD showing sulfur) spanning 42000-44000 b2k for all six ice cores (Greenland left, Antarctica right)

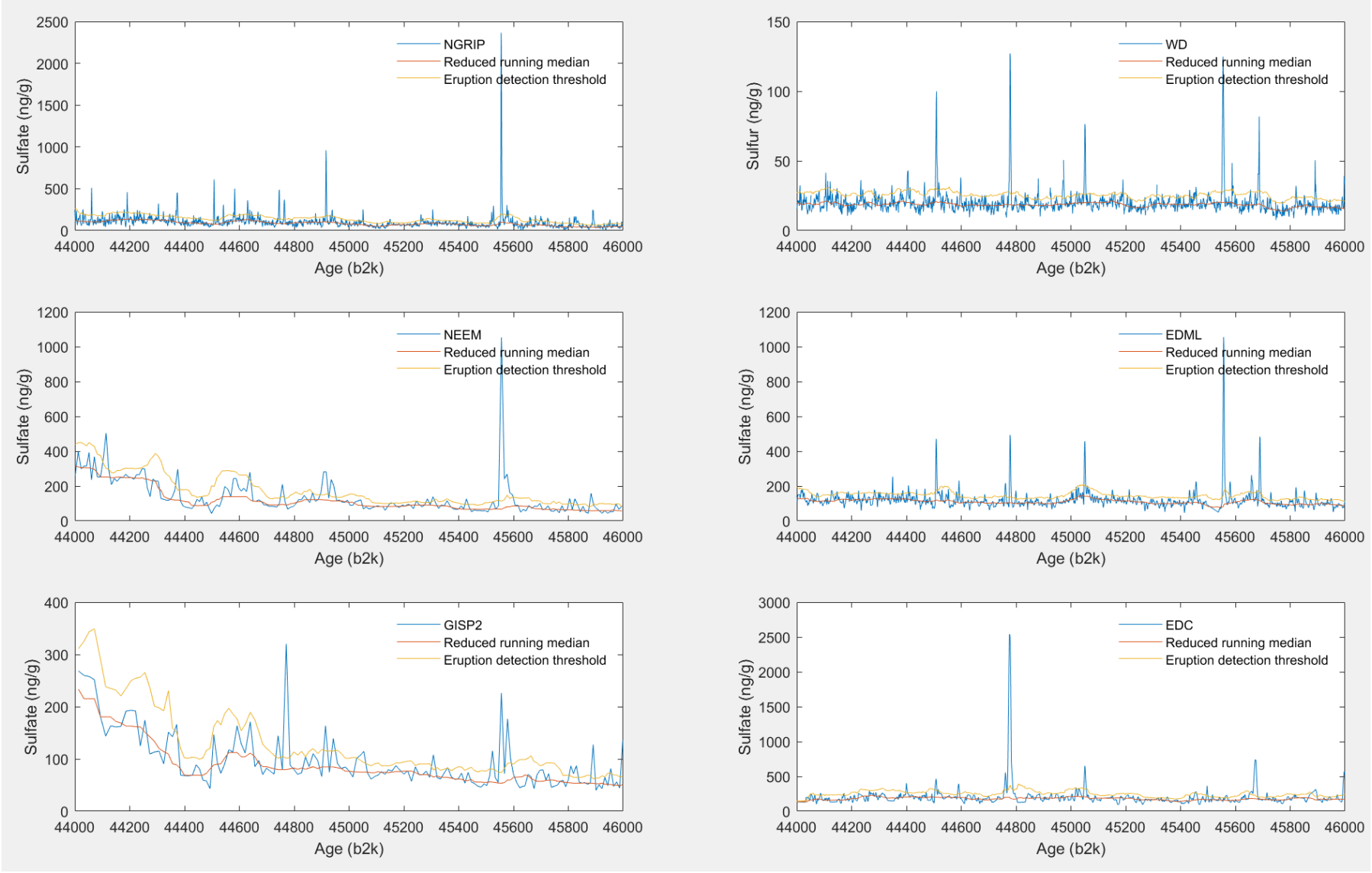


Figure 46: Record showing the sulfate concentration (WD showing sulfur) spanning 44000-46000 b2k for all six ice cores (Greenland left, Antarctica right)

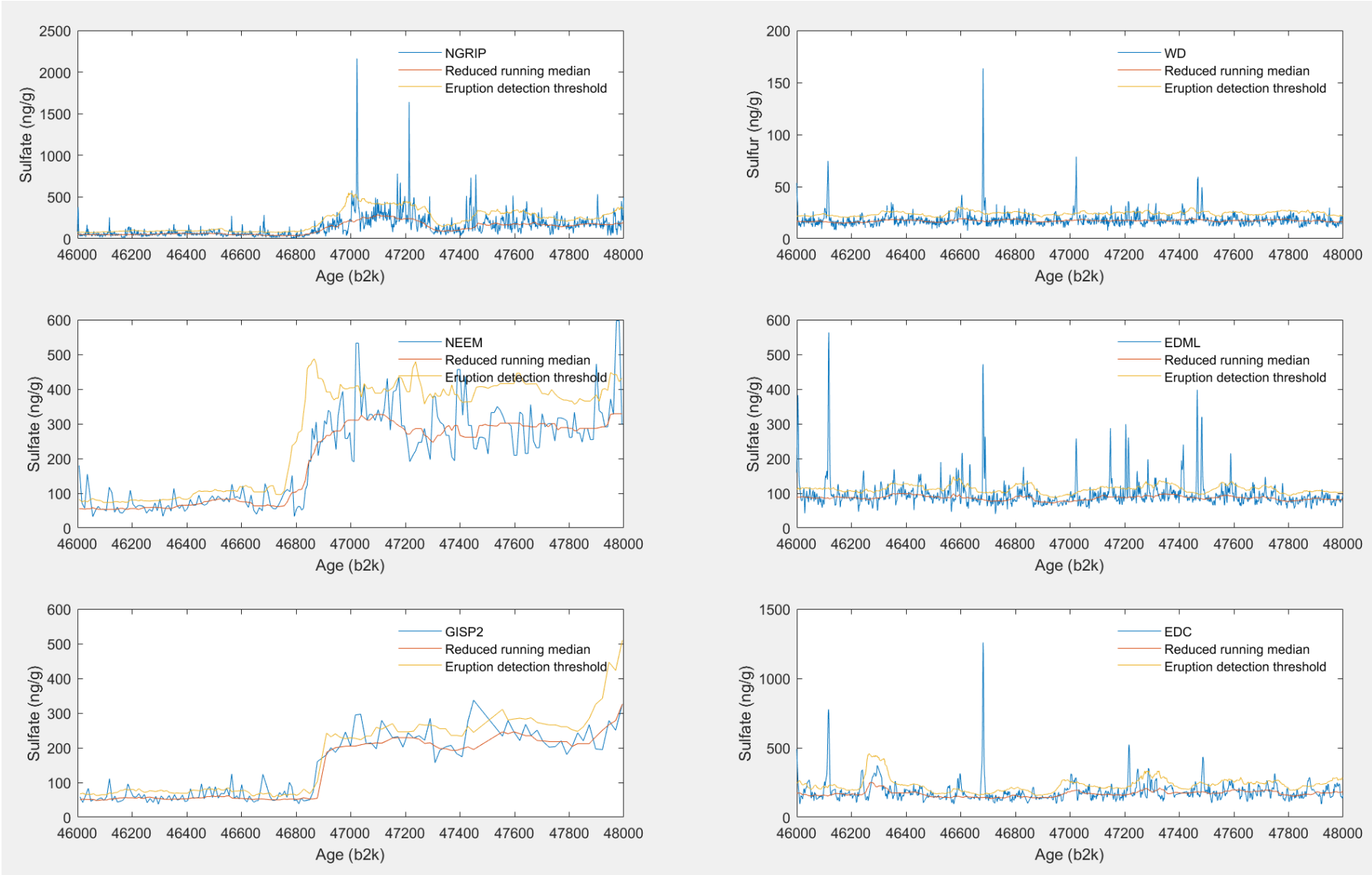


Figure 47: Record showing the sulfate concentration (WD showing sulfur) spanning 46000-48000 b2k for all six ice cores (Greenland left, Antarctica right)

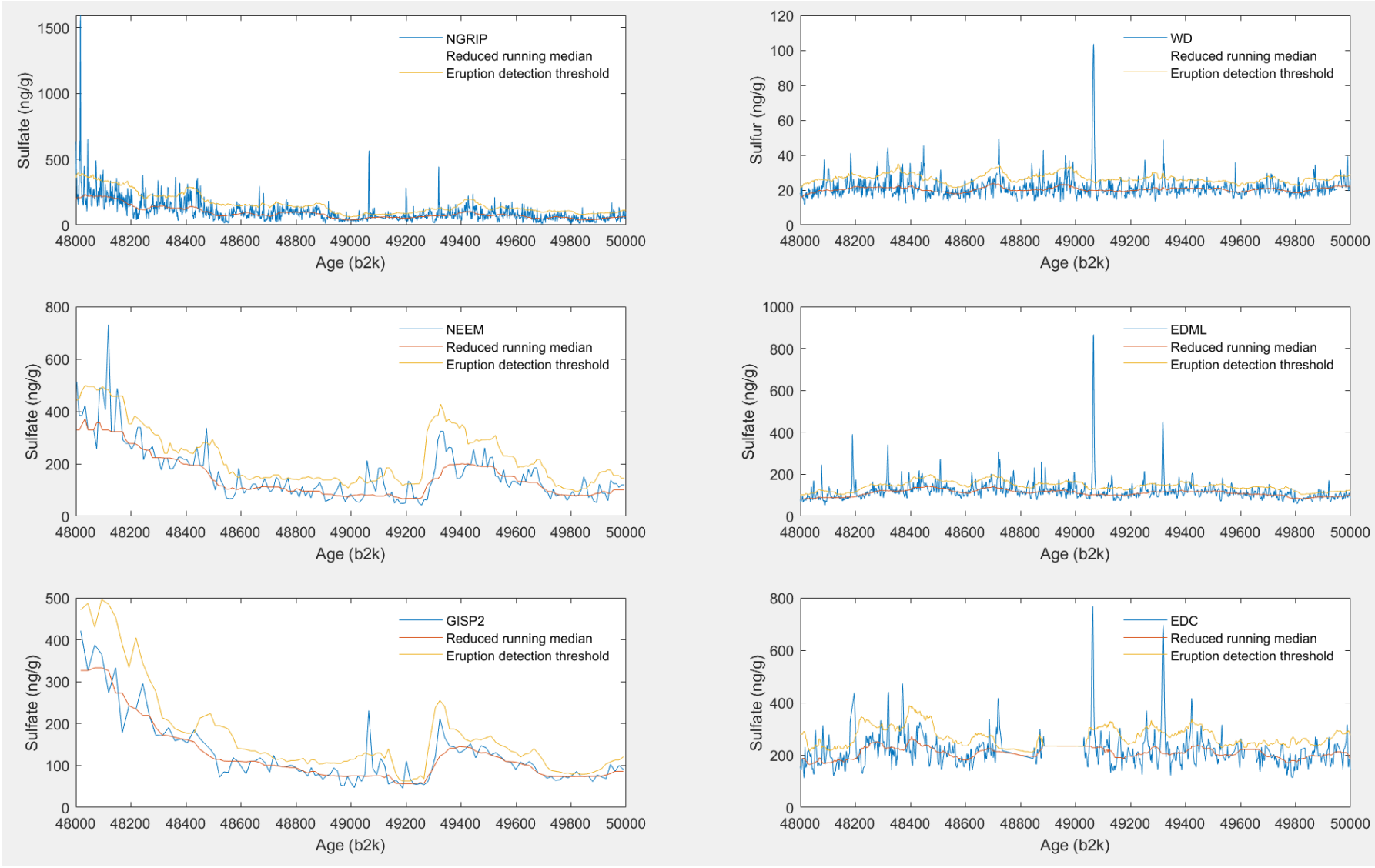


Figure 48: Record showing the sulfate concentration (WD showing sulfur) spanning 48000-50000 b2k for all six ice cores (Greenland left, Antarctica right)

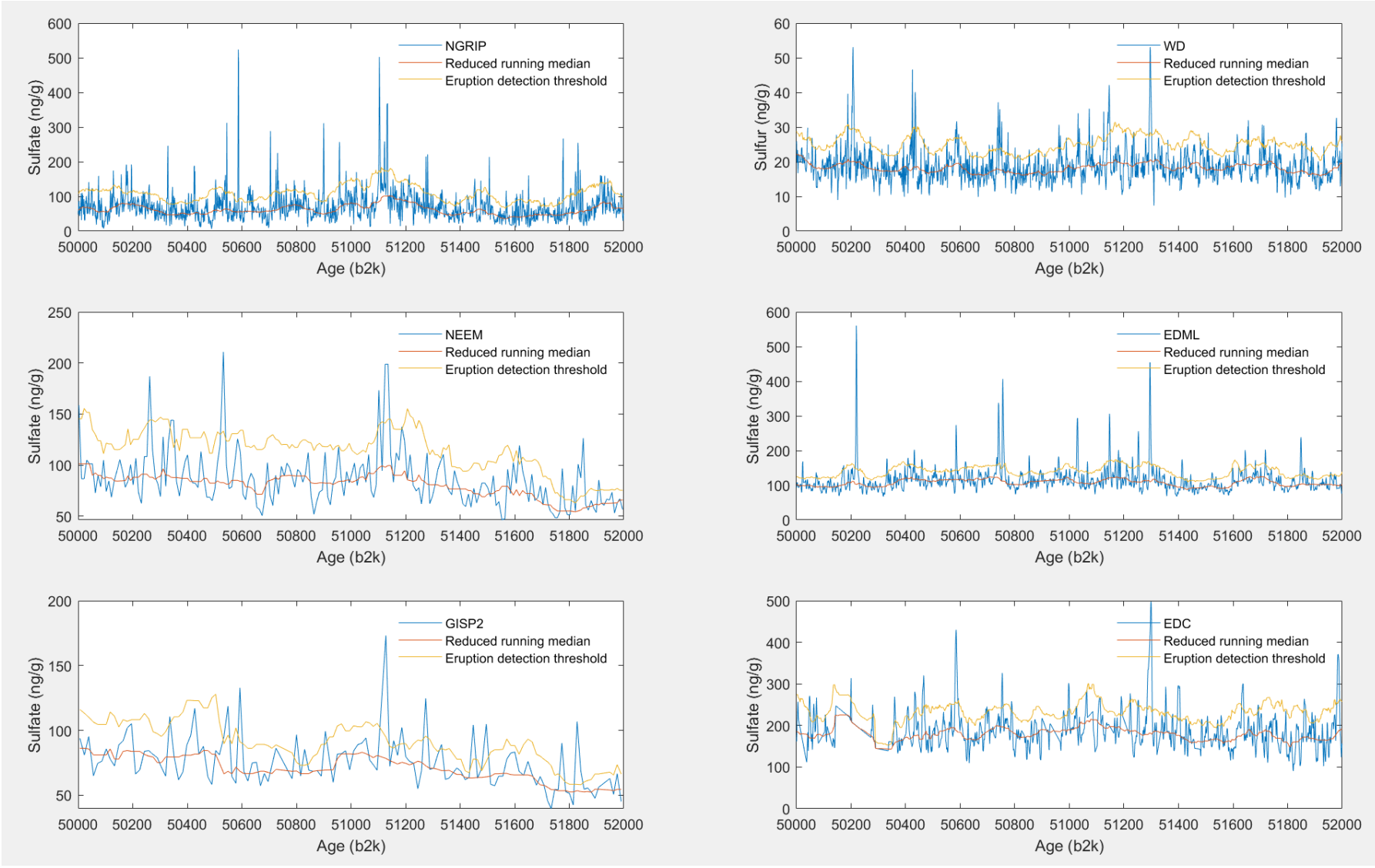


Figure 49: Record showing the sulfate concentration (WD showing sulfur) spanning 50000-52000 b2k for all six ice cores (Greenland left, Antarctica right)

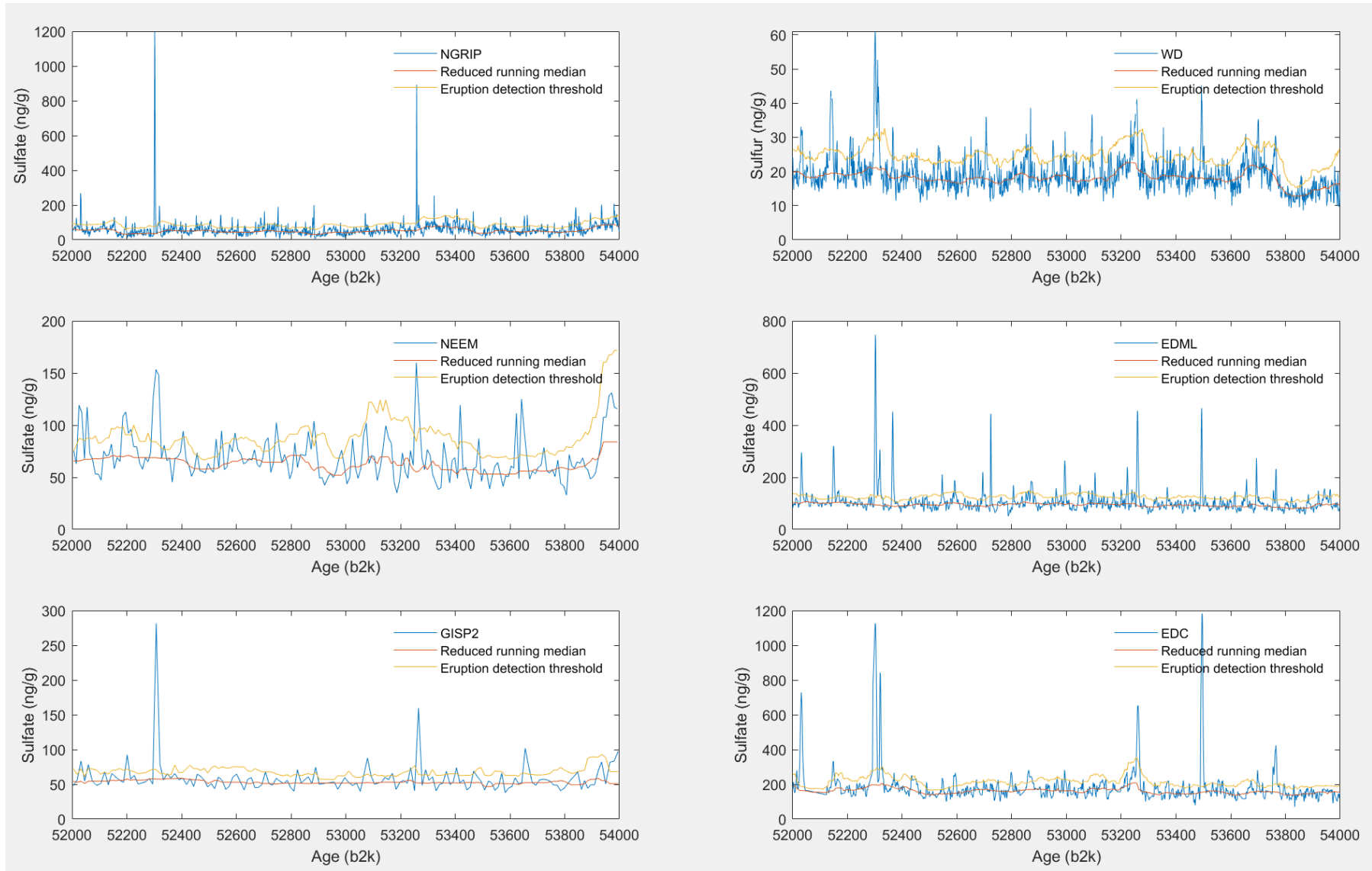


Figure 50: Record showing the sulfate concentration (WD showing sulfur) spanning 52000-54000 b2k for all six ice cores (Greenland left, Antarctica right)

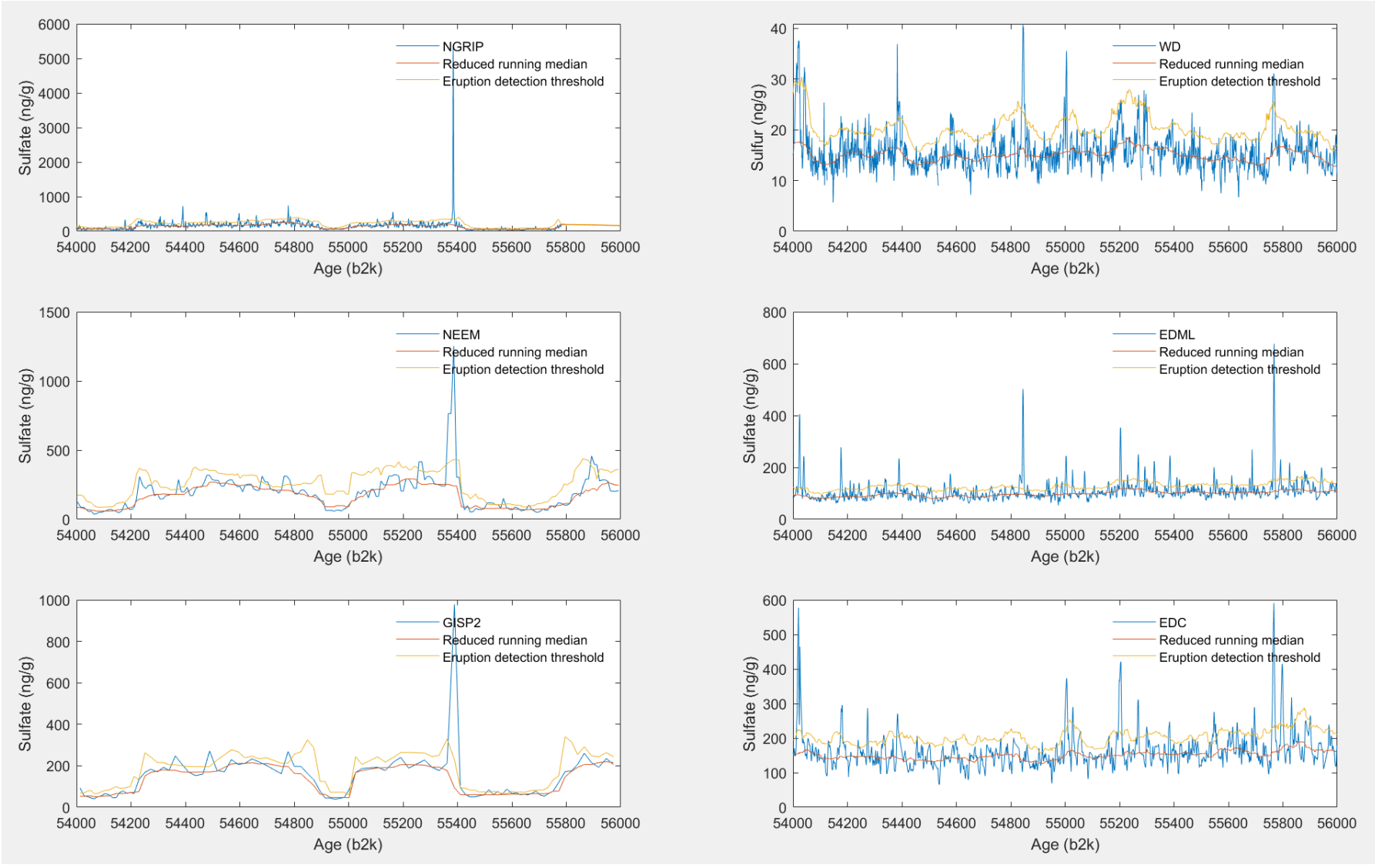


Figure 51: Record showing the sulfate concentration (WD showing sulfur) spanning 54000-56000 b2k for all six ice cores (Greenland left, Antarctica right)

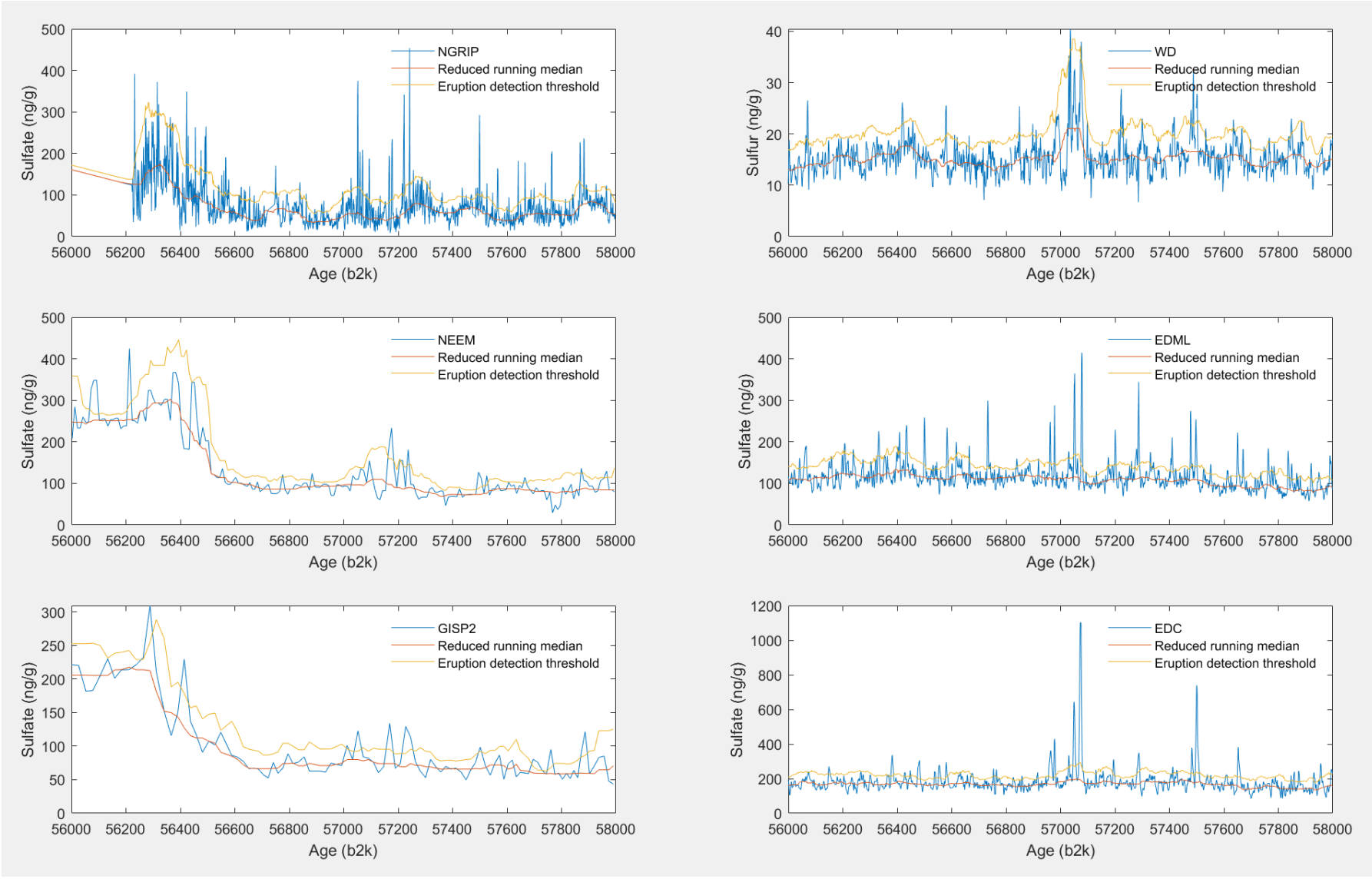


Figure 52: Record showing the sulfate concentration (WD showing sulfur) spanning 56000-58000 b2k for all six ice cores (Greenland left, Antarctica right)

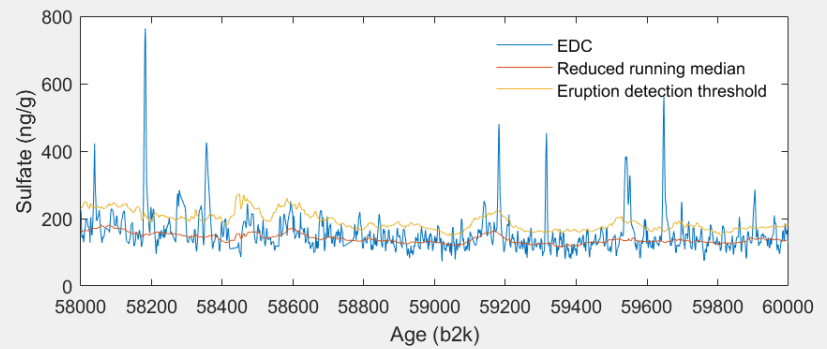
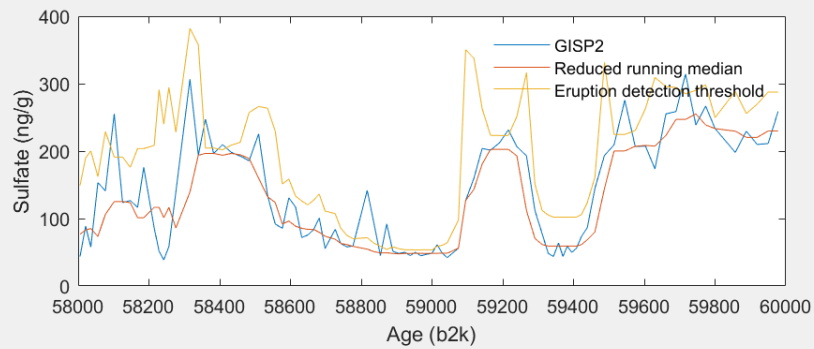
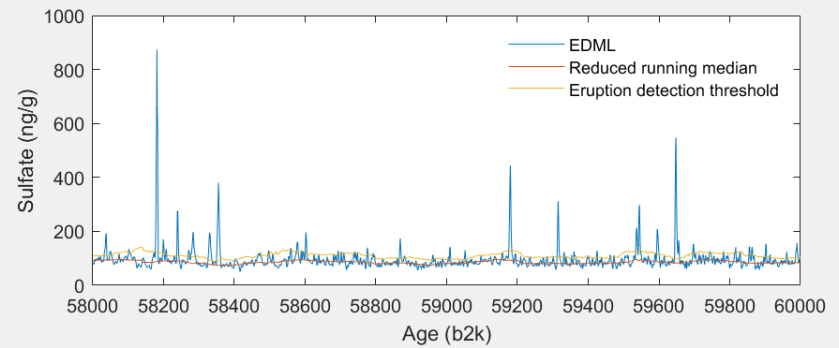
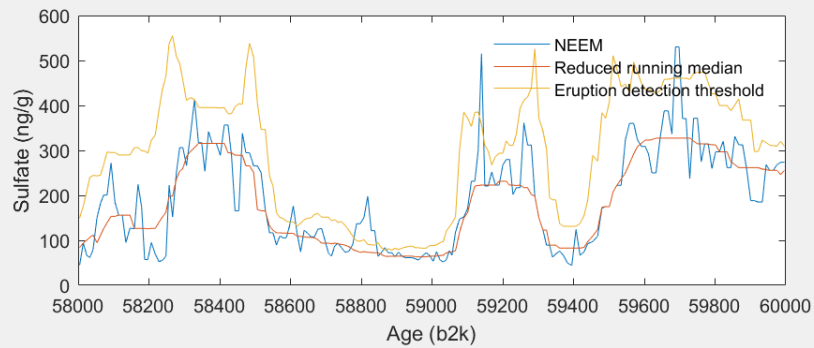
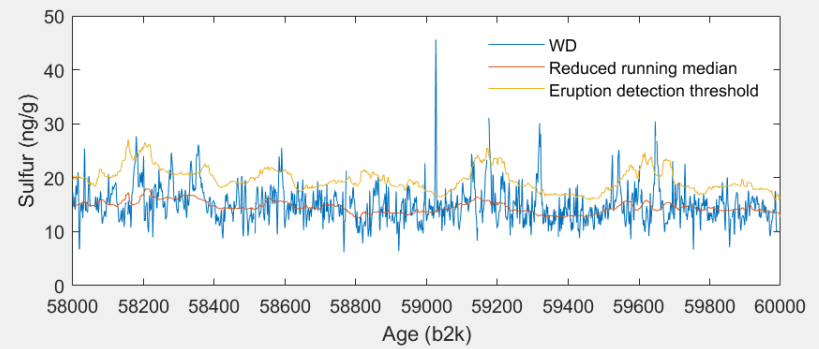
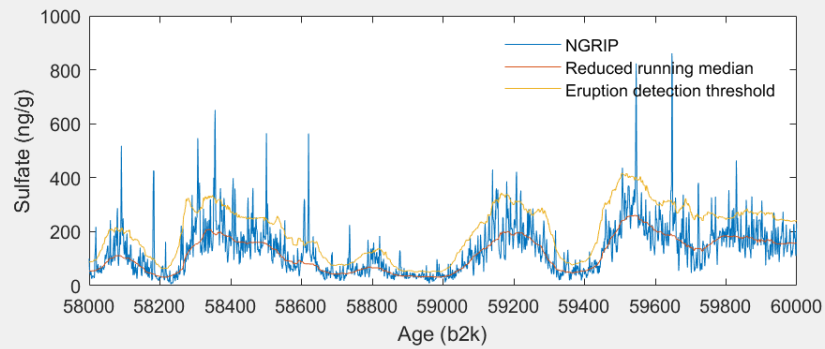


Figure 53: Record showing the sulfate concentration (WD showing sulfur) spanning 58000-60000 b2k for all six ice cores (Greenland left, Antarctica right)

